STRUCTURAL CHANGES IN THE *E. COLI* RIBOSOME DURING ASSEMBLY AND CELLULAR STRESS

by
Ryan Martin Hulscher

A dissertation submitted to Johns Hopkins University in conformity with the requirements for the degree of Doctor of Philosophy

Baltimore, Maryland
October, 2017

Abstract

The ribosome is a large ribonucleoprotein that undergoes structural changes throughout its lifecycle. In this work, I will present a method that I developed for pulse-labeling *E. coli* ribosomal RNA. This procedure was coupled with RNA probing techniques for the structural analysis of *in vivo* assembly intermediates. This method was able to identify global structural changes in the ribosome structure during assembly.

I also used RNA probing techniques to study structural changes that occur as the *E. coli* ribosome is degraded under bacterial stress. Cells that were grown in rich media to late stationary phase contained rRNA that was more accessible to DMS structure probing, suggesting increased disorder and the potential for degradation by cellular nucleases. The results of the DMS probing showed how cellular nuclease cleavage sites were more accessible in stressed cells. This change in the accessibility of the rRNA correlates well with the decrease in intracellular rRNA that I observed over the same time period.

The polysome profiles of stressed bacterial cells show that deprivation of different nutrients can result in different responses in how ribosome degradation is regulated. Ribosomes in cells deprived of magnesium will be degraded in a matter of hours, whereas nitrogen-starved cells still have ribosomal particles after 4 days of nitrogen depletion. The MRE600 cells used for the experiments maintain ribosomes during bacterial stress without forming the 100S hibernation ribosome.

Advisor and primary reader: Dr. Sarah A. Woodson

Secondary reader: Dr. Sua Myong

Committee members: Dr. Rachel Green, Dr. Karen L. Beemon, Dr. Jie Xiao

Acknowledgments

I would not be where I am at today without the help of many others. My family deserves special recognition. My mother for always believing in me and my endeavors, however outlandish they must have occasionally seemed. My father for teaching me from an early age that there is a logical explanation for everything and instilling in me a love of hard work. And my brother for being a far superior athlete and convincing me to focus on my studies. I love you all more than I could possibly say.

I am deeply indebted to my advisor Sarah. She took a chance on me when I needed a lab and trusted me with a project I probably had no right to attempt. For placing such confidence in me, however undue, I will be forever grateful. She has been amazing to work with. Even after knowing her all this time, I still marvel at her passion and drive and the high standard she sets. I can say without hesitation that I am an unequivocally better scientist, worker, and thinker for having received her guidance.

I would like to thank my past mentors, Steven Neshyba and David Draper. They were both instrumental in setting me on the course to intellectual independence.

I would also like to thank my committee members Rachel Green, Greg Bowman, Sua Myong, Jie Xiao, and Karen Beemon for their helpful suggestions through the years. Rachel Green deserves special thanks for sharing her lab space and resources with me. And for introducing me to Boris Zinshteyn, who was invaluable in helping me learn new techniques and troubleshoot my research. Though they were not on my thesis committee, Doug Barrick, Bertrand Garcia-Moreno, and Juliette Lecomte have all offered me sage advice and helped me navigate through grad school and I am deeply appreciative.

I have been blessed with wonderful labmates and would be remiss to not mention a few by name. I had a lot of fun, possibly too much, with Bobby Trachman and Nan Wang early in grad school. Mollie Rappé was a great travel companion on beamline trips. Indra Sharma was a constant source of optimism. Andrew Santiago-Frangos was a great gym buddy and conference travel companion. Subrata Panja and Arthur Korman were delightful for coffee talk and Yumeng Hao and Maggie Rodgers were so much fun to grab a beer with. My grad school experience would have been deeply diminished had I not had such a good assortment of colleagues.

I have also been blessed with outstanding classmates, half of whom I've lived with. They were a constant source of motivation and inspiration for me. A special thanks to Hesam Motlagh for many life-affirming late-night conversations.

I would like to thank my friends Jason Legan and Daniil Davydoff for their comradery through the years. And finally a deep thank you to my wife for her constant support, encouragement, and understanding, and for instigating so many of my happiest memories. This would all be unthinkably less enjoyable without her.

Table of Contents

List of Tables

List of Figures

CHAPTER 1: Introduction

1.1 The ribosome

The ribosome synthesizes the proteins of all living cells. This essential function requires cells to maintain a high concentration of ribosomes even in the face of dilution due to cell growth. Because of this, ribosomes must be rapidly and accurately synthesized. The ribosome is a 2.5 MDa macromolecule consisting of ribonucleic acids (RNA) and proteins. It has an asymmetric quaternary structure consisting of two subunits: a small subunit with a sedimentation coefficient of 30S and a large subunit with a sedimentation coefficient of 50S. The small subunit is composed of the 16S rRNA and 20 proteins (Figure 1.1a-b). It is responsible for initiating the interaction with mRNA and for decoding the mRNA. The large subunit is composed of the 23S and 5S ribosomal RNAs (rRNAs) and 33 proteins (Figure 1.1c). The large subunit contains the site of peptide bond formation.

The ribosomal subunits are each comprised of individual domains that are each closed by long-range base pairs (Noller 1981; Woese 1980). The small subunit possesses the 5' domain, the central domain, the 3' major domain, and the 3' minor domain. These domains were predicted from secondary structure and have each been shown to be able to be reconstituted *in vitro* with the appropriate subset of r-proteins (Agalarov 1998; Samaha 1994; Weitzmann 1993). These three major domains are joined by a central pseudoknot. This pseudoknot has been shown to form late in assembly (Holmes 2004), potentially occurring after the modular assembly of the 5', central, and 3' domains. The

three-dimensional structure of the small subunit is often described anthropomorphically. The 5' domain is referred to as the body and the 3' domain as the head. The central domain is referred to as the platform.

The large subunit can be thought of as containing six domains, defined by the secondary structure. However, the tertiary structures of these domains are more intertwined than what is seen in the small subunit (Steitz 1999). They also contain a much more extensive network of distal tertiary contacts and r-proteins bridging multiple domains. As a result of this greater complexity, the large subunit assembles far less efficiently *in vitro* than the small subunit does and requires a greater degree of thermal and ionic manipulation to achieve proper maturation (Dohme 1976; Shajani 2011). Unlike the small subunit, the domains of the large subunit have not been able to be individually reconstituted *in vitro*. For these reasons, assembly of the large subunit has been studied less than assembly of the small subunit.

1.2 *In vitro* ribosome assembly

The field of ribosome assembly research began to emerge in the late 1960s when it was demonstrated that the 30S subunit of *E. coli* could be reconstituted *in vitro* from its constituent RNA and proteins (Traub 1968). With this established, more detailed experiments were possible. The *in vitro* order of r-protein binding was soon determined (Held 1974, 1973). An *in vitro* assembly map showing the assembly dependencies of the r-proteins was determined by altering the order of protein addition (Held 1974, 1973; Mizushima 1970). It was shown that certain r-proteins can bind to naked 16S rRNA

(primary binding proteins). The remaining proteins require the binding of one (secondary binding proteins) or more (tertiary binding proteins) r-proteins to the rRNA (Figure 1.2a). The primary and secondary proteins are able to bind to the 16S rRNA at low temperatures and form what is known as the reconstitution intermediate. This reconstitution intermediate cannot bind tertiary proteins unless the temperature is raised to 42 °C (Traub 1968). At this higher temperature, conformational changes take place in the molecule resulting in an intermediate which is competent to bind tertiary proteins and form a functional 30S subunit.

In vitro assembly can occur by combining native 16S rRNA with total proteins purified from 30S subunits (Traub 1968), individually purified r-proteins (Held 1973), or recombinant r-proteins (Culver 1999). It is also possible to reconstitute 30S subunits using *in vitro*-transcribed 16S rRNA (Krzyzosiak 1987). Within the cell, the 16S rRNA is post-transcriptionally modified with 10 base-methylations and one pseudouridylation. An *in vitro* transcript would not contain these modifications.

In vitro studies have been performed on the assembling 30S ribosome using time-resolved hydroxyl radical footprinting (Adilakshmi 2008), quantitative mass spectrometry (Talkington 2005), and time-resolved electron microscopy (Mulder 2010). These studies have suggested that multiple parallel assembly pathways are present *in vitro*. By combining quantitative mass spectrometry and time-resolved electron microscopy, fourteen structural intermediates were identified (Mulder 2010). Given their differences in protein occupancy, a kinetic assembly map was constructed showing the relationship between each of the intermediates, and the parallel pathways that could be followed for each intermediate (Figure 1.3).

The assembly of the 50S subunit has also been studied through *in vitro* reconstitution experiments (Nierhaus 1979). Like the small subunit, the large subunit also has structural intermediates that can be isolated based on the temperature and the ionic conditions. At low temperatures and 4 mM Mg^{2+}, the 23S and 5S rRNA and 22 r-proteins are able to form a first structural intermediate. By raising the temperature to 44 °C, there is a structural transition that renders the intermediate competent to bind the remaining r-proteins (Sieber 1978). This results in an inactive subunit which becomes functional by increasing the temperature to 50 °C and the magnesium concentration to 20 mM.

1.3 *In vivo* ribosome assembly in eubacteria

Assembly of the ribosomal subunits is coupled with pre-rRNA synthesis (Lewicki 1993; Powers 1993; Spillmann 1977) and requires only a few minutes during logarithmic growth (Lindahl 1975). Near the end of the assembly process, an intermediate form of the pre-rRNA is trimmed to its mature (16S) length in several steps by ribonucleases. Several features likely contribute to the rapidity of subunit biogenesis in the cell. First, the 5'-to-3' polarity of co-transcriptional assembly limits the opportunities of forming non-native RNA secondary structures, because 5' regions of the rRNA are able to fold before the 3' regions have been transcribed (Lewicki 1993). Second, more than 15 assembly factors and additional RNA and protein modification enzymes facilitate assembly and carry out the final steps of subunit maturation (Kaczanowska 2007; Wilson 2007). Third, homeostasis of free ribosomal proteins ensures a constant pool of protein components (Chen 2012). In eukaryotes, ribosome assembly is aided by over 200 assembly factors

and is also coupled to transport of assembly intermediates from the site of transcription in the nucleolus to the cytoplasm (Hage 2014).

The rRNA for the entire ribosome is transcribed as a single transcript. There are three cleavage events which produce the final 16S rRNA (Figure 1.4). RNase III makes a double-stranded cut and produces a 16S precursor rRNA with a 115 nt 5' leader and a 33 nt tail at the 3' end. This precursor is known as 17S rRNA. RNase III cleavage takes place before the *rrn* operon has been fully transcribed. A transcript containing the entire *rrn* operon is undetectable *in vivo* (Gegenheimer 1975). The 3' tail is cleaved by polynucleotide phosphorylase (PNPase) and RNases II, R, and PH. The 5' leader is then cleaved by RNase E leaving a 66nt leader. This precursor sediments at 16.3S. Finally, RNase G cleaves the remaining 5' leader and the result is 16S rRNA. There is evidence that the 5' leader influences folding of the 16S rRNA. Mutations made in the leader sequences of *rrn* operons show changes in the structure of the 30S ribosomal subunit (Balzer 1998). Cross-linking studies have also suggested that the leader interacts with the 5' domain of the 16S rRNA (Pardon 1995). The leader also affects the kinetics of the folding of the 5' domain (Besançon 1999).

The 16S rRNA is subject to 11 post-transcriptional modifications. Quantitative mass spectrometry has been used to determine the relative order of the modifications. The modifications to the 5' domain occur earliest, followed by the 3' major domain, and finally the 3' minor domain is modified (Popova 2014). The modifications are late events of *in vivo* assembly. As mentioned earlier, the modifications are not absolutely necessary for assembly *in vitro*.

After cleavage by RNase III, the 23S precursor rRNA contains 7 nt at the 5' end

and 8 nt at the 3' end. The 3' end is further processed by the exoribonucleases RNase PH, RNase II, and PNPase, leaving 1 to 4 nt (Gutgsell 2012). These final nucleotides at the 3' end are removed by RNase T (Gutgsell 2012). The 5' end processing occurs independently by an unknown nuclease. The 23S rRNA is subject to 25 post-transcriptional modifications.

Cleavage by RNase III results in a transcript containing both the 5S rRNA and a variable distal sequence which can contain one or two tRNAs (King 1983). After processing by RNase P, the tRNA is removed and a precursor containing the 5S rRNA with 84 additional nt at the 5' end and 42 nt at the 3' end is generated (Guerrier-Takada 1983). This is known as the 9S rRNA. RNase E processes both termini and the 5S rRNA is left with 3 additional nt at each termini (Roy 1983). Processing at the 3' end has been shown to require RNase T (Li 1995). The nuclease responsible for processing the 5' end has not yet been identified.

Recent technical advances, notably in the area of electron microscopy, have resulted in great increase in the understanding of *in vivo* ribosome assembly. In the small subunit, a number of *in vivo* assembly intermediates were able to be identified from fractions of the *E. coli* 30S peak on a sucrose gradient (Sashital 2014). Intermediates were grouped according to their r-protein content and their conformation, as determined by quantitative mass spectrometry (qMS) and negative-stain electron microscopy, respectively. The intermediates were structurally divided into five main groups (Figure 1.5). Group I intermediates were the least mature, with the body and platform assembled, but no density for the head (Figure 1.5a). Group II and III both contained head density, with the head undocked in Group II (Figure 1.5b) and merely out of position in Group III

(Figure 1.5c). The study also noted a significant destabilization of the central pseudoknot in the Group II intermediates. This is consistent with the previous *in vitro* finding that the central pseudoknot forms late in assembly (Holmes 2004). This hinged head movement was also observed in EM structures (Mulder 2010) of *in vitro* 30S assembly intermediates (Figure 1.3). Group IV and V intermediates were nearly mature, only missing the late-binding r-proteins S2, S3, and S21 (Figure 1.5e-g).

The use of cryo-EM has been increasingly important in the study of the 50S subunit. A number of 50S assembly intermediates have been characterized in this manner (Jomaa 2014; Li 2013). These intermediates were found to lack density in the central protuberance and the peptidyl transferase center, suggesting that these regions form late in assembly. Recent analysis of large subunit intermediates obtained through limited expression of the essential r-protein L17 identified thirteen structural intermediates through the use of qMS and cryo-EM (Davis 2016). By coordinating the occupancy of r-proteins via qMS and the presence of RNA helical density in the cryo-EM maps, five highly-correlated structural blocks were identified in the large subunit (Figure 1.6a). The linkage between the helical folding and r-protein binding suggests that these regions can individually form as cooperative folding blocks. Interestingly, these folding blocks connect multiple rRNA secondary structure domains (Figure 1.6b). These independent folding blocks suggest that multiple parallel assembly pathways are available to connect the thirteen assembly intermediates characterized in the study.

1.4 *In vivo* RNA probing using hydroxyl radical and DMS probing

The use of EM has produced increasingly well-resolved global structures of assembly intermediates, and the use of qMS has characterized the protein occupancy of the various intermediates and allowed kinetic assembly maps to be constructed. However, qMS studies do not provide structural information on the rRNA and cryo-EM studies are unable to probe RNA structure in cell or over time. Cryo-EM also fails to provide information on disordered regions of the ribosome. In contrast, RNA chemical probing can be used to obtain the rRNA structure with single-nucleotide resolution in the cell over time. By using RNA chemical probing, a more complete picture of the ribosome assembly process can be attained.

A number of chemical probing techniques are available for the structural examination of RNA *in vivo*. All of these methods work by modifying either the base or the sugar moiety of a nucleotide in the RNA structure. Two specific techniques will be presented here: hydroxyl radical probing and dimethyl sulfate (DMS) probing. These reagents act upon the RNA in very different ways. Hydroxyl radicals attack the sugar ring, resulting in the breaking of the phosphate backbone at the location of probing (Tullius 2005). DMS methylates the adenine and cytosine bases on their Watson-Crick faces and guanine on its Hoogsteen face (Peattie 1980). In both cases, the modifications can be observed by reverse transcribing the probed RNA and generating cDNA (Inoue 1985; Stern 1988). For RNA exposed to hydroxyl radical, the cDNA will terminate at the point of cleavage. For RNA methylated with DMS, there are two possible outcomes depending on the reverse transcriptase used. Most reverse transcriptases will fall off the RNA when a methylation A or C is encountered, resulting in a cDNA that terminates one

base prior to the methylated base. A recently developed reverse transcriptase is able to process through methylated bases, resulting in mismatches in the cDNA at the sites on DMS methylation (Katibah 2014; Mohr 2013).

The hydroxyl radicals break the RNA strand by abstracting a proton from the ribose C4', C5' or C1' (Tullius 2005). The probability of cleavage depends on the solvent accessibility of the ribose, and thus reflects the RNA tertiary structure or protein interactions. Because hydroxyl radicals cleave the RNA backbone in a base-independent manner, hydroxyl radical footprinting provides structural data on the RNA at single-nucleotide resolution, unlike many other chemical probing techniques.

Unlike the *in vitro* experiments, in which hydroxyl radicals are produced using Fe(II)-EDTA and millimolar concentration of H_2O_2 (Tullius 1986; Tullius 1987; Udenfriend 1954), the live cell samples are probed by hydroxyl radicals that are generated by ionizing radiation, as shown in the equation below.

$$H_2O \xrightarrow{h\nu} H_2O^+ + e^-_{aq} \xrightarrow{H_2O} H_3O^+ + \bullet OH + e^-_{aq}$$

This *in situ* method of generating hydroxyl radical avoids the deleterious effect of hydrogen peroxide on live cells. Both γ-rays from a ^{137}Cs source (Ottinger 2000) and X-rays from a synchrotron source (Bohon 2014; Gupta 2014; Sullivan 2008) produce hydroxyl radicals *in situ*. However, the higher flux density of a synchrotron beam delivers the necessary dose in a much shorter time, typically in less than 100 ms for frozen cells (Adilakshmi 2009) and 10–20 ms for liquid culture, and ensures the least perturbation to live cells.

Time-resolved X-ray-dependent hydroxyl radical footprinting has been used to study the kinetics of *in vitro* RNA folding (Adilakshmi 2008) because sufficient hydroxyl

radicals to probe RNA can be generated in a few milliseconds using a synchrotron X-ray source with high flux density (Sclavi 1998). X-ray footprinting has also been used on frozen *E. coli* cells to characterize the structure of the small subunit of the ribosome and examine the effect of ribosome assembly factor deletion (Clatterbuck Soper 2013). Because the hydroxyl radical is produced *in situ* by photolysis of the water, no harmful permeabilization of the cell is needed. Another advantage of X-ray footprinting is that the extent of cleavage can be controlled by varying the X-ray dose (Ralston 2000).

The quality of the footprinting results depends greatly on minimizing X-ray-independent RNA cleavage, which leads to undesired background in the sequence analysis. MRE600 cells lack RNase I, a periplasmic protein that can degrade RNA during extraction (Deutscher 2009). Using this strain reduces non-specific RNA degradation. To further limit RNA degradation, samples can be treated with RNAprotect (Qiagen) to stabilize the RNA. The culture and RNAprotect should be mixed as soon as possible after each fraction is collected. If the samples will be shipped to another location for analysis, they should be packaged in ample dry ice to guard against partial thawing during shipment. Cells should be stored at -80 °C until the RNA can be extracted.

RNA can also be modified with chemical reagents. Dimethyl sulfate (DMS) is a lipophilic molecule that readily passes the cell membrane and can modify RNA bases (Ephrussi 1985; Waldsich 2002). In contrast to hydroxyl radical, DMS methylates adenine N1, cytosine N3 and guanine N7, and therefore the extent of modification reports on the RNA secondary structure and other interactions with the RNA bases. Methylation of A N1 and C N3 is detected by pausing of reverse transcriptase during primer extension. Methylation of G N7 is usually only detected by primer extension if it

subsequently causes depurination. DMS has been extensively used to probe RNA *in vitro* (Merryman 1999; Nguyenle 2006; Stern 1989), and because it is highly reactive, can also be used to monitor RNA assembly in real time (Powers 1995). It has also been used *in vivo* for transcriptomics studies (Rouskin 2014). High-throughput DMS probing of rRNA structure has been performed in bacteria, yeast, and mammalian cells (Rouskin 2014; Swiatkowska 2012; Talkish 2014). While DMS only modifies certain bases, it does not require a synchrotron, is reproducible, and easy to scale up.

1.5 Regulation of ribosome assembly and rRNA synthesis

Ribosome biogenesis is directly related to cellular growth conditions. The number of *E. coli* ribosomes (per unit of cellular protein) is linearly proportional to the cellular growth rate (μ) and the rate of ribosome synthesis is proportional to μ^2 (Kjeldgaard 1966). Ribosomal RNA synthesis is greatly inhibited under conditions that preclude cellular growth.

The synthesis of rRNA is controlled primarily at the level of transcription initiation, in response to the amount of free rRNA available for r-protein binding (Gourse 1996, 1984). As a result, transcription of rRNA is the rate-limiting step in ribosome biogenesis. Transcription of rRNA uses two promoters: *rrn* P1 and *rrn* P2 (Kaczanowska 2007; Murray 2003; Paul 2004). The *rrn* P2 promoter is particularly important in regulating rRNA transcription during the transition into the stationary phase and also during outgrowth from stationary phase (Murray 2004). The promoter open complex is short-lived and, as such, is sensitive to the concentration of the initiating NTP (Gaal 1997; Paul 2004; Schneider 2004). During exponential phase growth, NTPs are abundant

(each ~1mM). In the stationary phase, NTP pools decrease 15- to 20-fold (Walker 2004). The *rrn* P2 promoter open complex is also sensitive to the presence of guanosine-5'-diphosphate-3'-diphosphate (ppGpp) (Murray 2003). This molecule is present in increased concentrations during the stationary phase and during the stringent response. The decrease in NTPs and the increase in ppGpp both result in rRNA synthesis being greatly reduced during the stationary phase as both promoters are inhibited (Kaczanowska 2007).

1.6 Ribosomal response to bacterial starvation

Structural changes occur in the ribosome throughout its lifecycle. In contrast to the maturation and increased stability that occurs during assembly, ribosomes are known to become unstable during starvation. The total RNA content in a bacterial cell decreases during periods of nutrient starvation (Ben-Hamida 1966; Jacobson 1968; Maruyama 1970; McCarthy 1962). Ribosomes account for the majority of cellular RNA and the RNA degradation observed during starvation is largely resulting from rRNA degradation.

Ribosomal degradation appears to be an all-or-none process where ribosomes are completely broken down once degradation begins (Davis 1986; Jacobson 1968; Kaplan 1975). During carbon starvation, several RNases have been implicated in the ribosome degradation process (Basturea 2011). In the 16S rRNA (Figure 1.7a), the 3' end is trimmed by the exoribonuclease RNase PH during starvation. This step can lead to the removal of the entire 3' minor domain and appears to be required for efficient rRNA degradation. The 3' minor domain, which contains the mRNA decoding site, forms a

significant portion of the subunit interface in the 70S ribosome. During periods of starvation, the 16S rRNA is cleaved by RNase E between A919 and U920, near the central pseudoknot (Sulthana 2016). It also appears to cleave near U820. The processive exoribonucleases RNase II and RNase R rapidly degrade the downstream fragment generated by the cleavage between A919 and U920. The enzymes responsible for degrading the upstream fragment have not yet been identified. In the 23S rRNA (Figure 1.7b), RNase E cleaves between C1492 and C1943 in Helix 71. No other fragments are seen for the 23S, suggesting the degradation of the fragments continues by the action of exoribonucleases. The sites of RNase E cleavage in both subunits reside in the interfacial region and would be exposed following removal of the 3' minor domain by RNase PH.

Although the enzymes involved in the degradation of stable RNA during starvation conditions have largely been identified, the mechanism by which they first begin to degrade stable rRNA is not understood. Two possibilities are that the structure of the ribosomes is altered in such a way that rRNA becomes more accessible for RNase cleavage or that RNase activity becomes elevated during periods of starvation. Understanding the structural mechanism of degradation would provide valuable insight into RNA metabolism.

1.7 Specific aims

The goal of my work is to better understand the structural changes that occur during the lifecycle of the *E. coli* ribosome *in vivo*. To accomplish this, I developed a novel technique for labeling and isolating ribosomes that are newly synthesized and in

the process of being assembled *in vivo*. I also developed two techniques for synchronizing the transcription of ribosomal RNA: one by manipulating the cellular growth media and one by treating exponential phase cells with an antibiotic. I have used probed RNA *in vivo* using both DMS and hydroxyl radicals in an effort to examine the structures of ribosomal assembly intermediates as they actually exist in the cell. I have also applied these probing techniques to study ribosomes during periods of bacterial stress in which the ribosomes are undergoing degradative processes in order to observe structural changes occurring at the end of the bacterial lifecycle.

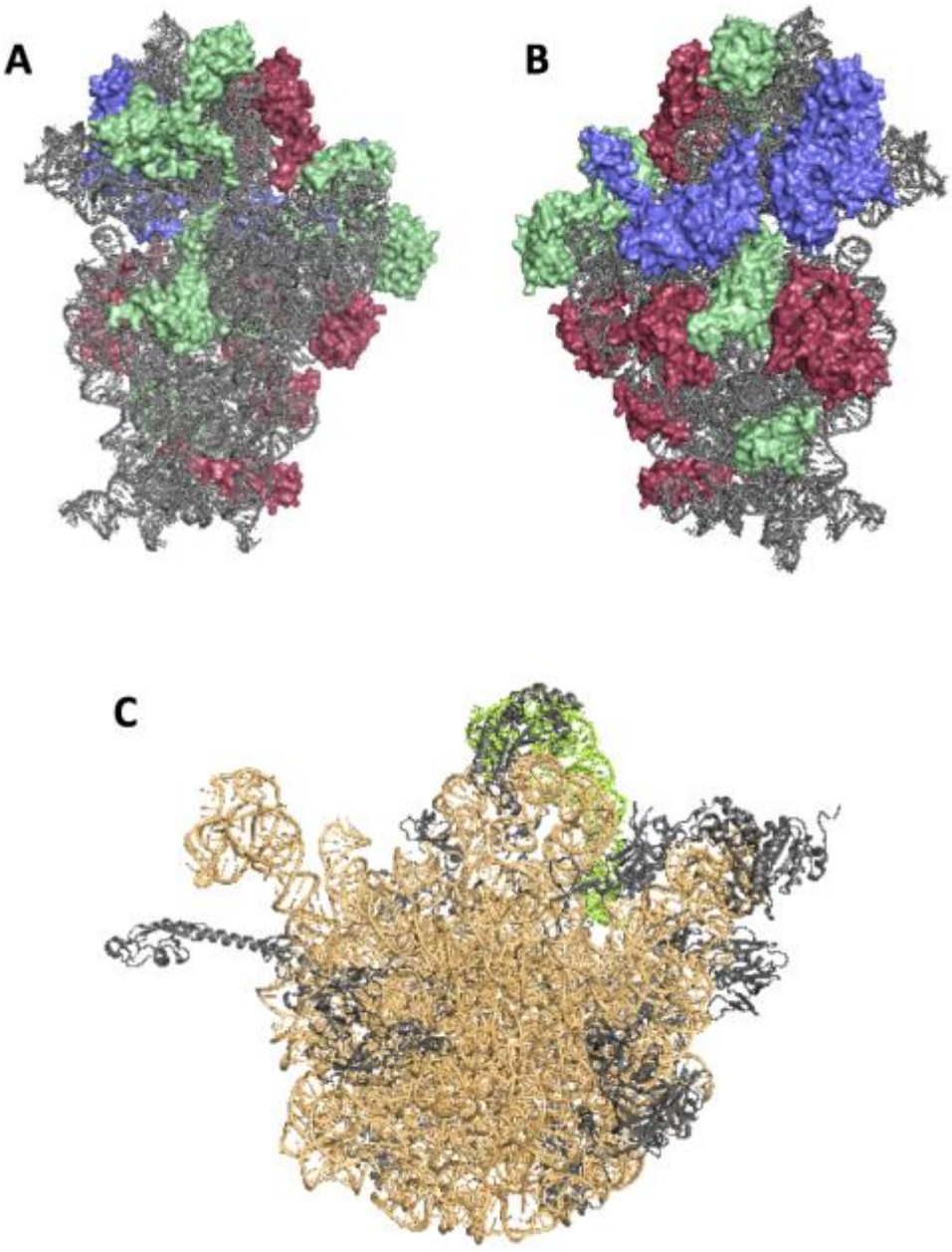

Figure 1.1. The crystal structure of the *E. coli* ribosome (a) The interface view of the 30S subunit. The 16S rRNA is represented in grey. The primary binding proteins are represented in red, the secondary binding proteins are in green, and the tertiary binding proteins are in purple. (b) The solvent view of the 30S subunit. (c) The interface view of the 50S subunit. The 23S rRNA is orange and the 5S rRNA is green. All proteins are depicted in grey. PDB ID 4YBB.

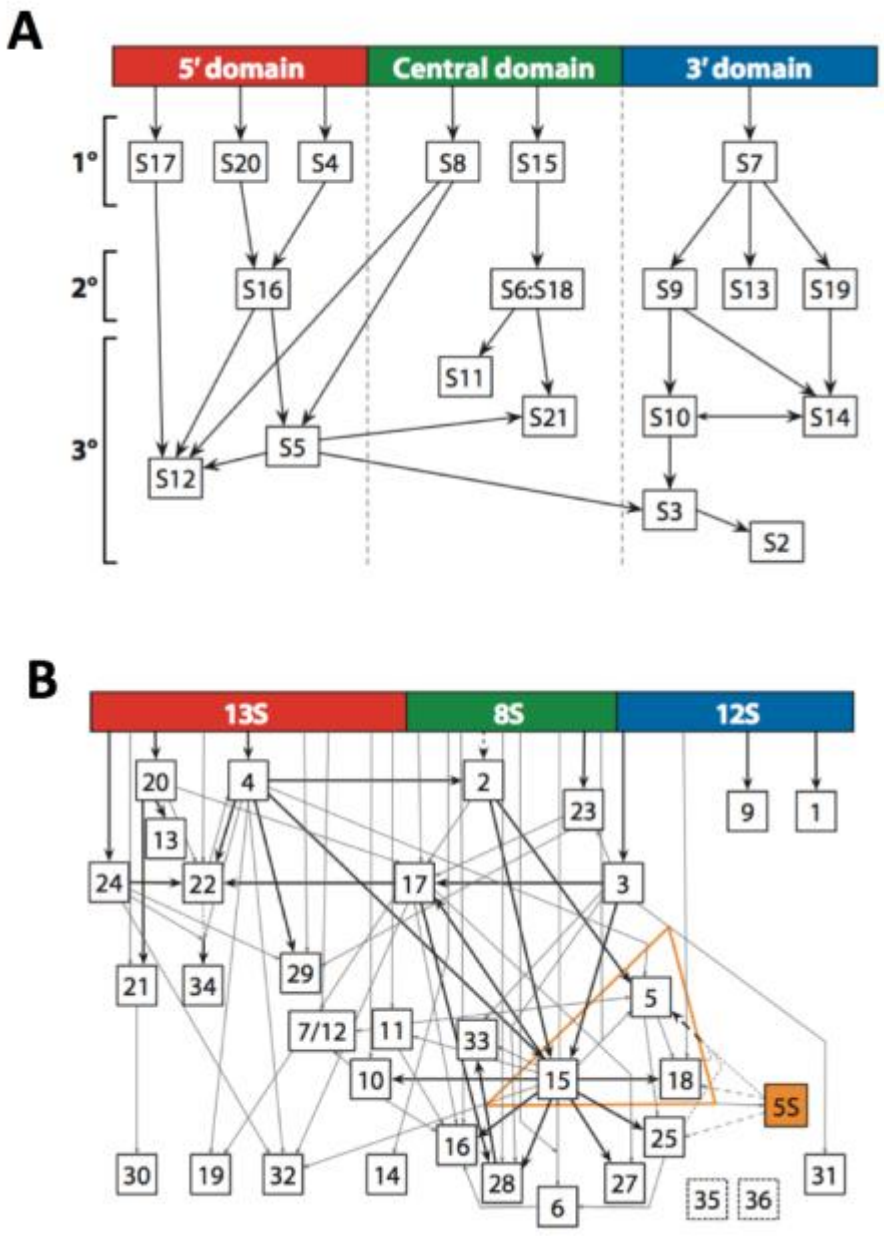

Figure 1.2. Assembly maps of the thermodynamic binding dependencies in the ribosome subunits (a) The Nomura assembly map depicts the protein binding hierarchy in the 30S subunit. Primary binding proteins are able to bind directly to rRNA. Secondary binding proteins require primary binding proteins to first be bound to the rRNA before they will bind. Tertiary binding proteins require secondary binding proteins to be bound. The domains colored at the top of the chart depict the locations on the rRNA to which the proteins bind. (b) The Nierhaus assembly map depicts the binding hierarchy in the 50S subunit. The binding of the 5S rRNA is dependent on the binding of proteins L5, L15, and L18. From (Shajani 2011). Reprinted with permission.

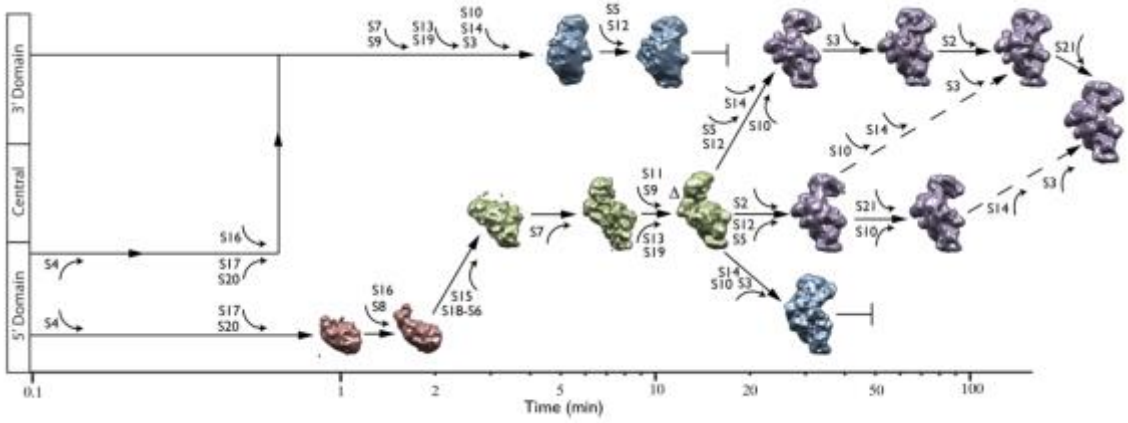

Figure 1.3. Kinetic assembly map of *in vitro* 30S assembly shows multiple parallel assembly pathways The vertical axis represents the 16S rRNA. The structures shown are fourteen structural intermediates identified by time-resolved electron microscopy. Assembly can nucleate from various points, but not all pathways are on target. The order of r-protein binding is shown along the arrows between structures. From (Mulder 2010). Reprinted with permission from AAAS.

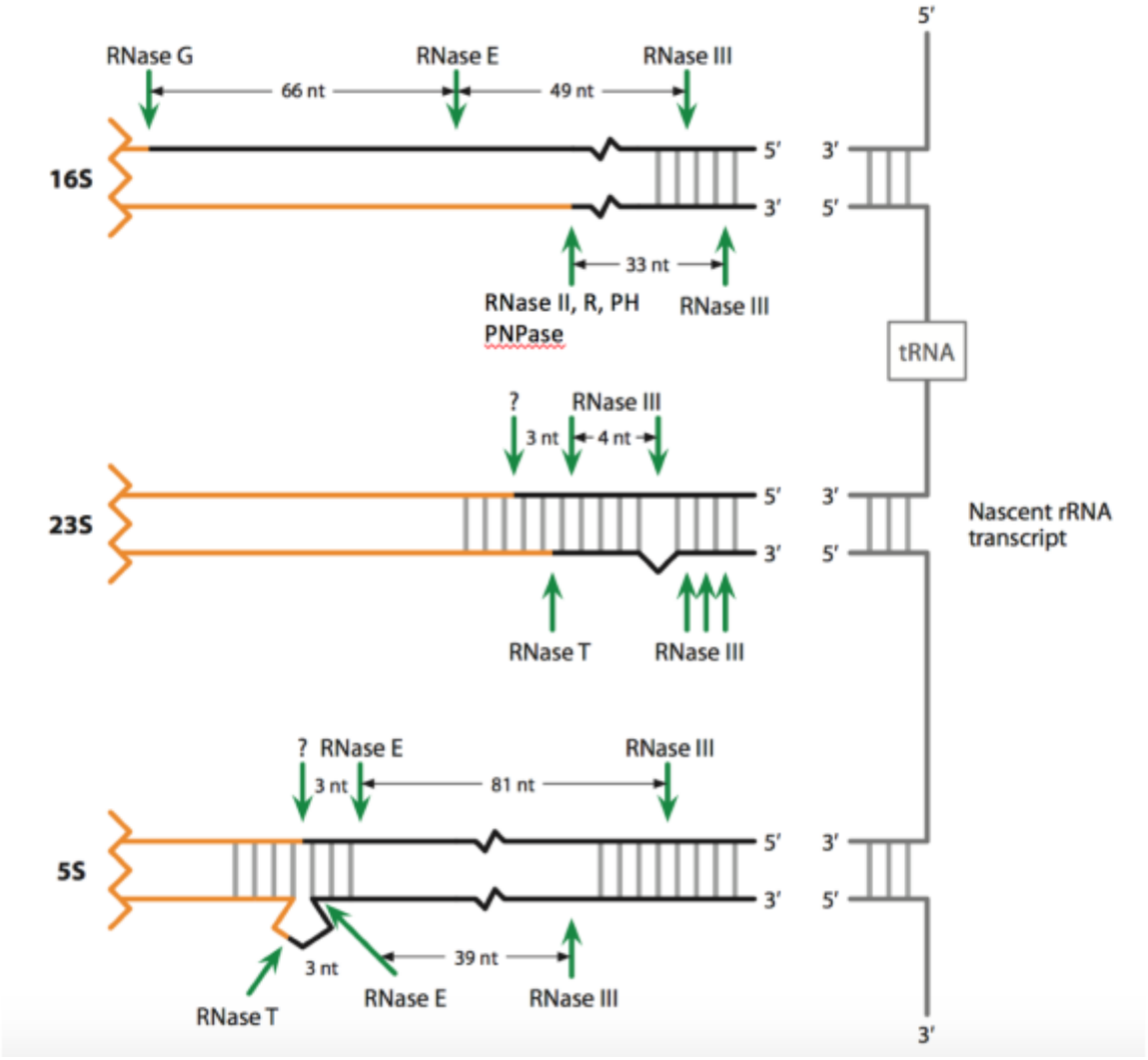

Figure 1.4. Maturation of precursor rRNAs The 16S, 23S, and 5S rRNAs are transcribed as part of a single transcript. The full transcript is cleaved by RNase III to produce precursor versions of each of the rRNAs (Bram 1980; Young 1978). These are processed by a further series of RNases to produce the mature rRNAs. Cleavage sites are depicted by green arrows. Mature rRNAs are shown in orange. Cleavage events for which the responsible RNase has not been identified are marked with a question mark. Adapted from (Shajani 2011). Reprinted with permission.

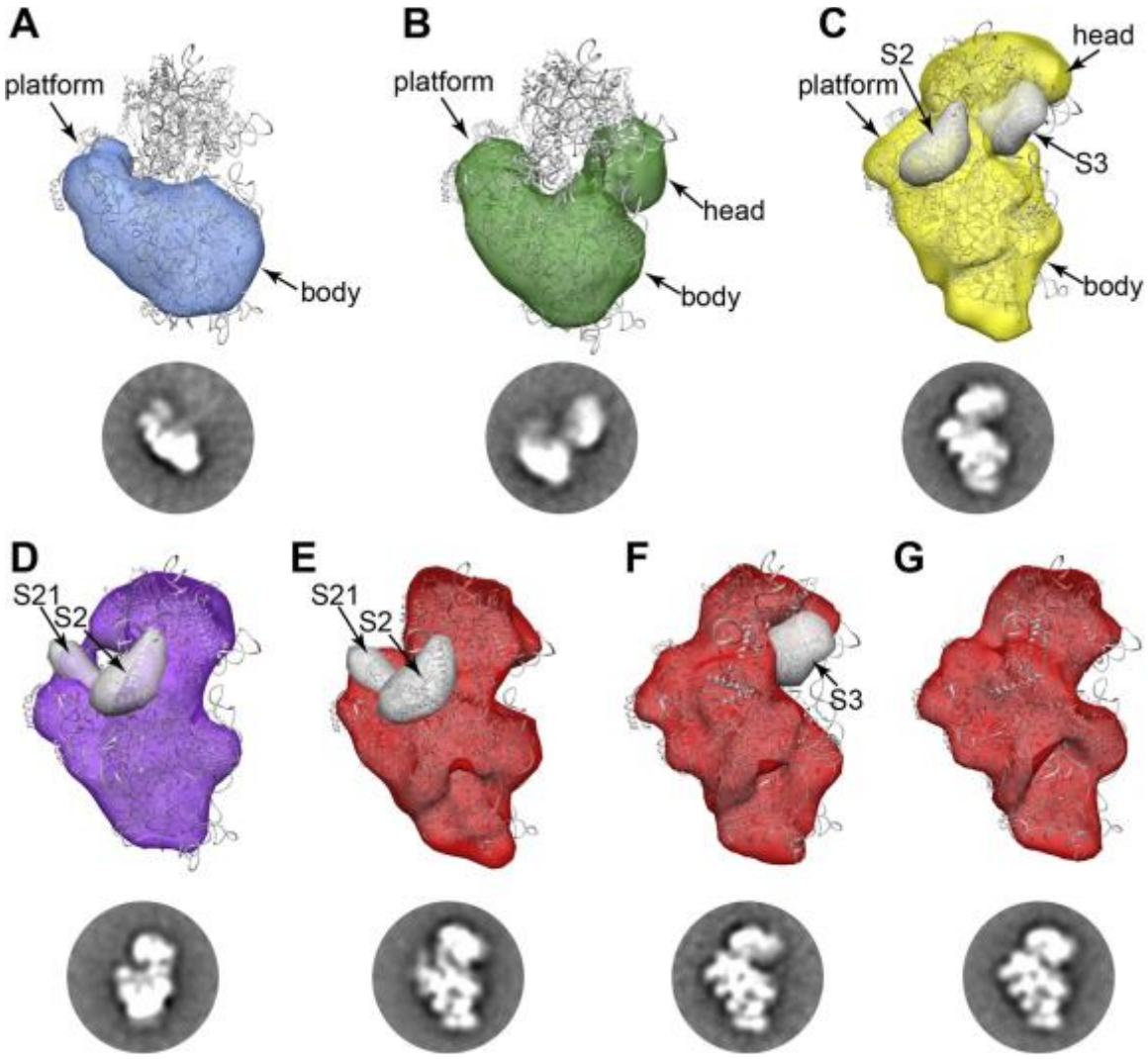

Figure 1.5. Assembly intermediates of the *E. coli* 30S subunit Representative random conical tilt reconstructions of the cryo-EM maps are aligned with the crystal structure of the mature 30S. (a) Group I intermediate. This intermediate lacks all density for the 3' domain ('head'). (b) Group II intermediate. Density is present for the 3' domain, but it is detached from the other domains. (c) Group III intermediate. Density is present for the head domain, but it is not in the mature orientation, (d) Group IV intermediate. Some density is missing in the platform domain and these intermediates generally lack S2 and S21. (e) Group V intermediate lacking S2 and S21 density. (f) Group V intermediate lacking S3 density. (g) Fully-mature Group V intermediate. From (Sashital 2014). Reprinted with permission.

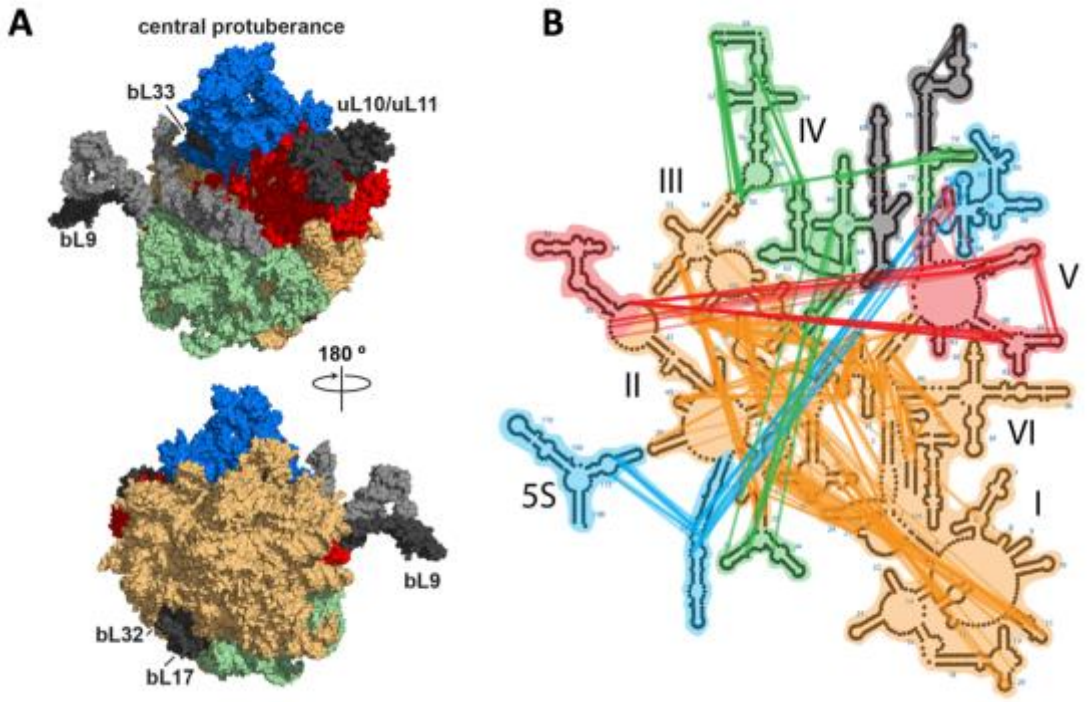

Figure 1.6. Cooperative folding domains in the 50S ribosome subunit (a) Regions of the 50S were clustered according to r-protein and rRNA helix occupancy. The 50S subunit is shown here with each independent folding region a different color. (b) The 23S secondary structure map. The colored lines represent tertiary contacts between helices in the same folding domain. From (Davis 2016). Reprinted with permission from Elsevier.

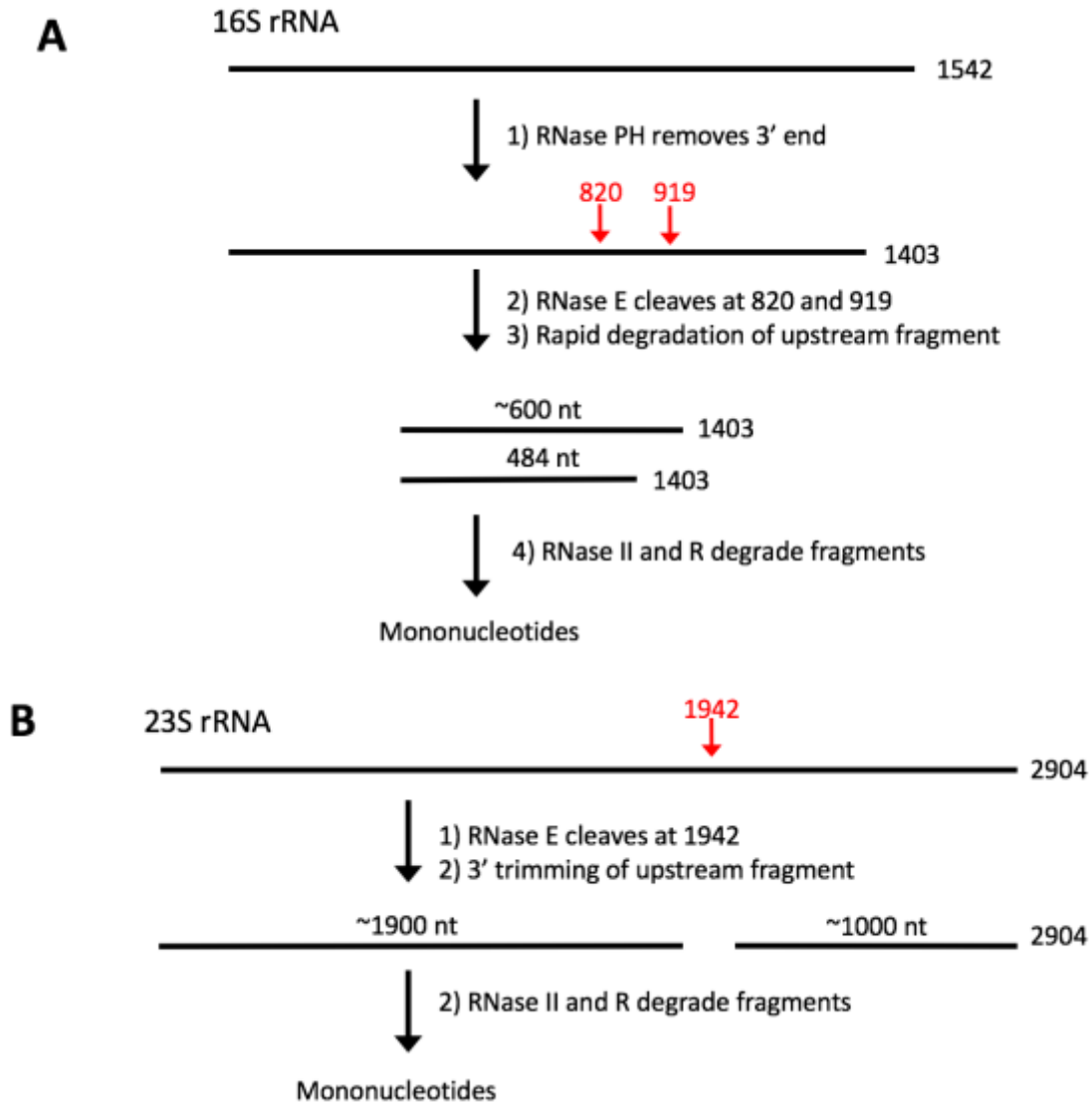

Figure 1.7. Summary of rRNA degradation pathways during carbon starvation (a) 16S rRNA. (b) 23S rRNA. Adapted from (Sulthana 2016).

CHAPTER 2: Probing the structure of ribosome assembly intermediates *in vivo* using DMS and hydroxyl radical footprinting

2.1 Introduction

Ribonucleoprotein (RNP) complexes typically undergo many structural changes during their lifecycles, from transcription of the RNA to maturation of the complex and degradation. Because the full lifecycle of an RNP cannot often be reconstituted in the test tube, footprinting methods for probing RNA structure in the cell have gained increasing attention (Kubota 2015; Mortimer 2014). In this chapter, I will present a method for probing the structure of the 16S ribosomal RNA in *Escherichia coli* cells following metabolic labeling of pre-rRNA that can be generalized for use on other intracellular RNPs.

The bacterial ribosomal subunits have long served as a model for the assembly of ribonucleoprotein complexes because they can be reconstituted *in vitro* using only free rRNA and ribosomal proteins (Held 1974; Nierhaus 1974). Despite this, ribosome biogenesis in living cells remains poorly understood. One reason for this is the low abundance of assembly intermediates, which constitute 2–5% of total rRNA in *E. coli* under normal growth conditions (Lindahl 1975). Moreover, the predominant intermediates are difficult to isolate using sucrose gradient sedimentation, because they tend to migrate near the mature subunits.

Previous studies increased the concentration of ribosomal intermediates by using temperature-sensitive strains or conditional mutations that stall assembly under non-permissive conditions such as low temperature (Culver 2003). Ideally, one should study the path of assembly in real time, under normal conditions. The kinetics of ribosome synthesis or protein binding has been measured by pulse-labeling cells with isotopically-modified nucleosides or amino acids and then analyzing via scintillation counting (Lindahl 1975) or mass spectrometry (Chen 2013). These approaches reveal the protein composition of assembly intermediates. When complemented by structure probing of the RNA, a more complete picture of the assembly process can be obtained.

During normal cell growth, the ribosomes being synthesized in the cell are in various states of assembly, giving a time-average of the different pre-rRNA intermediates. By synchronizing their transcription, it is possible to study individual assembly states. Using the effects of two small molecule effectors, it is possible to regulate the initiation of bacterial transcription. These effectors can be manipulated by altering the nutrients available to the bacteria.

In *E. coli*, rRNA transcription is repressed during starvation through both the stringent response (ppGpp) and the concentration of the initiating NTP (Murray 2003). During the late stationary phase and extended periods of starvation, the concentration of the initiating NTP becomes the primary repressor of ribosomal RNA operon (*rrn*) promoter activity (Murray 2003). When nutrients become available, there is a rapid increase in intracellular NTP concentration and pre-rRNA synthesis is reactivated (Figure 2.1). For exponential phase cells subject to a nutrient upshift and cells diluted from

stationary phase into fresh media, rrn promoter activity increases within 1 min (Murray 2003).

In order to label nascent transcripts when pre-rRNA transcription resumes, starved cells are pulse-labeled with 4-thiouridine (4sU) just before feeding (Favre 1986). After extracting the total RNA from the cells, the nascent RNA labeled with 4sU can be conjugated to a biotinylation reagent via a reversible disulfide bond (Dölken 2008). The labeled RNA is captured on streptavidin beads and analyzed by direct primer extension (as described in this chapter) or high-throughput sequencing (as described in Chapter 3). In this way, it is possible to get snapshots of the ribosome assembly process after transcription begins again.

2.2 Materials and methods

2.2.1 Cellular recovery from starvation

To prepare cultures, 3–5 mL of LB media were inoculated with a single MRE600 colony and grown overnight at 37 °C with shaking. The following day, the culture was diluted at a ratio of 1:100 to 1:1000 into 500 mL media. After the cells reached stationary phase, they were harvested by centrifugation, and resuspended in a defined minimal medium lacking phosphate (100 mM Tris-HCl, 25 mM KCl, 10 mM NaCl, 20 mM NH_4Cl, 1 mM $MgSO_4$, 0.1 mM $CaCl_2$, 2 μM thiamine, 0.4% glucose, pH 7.8). The cells were harvested and resuspended twice more to remove excess phosphate. On the final step, minimal media was added until the cells were diluted to the desired final volume (75 mL per time course, or 675 mL for 9 trials) and had an OD_{600} in the mid-log range (0.6–

0.8). The cells were incubated in minimal media at 37 °C with shaking for 4 h to arrest pre-rRNA transcription. At the end of this starvation period, and approximately 2 min before rRNA transcription was induced, a 250-mM stock solution of the modified nucleotide 4-thiouridine (4sU) was added to the media to a final concentration of 0.5 mM. This concentration of 4sU minimally affects the growth rate of MRE600 (data not shown). The stock solution of 4sU should be kept away from light. Transcription and cell growth were restarted by adding 10X rich medium to the culture (5 g tryptone, 2.5 g yeast extract, 15 g Na_2HPO_4, 8.25 g KH_2PO_4 in 50 mL). The culture was grown with shaking for the desired period before treatment with DMS or hydroxyl radical as described below.

2.2.2 Hydroxyl radical footprinting using live culture

Liquid culture irradiation was performed using a custom capillary holder and slit assembly capable of being water-cooled (Bohon 2014). The apparatus is shown in Figure 2.2. At the start of the footprinting experiment, the cell culture was transferred to a 37 °C water bath in the beamline experiment end-station enclosure (‘‘hutch”). During this transfer, two 0.75 mL fractions to serve as ‘‘No Hutch” controls were collected to determine the amount of background signal that can be attributed to sources outside the beamline enclosure. A magnetic stirrer was used to aerate and mix the culture during the footprinting experiment.

The cells were exposed to the synchrotron X-ray beam by pumping the culture through a flow cell placed in the path of the beam using an M50 pump (VICI®) at a continuous flow rate of 5 mL/min. Silica tubing ran from the pump inlet to the bottom of the culture flask, with care being taken to not aspirate air into the flow path. A second

piece of silica tubing connected the M50 pump outlet with the flow cell and fraction collector. For the flow cell, silica tubing between 0.54 and 0.7 mm internal diameter (Polymicro Technologies™, molex) was used. The X-ray beam covered the entire internal diameter of the flow cell tubing with as homogenous an intensity profile as possible to obtain uniform cleavage of intracellular RNA. The beam was focused to the smallest area (cross-section) that still covered the sample to achieve high levels of cleavage.

To induce outgrowth and pre-rRNA transcription, 10X rich medium (5 g tryptone, 2.5 g yeast extract, 15 g Na_2HPO_4, 8.25 g KH_2PO_4 in 50 mL) was added to the starved culture using a dispensing syringe pump. The syringe pump was first primed with the 10X rich medium and the outlet connected to the culture flask (Figure 2.2). The fraction collector was filled with at least 60 2-mL screw-cap microcentrifuge tubes. As the culture was pumped past the X-ray beam, fractions were collected at different time points. Each microcentrifuge tube contained 1mL RNAprotect Bacteria Reagent (Qiagen) to protect the RNA from being degraded during isolation.

The pumps, fraction collector, and beam shutter were interfaced with a computer outside the enclosure and controlled by a computer macro in LabView (Gupta 2007). The instruments were programmed to collect two 0.75 mL fractions of 4sU-containing culture before opening the beam shutter ("Pre-Food, No Dose"). Next, the shutter was opened, and two fractions in which the starving cells were exposed to the X-ray beam ("Pre-Food") were collected as controls for the RNA cleavage pattern in the starved cells. After these control samples were collected, the M50 pump and fraction collector were stopped, and the beam shutter closed. During this time, food was added to the culture flask using

the syringe pump, and mixed for 10 s to induce pre-rRNA synthesis. After inducer was added, the shutter was opened, the pump and fraction collector were restarted, and 52 0.75-mL fractions were collected at 5 mL/min (9 s per fraction).

At the end of the run, two 0.75 mL samples were collected from the culture flask ("Post-Food, No Dose") to test for stray radiation in the experiment end-station enclosure. After the run, the tubes were capped and inverted to mix the culture with the RNAprotect. Tubes were placed in a microcentrifuge to pellet the cells. After decanting the supernatant, the cell pellets were immediately placed on dry ice, and stored at -80 °C as promptly as possible to reduce background RNA degradation.

2.2.3 Footprinting rRNA in live culture using DMS

To probe the rRNA secondary structure with dimethyl sulfate (DMS), the *in vivo* DMS probing and quenching conditions of Wells et al. (Wells 2000) were adapted.

For each sample treated with DMS, the desired amount of DMS diluted 1:2 (v/v) in 95% ethanol was placed in a 50-mL screwcap conical tube. Because DMS is toxic and mutagenic, tubes were placed in a chemical fumehood. Eye shields and protective gloves and clothing should be worn. Inhalation and contact with the skin should be avoided. Ethanol interferes with phospholipid bilayers, so the amount of DMS and ethanol added to samples should be as low as possible while still giving sufficient probing. The ratio of DMS-ethanol solution to culture medium was typically 1:25 (v/v) in these experiments.

At the desired times, an aliquot (*e.g.* 20 mL) was removed from the main culture and added to one of the DMS-containing 50 mL tubes. After 30 s, the methylation reaction was quenched by the addition of a 1/2 vol (*e.g.* 10 mL) of ice-cold 0.6 M β-

mercaptoethanol and a 1/2 vol of water-saturated isoamyl alcohol (Wells 2000). For each time point, a sample to which DMS was not added was also collected to correct for any background changes in the RNA.

After DMS treatment, cells in each sample were pelleted by centrifugation and resuspended in one culture volume (e.g. 20 mL) 0.6 M β-mercaptoethanol (Wells 2000). Cells were harvested again and the supernatant decanted. At this point, RNA can be extracted from the cells, or the cell pellets can be stored at -80 °C until ready to extract the RNA.

2.2.4 Isolation of 4sU-labeled rRNA from *E. coli*

RNeasy spin columns (Qiagen) were used to extract total RNA from treated bacterial cell pellets. To isolate nascent 4sU-labeled RNA, 4sU was first biotinylated and then captured on streptavidin beads (Figure 2.3). The purification protocol that follows is based on that of Dölken et al. (Dölken 2008) with slight modifications to the buffers and the incubation durations.

The 4sU-labeled RNA was modified using EZ-Link HPDP-Biotin (Pierce), freshly dissolved in dimethylformamide to a concentration of 2.2 mg/mL. The RNA was diluted to 100 ng/μL in 10 mM Tris-HCl pH 7.6, 1 mM EDTA, and the HPDP-Biotin reagent was added to a final concentration of 0.4 mg/mL, for 10 min at 65 °C.

Unbound biotin was removed by extracting the biotinylation reaction with an equal volume of chloroform/isoamyl alcohol (39:1). The upper aqueous layer was collected using Phase Lock Gel (Heavy) tubes (Eppendorf). The RNA (200–300 μL) was precipitated by adding 1/10 volume 3M sodium acetate (pH 5.5) and 3 volumes 100%

ethanol. The RNA was precipitated by incubating 1 h at -80 °C and pelleted by centrifugation at 13,000 × g at 4 °C for 30 min. The pellet was washed with 1 volume 75% ethanol, centrifuged again for 10 min, and dried under vacuum. The pellet was resuspended in 100 μL binding buffer (20 mM Tris-HCl pH 7.6, 1 mM EDTA, 0.5 M NaCl) before determining the RNA concentration (Nanodrop UV spectrometer).

The resuspended biotinylated RNA (50–150 μg) was added to 100–150 μL magnetic streptavidin beads (NEB) for 1 h at 4 °C with gentle shaking. Before adding the RNA, the beads were washed three times with binding buffer, blocked with 40 ng/mL glycogen in binding buffer, then washed once more with binding buffer. After the supernatant-containing unlabeled RNA was removed, the beads were washed three times with 1 volume wash buffer (100 mM Tris-HCl pH 7.6, 10 mM EDTA, 0.5 M NaCl, 0.5% Tween20) at 65 °C and three more times with wash buffer at room temperature.

The labeled RNA was eluted from the beads using 1 vol freshly prepared 100 mM dithiothreitol (DTT). This elution step was repeated, and the eluates combined. The RNA was precipitated from the eluate using 1/10 volume 3 M sodium acetate, 3 volumes 100% ethanol, and 40 ng/mL glycogen as a carrier. The RNA pellet was collected and washed as described above. The RNA was resuspended in 25 μL RNase-free water and the concentration determined by UV absorption.

2.2.5 Primer extension analysis of 4sU-labeled RNA

Primer extensions were performed using radiolabeled primers. 0.5–1 μg 4sU-labeled RNA was combined with 1 pmol ^{32}P-labeled primer. The reactions were heated to 65 °C for 5 min and placed on ice for at least 1 min. First Strand Buffer (Invitrogen), 1

mM dNTPs (final), and 5 mM dithiothreitol (final) was added to the samples. Primers were extended using 50 U SuperScript III reverse transcriptase (Invitrogen) at 60 °C for 30 min. Samples were separated on a 6% polyacrylamide gel at 55 W for 2-4 h. Phosphorimager screens were exposed to the gels. The band intensities in the gel were analyzed using ImageQuant (Molecular Dynamics) or the Semi-Automated Footprinting Analysis (SAFA) software package (Das 2005). To quantify the proportion of 16S and 17S rRNA, primer 161 was used (Table A.1). To determine locations of probed residues, primers 46, 161, 323, 540, 812, 1046, 1257, or 1486 were used.

2.3 Results

2.3.1 Bacterial transcription can be halted and restarted

To study the *in vivo* assembly of ribosomes, I chose to synchronize the start of rRNA transcription as a means of temporally isolating intermediates at different stages of maturity. In an effort to achieve this synchronization, changes were made to the cellular growth media to manipulate the regulation of rRNA transcription. Cells were shifted from LB to a minimal medium lacking phosphate. After various incubation periods, cells were fed with rich media high in phosphate. As illustrated in Figure 2.4, the intracellular concentration of 17S pre-rRNA in *E. coli* MRE600 cells suspended in a minimal medium lacking phosphate decreased as incubation continued. Upon addition of a rich medium containing phosphate, 17S pre-rRNA was detected within 1–2 min, consistent with the kinetics of pre-rRNA synthesis during recovery from stationary phase (Murray 2003).

When the modified nucleotide 4-thiouridine (4sU) was added to the medium before the food, 4sU-labeled pre-rRNA was recovered with similar kinetics.

2.3.2 Nascent RNA can be isolated using 4sU-labeling

With the start of transcription synchronized in MRE600 by phosphate starvation and feeding, it was necessary to be able to isolate the newly transcribed ribosome assembly intermediates for downstream analysis. To label nascent RNA, 4sU was added to the media 2 min before outgrowth was induced with rich medium. Samples were collected over the first 10 min of outgrowth to follow the course of RNA synthesis. The total RNA from treated bacterial cell pellets was extracted using RNeasy spin columns (Qiagen). Nascent 4sU-labeled RNA was biotinylated and captured on streptavidin beads (Figure 2.3). The RNA was analyzed by extending a ^{32}P-labeled primer on RNA recovered from the wash and elution fractions. The nascent pre-rRNA was found primarily found in the eluted fraction (Figure 2.5). The nascent rRNA constituted approximately 1% of the total RNA, as evaluated by band intensity and the A_{260} of the RNA pulldown fractions.

2.3.3 An X-ray dose resulting in single-hit kinetics can be determined

The structures of ribosome assembly intermediates were probed using hydroxyl radical footprinting. This probing method was ultimately unable to provide an appropriate yield of nascent rRNA in the short time necessary for ribosome assembly, but was otherwise optimized for the purpose of studying ribosome assembly *in vivo*.

For reliable analysis of the hydroxyl radical cleavage pattern by primer extension, the RNA should be cleaved no more than once within each detection window (Hsieh 1996). If an RNA strand is cleaved multiple times, those events nearer to the location of priming will be preferentially detected over events further from the site of priming. Thus, for analysis by traditional gene-specific priming, the X-ray dose should be adjusted such that 70–90% of the RNA is full-length. Assuming the cleavage events follow a Poisson distribution, if 80% of the RNA is uncleaved, ~19% will be cleaved once, and the remaining ~1% will be cleaved twice. If high-throughput sequencing is used to analyze the footprinting pattern, the RNA is typically fragmented to ~200 nucleotides before library construction (Talkish 2014). In this instance, a much higher X-ray dose, sufficient to cleave the RNA once per 200 nucleotides, is needed to ensure good signal-to-noise.

To determine the correct X-ray exposure, a dose-response curve was generated by placing aluminum sheets of different thickness in front of the flow cell to attenuate the beam intensity incident on the sample. Alternatively, the X-ray dose can be varied by changing the sample flow rate, which alters the time needed for the sample to traverse the beam. After exposing the cells to the X-ray beam, the amount of full-length 16S RNA remaining in each sample was determined by isolating total RNA, and extending a radiolabeled primer complementary to nucleotides 1486–1510 at the 3'-end of the 16S rRNA. The percent full-length cDNA (normalized to an unexposed sample) was plotted versus the aluminum thickness, and fit to a line (Figure 2.6). This dose-response plot was used to empirically determine the appropriate beam attenuation needed to obtain the desired level of cleavage (Figure 2.6).

2.3.4 16S rRNA helices 27 and 33 show prominent exposure during assembly

DMS probing was used to generate structural data on *in vivo* ribosome assembly intermediates. A 220-mL culture of phosphate-starved cells was pulse-labeled with 4sU to a final concentration of 0.5 mM and probed with DMS at time points before and during outgrowth. A total of 14 15-mL time points and controls were collected. Samples were treated with DMS immediately before the food was added to start outgrowth, and then over the first 8 min after feeding. 'No DMS' controls were collected immediately before feeding, and at 4 min and 8 min after feeding. The 4sU RNA was isolated as described above, and the methylation patterns were analyzed by traditional primer extension sequencing, using primers complementary to the 16S rRNA (Figure 2.7a). Band intensities were analyzed using SAFA (Figure 2.7b).

The initial results using this technique are consistent with earlier findings regarding the folding of the central platform and 3' domain of the 30S ribosome (Figure 2.7c). For example, nucleotides 890–920 in the central domain are strongly exposed to methylation in the newly transcribed 4sU-labeled pre-rRNA. Nucleotides 885–912 form helix 27, which supports the decoding site helix 44. Nucleotides 917–919 form part of the central pseudoknot, a structure that draws together the 5', central, and 3' domains and that is known to form late in 30S assembly (Holmes 2005). Also prominently exposed in the 17S pre-rRNA is helix 33, which forms the ''beak" of the 30S ribosome and is known to fold late in assembly (Holmes 2005). More surprisingly, certain nucleotides in the 5' domain also take about 6 min to become fully protected, although this region is the first domain to be transcribed. Thus, this method can pinpoint RNA interactions that form late

during assembly of the 30S ribosomal subunit, or that lie on the interface with 50S subunits.

In this experiment, many residues became more strongly modified as assembly continued. This is somewhat paradoxical because modification patterns should approach those present in exponential phase cells as assembly continues. This finding actually reflects the fact that 4sU-labeled RNA is synthesized throughout the experiment. Over time, the isolated RNA will represent an increasingly heterogeneous mixture of assembly intermediates. Further, any slow-folding intermediates will begin to dominate the pre-rRNA pool.

2.4 Discussion

This method of isolating nascent RNA over time, combined with the *in vivo* RNA probing techniques of hydroxyl radical and DMS footprinting, has the potential to allow the kinetics of structural changes in rRNA during ribosome biogenesis to be determined. This is a novel way of examining ribosome assembly intermediates that does not require the use of temperature-sensitive cells strains or conditional mutants. The time resolution currently attainable with these probing methods is appropriate for the study of ribosome biogenesis, and may be improved in the future. This technique has the potential to heighten our understanding of ribosome biogenesis in ways that would not be possible by *in vitro* studies. For example, this method would be very conducive to studies of ribosome assembly factors *in vivo*. By using cell strains lacking ribosome assembly factors, it should be possible to use this technique to determine not just where these

proteins interact with the assembling ribosome, but when they interact as well. This method can also be adapted to map time-dependent conformational changes in a wide range of stable, non-coding RNAs.

The use of hydroxyl radical footprinting was not able to generate a sufficient amount of probed rRNA for analysis. Only a small amount of culture can be flowed past a synchrotron X-ray beam in the time that ribosome assembly takes place. If improvements are made, either to allow higher flow rates or to extend the time of ribosome assembly, the technique could provide sufficient yield for RNA structural analysis.

The degree of DMS structure probing would be expected to decrease over the course of assembly as rRNA becomes more structured. The results here do not reflect this because, after the 4sU pulse, all nascent rRNA synthesized during outgrowth are isolated and structural heterogeneity increases over time. To ameliorate this effect, the 4sU pulse is chased with an excess of unlabeled uridine in subsequent experiments. This pulse-chase protocol allows the products from a shorter transcription window to be analyzed. Based on the level of heterogeneity present, this step will be necessary to isolate individual intermediates.

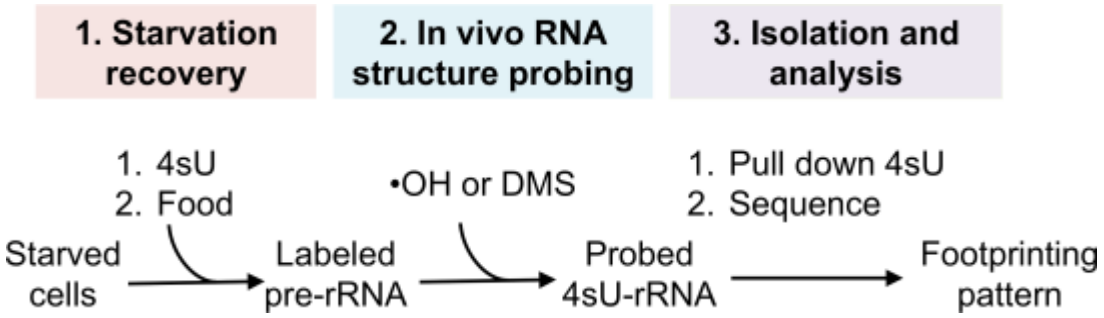

Figure 2.1. Overview of time-resolved *in vivo* footprinting protocol The method consists of three major parts: (1) starvation recovery, (2) in vivo RNA footprinting, and (3) isolation and analysis of the RNA. In the first phase, pre-rRNA transcription is synchronized by starving cells of phosphate, then adding nutrients and phosphate to trigger de novo ribosome biogenesis. The modified nucleotide 4-thiouridine (4sU) is added to the media prior to food. During the recovery from starvation, 4sU-labeled nascent rRNA is probed with hydroxyl radical or DMS in the second phase. In the third phase, the 4sU-labeled RNA is isolated from harvested cells and sequenced.

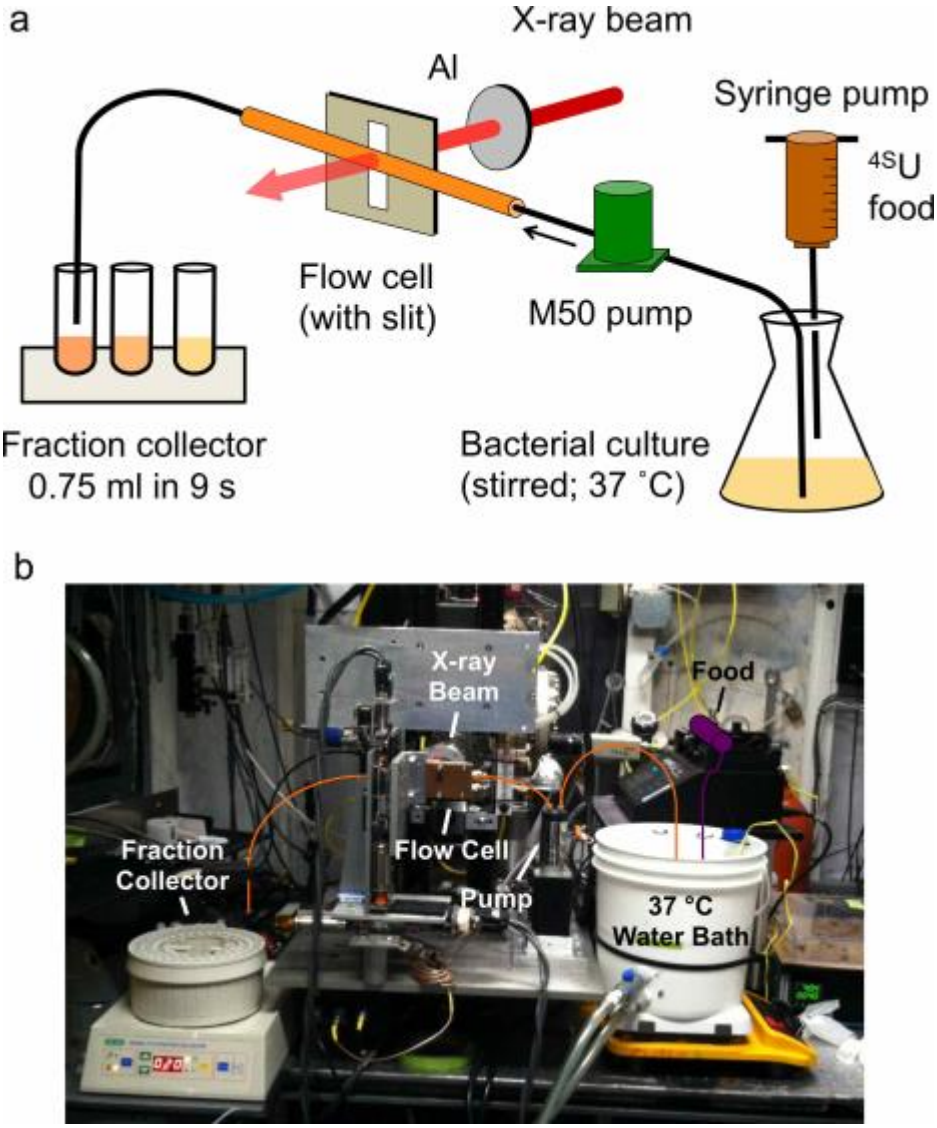

Figure 2.2. Apparatus for X-ray footprinting of live cultures (a) Schematic showing the flow of liquid culture past the X-ray beam and into a fraction collector. A syringe pump (Harvard Apparatus, PHD2000) is used to dispense nutrients into the culture at the desired time. A M50 pump (VICI®) displaces culture through a capillary flow cell in the path of the X-ray beam (Bohon 2014), at flow rates up to 5 mL/min. The X-ray dose depends on the flow rate, the length of tubing exposed to the beam (horizontal slit), and the X-ray flux density of the beam itself. The exposed culture is collected in 0.75–1 mL fractions. (b) Photograph of apparatus at NSLS X28C. The X-ray beam pipe is pointing toward the front of the image.

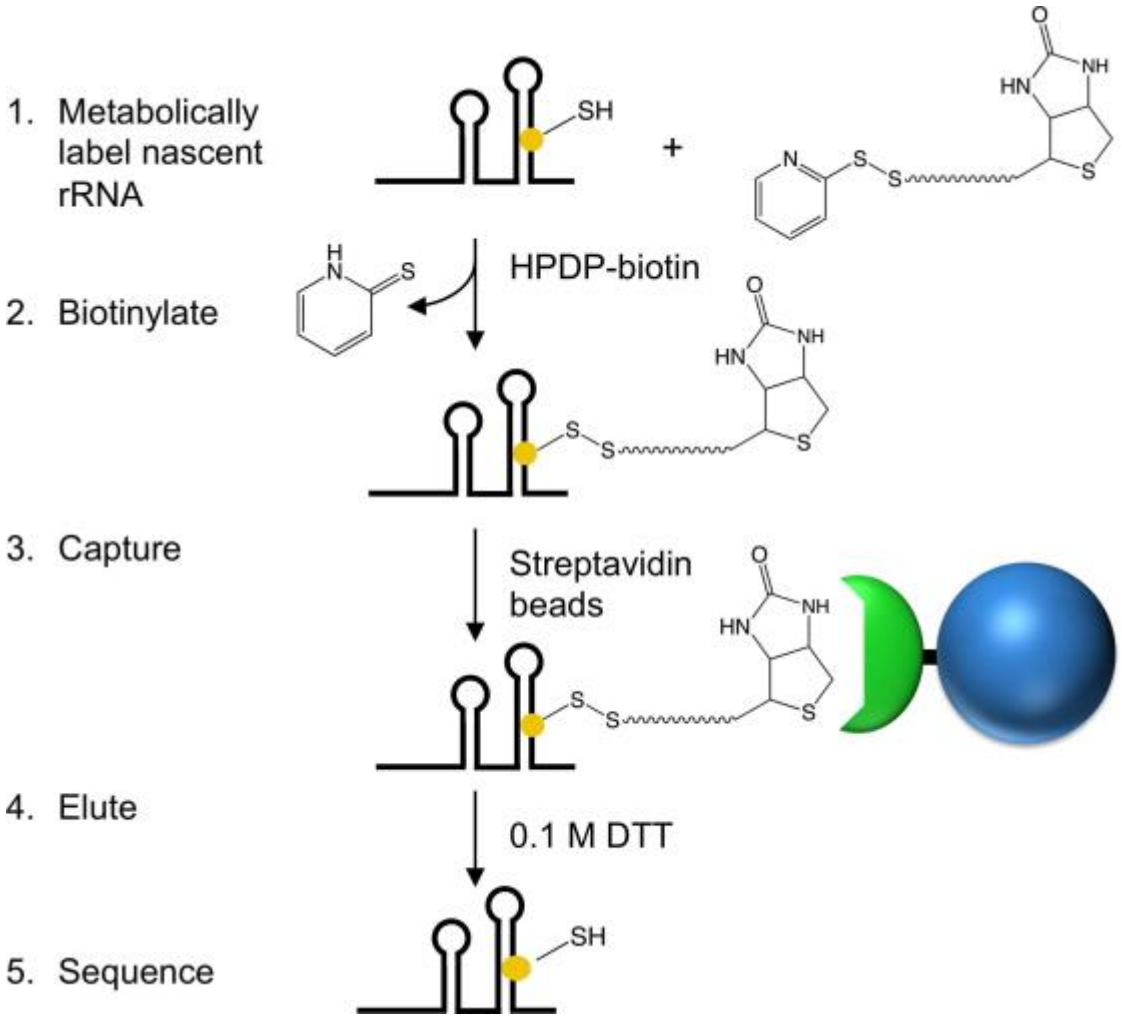

Figure 2.3. Scheme for isolation of 4sU-containing RNA Newly transcribed RNA is metabolically labeled with 4-thiouridine added to the medium just before outgrowth. 4sU is covalently modified with bifunctional HPDP-Biotin, which reacts with reduced thiols. The biotinylated RNA is captured on streptavidin beads, and then eluted with 0.1 M DTT. The purified RNA is analyzed by traditional or high- throughput sequencing.

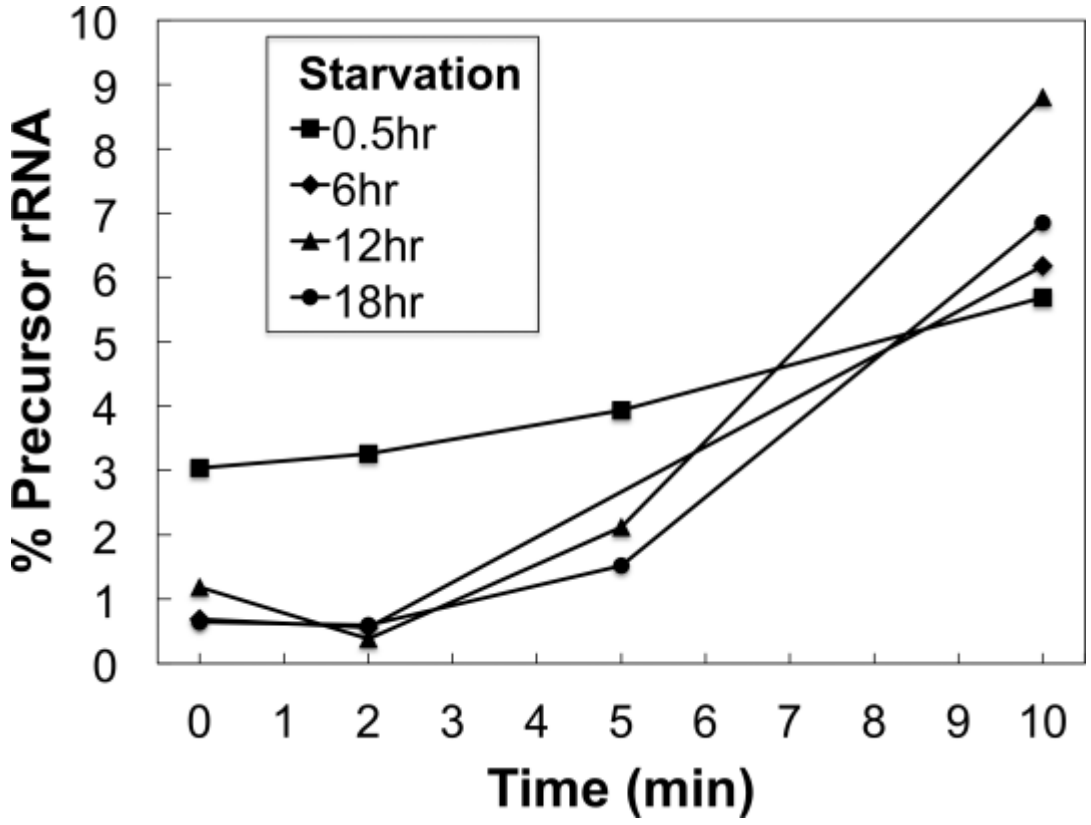

Figure 2.4. Pre-ribosomal RNA synthesis during starvation recovery Percent 17S pre- rRNA versus time after nutrients were added to MRE600 culture grown in minimal (low phosphate) medium for 0.5, 6, 12, or 18 h before feeding. The pre-existing pre-rRNA is usually depleted within 60–90min after transfer to low phosphate medium. In this example, pre-rRNA remains after 30 min, comprising 3% of the total rRNA. During exponential phase, the pre-rRNA makes up 2-5% of the total rRNA. The fraction of 17S rRNA was determined for each sample by primer extension, and calculated from f = cpm [17S]/(cpm [16S] + cpm [17S]).

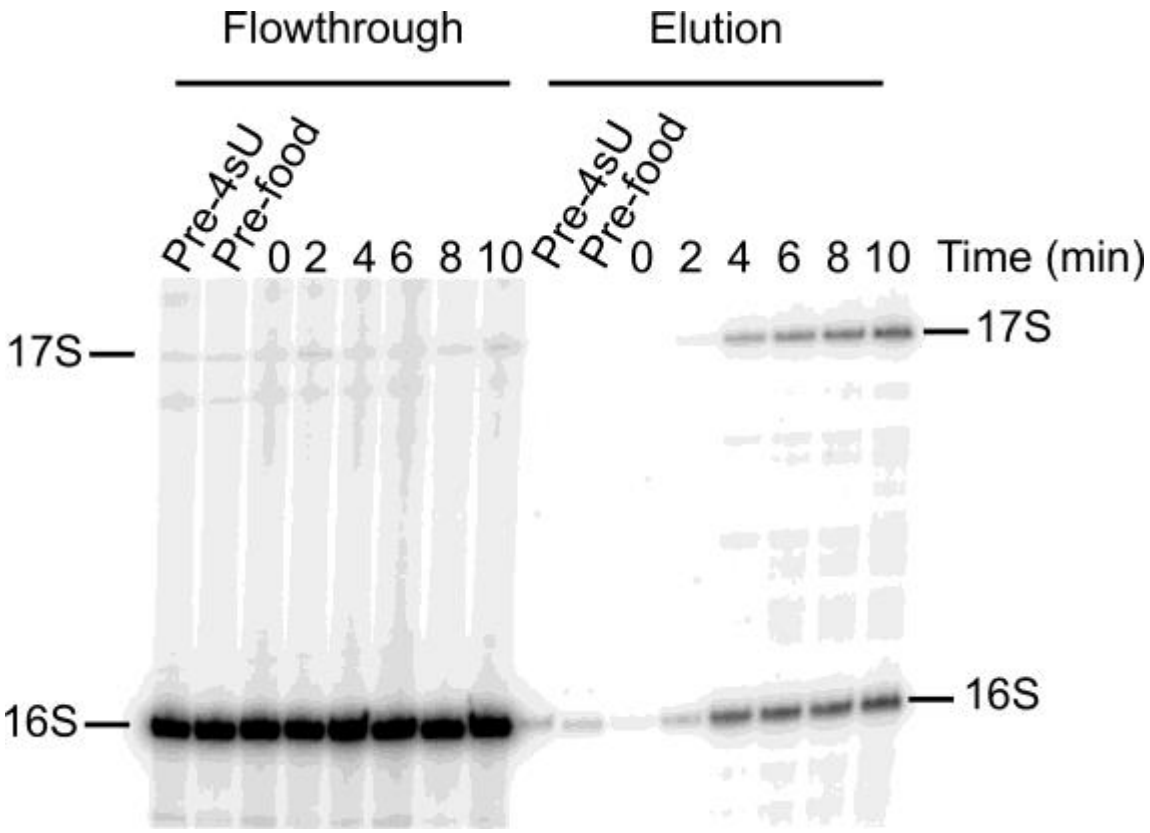

Figure 2.5. Analysis of 4sU-RNA purification 6% sequencing gel (1X TBE) showing the primer extension of RNA from elution and flow-through fractions of 4sU affinity purification (10 μg input RNA) as outlined in Figure 2.5. The unlabeled rRNA will be in the flow-through fractions. The pre-rRNA should be almost exclusively in the elution fractions. Based on the intensities of the 17S bands, 80-90% of the nascent rRNA is in the elution fraction. The primer used for probing the 5' end of the 17S anneals to nucleotides 162–178 of the 16S rRNA (Primer 161 in Table A.1).

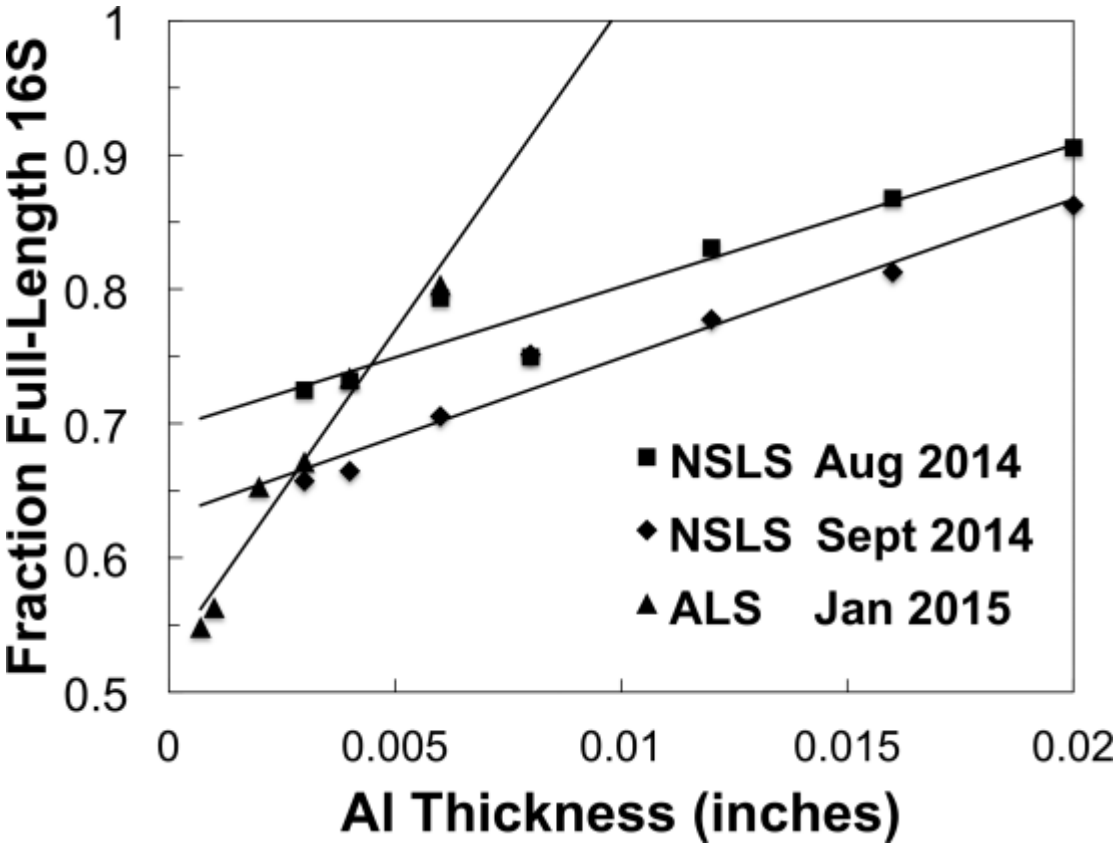

Figure 2.6. X-ray dose-response curves for RNA footprinting Full-length 16S rRNA remaining after exposure of log-phase MRE600 culture to an X-ray beam, using the flow apparatus described in Figure 2.3. The flow rate was 5 mL/min. The capillary tubing was 700 μm ID. The fraction full-length RNA was determined by primer extension and normalized to the amount of RNA in unirradiated controls. The X-ray dose was varied by attenuating the beam with aluminum sheets of varying thickness. The curves represent experiments performed on different dates at NSLS X28C (BNL) and ALS 5.3.1.

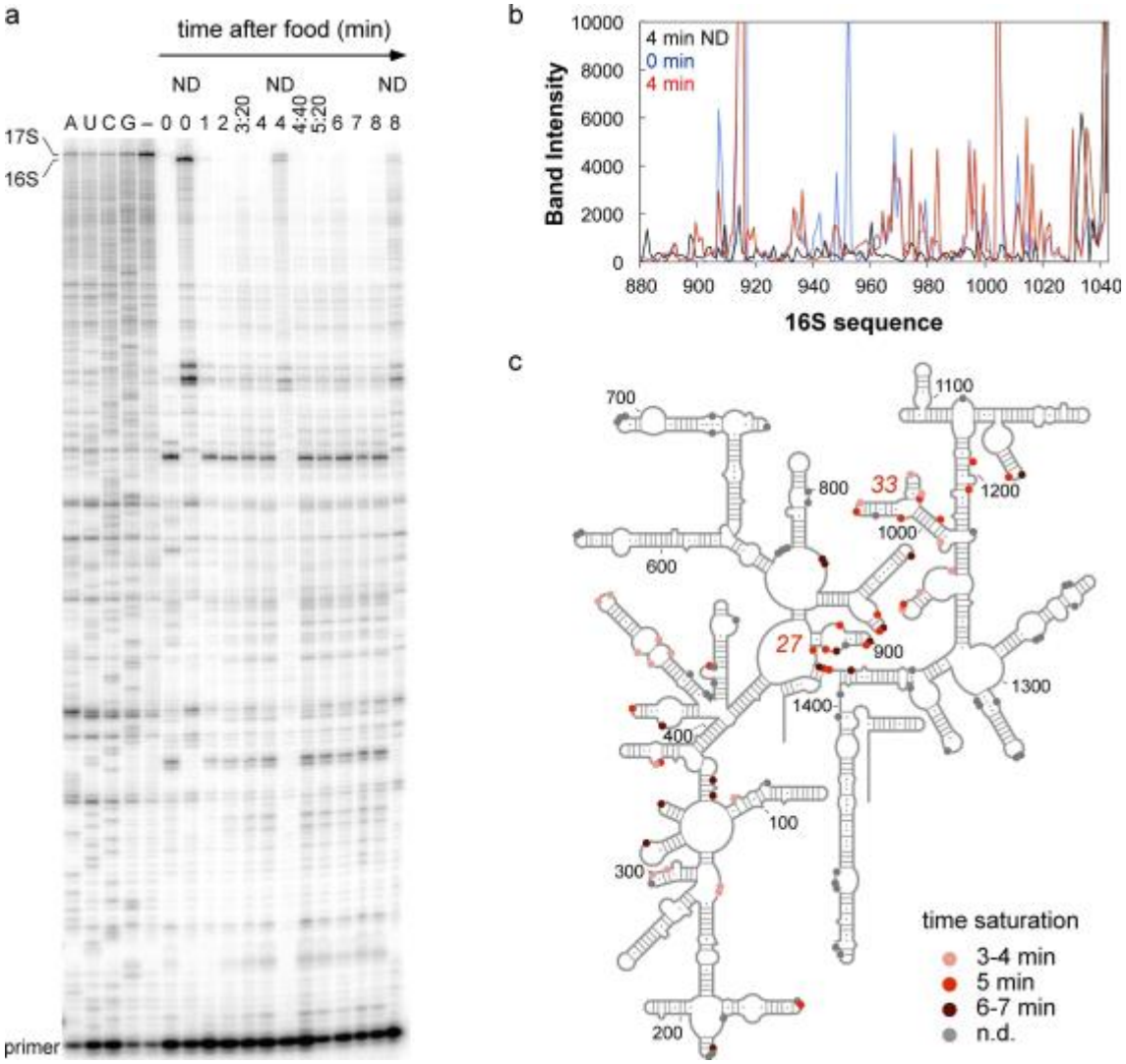

Figure 2.7. Time-resolved DMS footprinting of rRNA in E. coli (a) 6% sequencing gel (1X TBE) showing the change in the primer extension pattern from 0 to 8 min after the addition of food. Lanes ND indicate samples with no DMS. Sequencing standards are on the left. Examples of residues that become protected from DMS methylation with different kinetics are denoted as in (c). (b) Example of integrated band intensities for each nucleotide, for 16S nucleotides 880–1042. Black, no DMS treatment (4 min); blue, DMS treatment before feeding; red, DMS treatment 4 min after feeding. (c) Secondary structure and 3D ribbon (2i2p) of the E. coli 16S rRNA showing the folding kinetics for individual residues as the time to reach saturation (pink, red, brown); n.d. (gold), change in methylation but rate not determined.

CHAPTER 3: Kinetics of ribosome biogenesis and characterization of *in vivo* ribosome assembly intermediates

3.1 Introduction

Ribosome biogenesis *in vivo* is a complex process in which rRNA transcription, folding, and modification take place concurrently with the binding of ribosomal proteins. The co-transcriptional nature of *in vivo* assembly (Lewicki 1993; Powers 1993; Spillmann 1977), along with trans-acting assembly factors present in the cell, likely distinguishes *in vivo* assembly from the *in vitro* assembly pathway. For this reason, to properly understand ribosome assembly, it should be studied *in vivo*. The study of *in vivo* ribosome biogenesis has historically been difficult due to the fact that ribosome assembly intermediates are scarce (Lindahl 1975), heterogeneous, and difficult to isolate. To enrich the intracellular pool of ribosome assembly intermediates, protein deletion strains (Clatterbuck Soper 2013; Davis 2016) and chemical inhibitors (Sykes 2010) have been utilized. The isolation of assembly intermediates has also been improved by purification using affinity tags (Clatterbuck Soper 2013; Gupta 2014) and sucrose gradient sedimentation velocity (Chen 2013; Davis 2016; Sashital 2014; Sykes 2010). These techniques for enriching and isolating the ribosome assembly intermediates have been used to separate assembly intermediates into fairly homogeneous populations, and have been combined with techniques such as electron microscopy, quantitative mass spectrometry, and hydroxyl radical and chemical probing.

By using *in vivo* 4sU RNA labeling and DMS probing techniques (Figure 3.1), it should be possible to observe ribosome intermediates in the cell throughout the course of

assembly. This will result in a kinetic separation of the heterogeneous intermediates, where highly immature intermediates should be present during early time points and increasingly mature intermediates will appear as assembly progresses.

By combining this technique with high-throughput sequencing, the need for gene specific priming is eliminated. Such analysis will also provide secondary structure information on regions of the ribosomal subunit pre-cursors that are not present in the final structure. The use of high-throughput sequencing also allows the cDNA to be prepared by more robust methods. *In vivo* chemical modifications of RNA have historically been studied by observing reverse transcription truncation products, where the reverse transcriptase would terminate cDNA synthesis at the site of nucleotide modification (Inoue 1985). In cDNA truncation-based analysis, only one chemical modification site is observed per RNA molecule. Any distal modifications are not seen. For this reason, when using a truncation-based approach, it is necessary to probe the RNA at a rate low enough that there will be at most one modification per RNA. This results in ~80% of the RNA not being probed and only ~20% being modified. Because only one-fifth of the RNA is being probed, greater volumes are required, which can be prohibitive when studying RNA found in small quantities.

The work here uses a thermostable Group II intron reverse transcriptase (TGIRT), which encodes DMS modifications as cDNA mismatches (Figure 3.2) (Katibah 2014; Mohr 2013). The TGIRT does not terminate at modification sites, allowing for a higher degree of probing without introducing bias into the cDNA pool (Zubradt 2016). The function of the TGIRT enzyme has been optimized to detect DMS modifications while still maintaining high fidelity and processivity. The enzyme was adapted to produce

cDNA mismatches at endogenous m^1A and m^3C residues in tRNA (Katibah 2014; Mohr 2013). These are the same methylations associated with DMS. Using the probing techniques presented here, it is possible to study the structure of the ribosome in its native *in vivo* state and its structural changes during assembly.

3.2 Materials and methods

3.2.1 Cell growth for exponential phase and starvation recovery experiments.

3–5 mL of LB media were inoculated with a single MRE600 colony and grown overnight at 37 °C with shaking. The following day, the culture was diluted at a ratio of 1:100 to 1:1000 into the desired volume of media, which was typically around 1000 mL.

For experiments in exponential phase cells, cells were grown in LB to mid- to late-exponential phase (OD_{600} = 0.5 – 0.7). For starvation recovery experiments, MRE600 cultures were grown to late-exponential phase / early stationary phase (OD_{600} = 1 – 1.5). The cells were harvested by centrifugation and resuspended in a minimal medium lacking phosphate (100 mM Tris-HCl, 25 mM KCl, 10 mM NaCl, 20 mM NH_4Cl, 1 mM $MgSO_4$, 0.1 mM $CaCl_2$, 2 μM thiamine, 0.4% glucose, pH 7.8). The cells were harvested and resuspended twice more to remove excess phosphate. On the final step, minimal media was added until the cells were diluted to the desired final volume with an OD_{600} in the mid- to late-log range (0.5–0.7). The cells were incubated in minimal media at 37 °C with shaking for 4 h.

3.2.2 Analytical sucrose gradient preparation and fractionation

Analytical sucrose gradient preparations were based on the Spedding method (Spedding 1990). MRE600 cultures were grown to mid-exponential phase (OD_{600} ~ 0.5). Aliquots of 3-5 mL culture were chilled on ice in 14 mL Falcon tubes. These aliquots were centrifuged for 15 min at 5000 x *g* to pellet the cells. Pellets were resuspended in 500 µL cold buffer (10 mM Tris-HCl pH 7.5, 20 mM $MgCl_2$, 200 mM NH_4Cl, 3 mM β-mercaptoethanol). Pellets were then resuspended in 300 µL cold buffer (1 mg/mL lysozyme in 10 mM Tris-HCl pH 7.8, 15 mM $MgCl_2$), frozen in an ethanol-dry ice bath, and thawed at room temperature. The cell lysate was centrifuged 15 min at 5000 x *g*. The clarified lysate was loaded onto a 10 – 40% analytical sucrose gradient and centrifuged in an SW-41 swinging bucket rotor (Beckman Coulter) at 35,000 rpm (210,000 x *g*) for 4.5 h. Gradients were fractionated using a BioComp piston fractionator. UV absorbance traces at 254 nm were recorded using WINDAQ software (DataQ). The 10 – 40% sucrose gradients (sucrose in 20 mM Tris-HCl pH 7.8, 10 mM $MgCl_2$, 100 mM NH_4Cl, 2 mM DTT) were prepared using the BioComp Gradient Master.

3.2.3 *In vivo* labeling of rRNA using ^{3}H-uridine

For exponential phase cells, MRE600 cells were grown in LB to mid-exponential phase (OD_{600} ~ 0.5), typically at a volume of 300-500 mL. A 1/100 volume [^{3}H-5]-uridine was added to the media. The culture was grown with shaking for the desired period before preparing the cells as described in Section 3.2.2.

For cells recovering from phosphate starvation, a 1/100 volume [^{3}H-5]-uridine was added to the media at the end of this starvation period, approximately 2 min before

rRNA transcription was induced. Transcription and cell growth were restarted by adding 10X rich medium (5 g tryptone, 2.5 g yeast extract, 15 g Na_2HPO_4, 8.25 g KH_2PO_4 in 50 mL) to the culture. The culture was grown with shaking for the desired period before preparing the cells as described in Section 3.2.2.

3.2.4 Metabolic labeling of rRNA using 4-thiouridine

For cells recovering from phosphate starvation, a 250 mM stock solution of the modified nucleotide 4-thiouridine (4sU) was added to the media to a final concentration of 0.25 mM at the end of the phosphate starvation period, approximately 2 min before rRNA transcription was induced. Transcription and cell growth were restarted by adding 10X rich medium (5 g tryptone, 2.5 g yeast extract, 15 g Na_2HPO_4, 8.25 g KH_2PO_4 in 50 mL) to the culture. After 60 s of cellular outgrowth, uridine was added to the culture to a final concentration of 5 mM (a 20-fold excess over 4sU). The culture was grown with shaking for the desired period before treatment with DMS.

Exponential phase cells were also used for labeling of nascent RNA. MRE600 cells were grown in LB to mid-exponential phase (OD_{600} ~ 0.5). To label nascent RNA, a 250 mM stock solution of 4sU was added to a final concentration of 0.5 mM. After 1 min of labeling, a 50 mg/mL stock solution of rifampicin diluted in DMSO was added to the culture to a final concentration of 200 μg/mL. The culture was grown with shaking for the desired period before treatment with DMS.

3.2.5 Preparation of cDNA libraries from nascent rRNA

The protocol used here is based on the DMS-MaPseq method (Zubradt 2016). The RNA was modified *in vivo* with DMS as described in Section 2.2.3. RNA was extracted using RNeasy Spin Columns (Qiagen). For each sample, 4 µg RNA in 10 mM Tris-HCl pH 7.0 was denatured by incubating 2 min at 95 °C and transferred to ice. 100 mM $ZnCl_2$ was added to the RNA to a final reaction concentration of 10 mM $ZnCl_2$ and mixed well. The final reaction volume was 60 µL. The RNA was fragmented at 95 °C for 2 min and moved to ice. The Zn^{2+} in the fragmentation reaction was quenched by the addition of 60 µL 40 mM EDTA. The fragmentation reaction was added to 380 µL H_2O, 44 µL 3 M sodium acetate (NaOAc), 1 µL GlycoBlue, 500 µL 100% isopropanol and incubated on dry ice for 15 min to precipitate the RNA. Samples were centrifuged 30 min at 4 °C at 20,000 x *g*. Pellets were washed with 75% ethanol and air dried. The pellets were resuspended in 6.5 µL H_2O and 1 µL 10X polynucleotide kinase (PNK) buffer (New England Biolabs).

To dephosphorylate the 3' ends of the RNA fragments in preparation for linker ligation, 2 µL PNK enzyme (New England Biolabs) was added to the 7.5 µL RNA. The 3' ends of the fragments were dephosphorylated by incubating 1 h at 37 °C. The PNK enzyme was then inactivated by incubating 20 min at 65 °C.

For linker ligation, 6 µL 50% PEG8000, 0.2 µL 50 µM Linker-2, 2 µL 10X T4 RNA Ligase buffer, 0.2 µL 100 mM DTT, 1.1 µL water, and 1 µL T4 RNA Ligase 2, truncated were pre-mixed. The heat-inactivated PNK reaction was added to this, mixed well, and incubated at 30 °C for 2 h. The T4 RNA Ligase was inactivated by heating 20 min at 65 °C. The reaction was added to 160 µL H_2O, 18 µL 3 M NaOAc, 1.5 µL

GlycoBlue, and 200 μL 100% isopropanol, mixed well, and incubated on dry ice for 15 min to precipitate RNA. Samples were centrifuged 30 min at 4 °C at 20,000 x *g*. Pellets were washed with 75% ethanol and air dried. Pellets were resuspended in 10 μL 10 mM Tris-HCl pH 7.0.

To produce cDNA from the ligated RNA, 5 μL of the RNA from the above reaction was combined with 2 μL First Strand Synthesis buffer, 0.5 μL dNTPs (10 mM each), 0.5 μL 0.1 M DTT, 0.5 μL 2 μM Linker2 RT Primer, and 0.5 μL TGIRT-III enzyme (InGex), mixed well, and incubated for 90 min at 60 °C.

To degrade the original RNA, 1 μL 5 N NaOH was added to the reaction and incubated at 95 °C for 3 min. 10 μL 2X TBE-urea loading dye was added to the reaction and all of the RNA-dye was loaded onto a 0.5-mm thick 6% TBE-urea minigel. Samples were run for 30-40 min at 200 V. The gel was stained with 1X SYBR Gold (Thermo-Fisher) and visualized on a Typhoon 9410 Molecular Imager (GE Healthcare). The region of the gel containing cDNA fragments 80-200 nt longer than the RT oligomer was excised.

To extract the cDNA from the gel slice, several holes were poked in the bottom of a 0.5 mL Eppendorf tube with a 20-gauge needle and the tube was nested in an uncapped 2 mL screw-cap tube. The cut gel piece was placed in the smaller tube and the nested tubes were centrifuged for 3 min at 20,000 x *g*. Any remaining gel pieces from the 0.5 mL tube were transferred to the 2 mL tube and the smaller tube discarded. 300 μL H_2O was added to the larger tube and incubated at 70 °C for 15 min. The gel slurry was transferred to a Costar Spin-X column using a 1000 μL pipet tip with the end trimmed using a sterile razor blade. The column was centrifuged for 3 min at 20,000 x *g* and the

flowthrough transferred to a 1.5 mL Eppendorf tube. 33 μL NaOAc pH 5.5, 500 μL isopropanol, and 2 μL GlycoBlue were added to the flowthrough and incubated on dry ice for 15 min to precipitate RNA. Samples were centrifuged 30 min at 4 °C at 20,000 x *g*. The pellets were washed with 75% EtOH and air dried. The pellets were resuspended in 15 μL 10 mM Tris-HCl pH 8.0.

The cDNA was circularized using the CircLigase ssDNA Ligase Kit (Epicentre). To each of the 15 μL 10 mM cDNA/Tris pH 8.0 samples from the above reaction, 2 μL 10X CircLigase buffer, 1 μL 1 mM ATP, and 1 μL 50 mM $MnCl_2$ were added. 1 μL CircLigase ssDNA Ligase was added and the reaction was mixed and incubated at 60 °C for 2 h. The ligase was heat inactivated by incubating 10 min at 80 °C.

Illumina sequencing adaptors were introduced by 10-18 cycles of PCR using Phusion High Fidelity Polymerase (NEB), primer NINI2 (Table A.1), and indexing primers with TruSeq 6 bp indices (RMH001 – RMH024 in Table A.1). For a 60 μL final reaction volume, 12 μL 5X Phusion High Fidelity buffer, 1.2 μL 10 mM dNTPs, 0.3 μL 100 μM NINI2, 0.6 μL Phusion High Fidelity Polymerase, 39.9 μL H_2O, 3 μL 10 μM indexing oligonucleotide, and 3 μL circular ligation product were mixed. The reaction underwent an initial denaturation at 98 °C for 30 s followed by 10-18 cycles with the following settings: denaturation for 10 s at 98 °C, annealing for 10 s at 65 °C, extension for 10 s at 72 °C. To the reaction, 12 μL 6X DNA Loading Dye was added. The sample was loaded on a 6% TBE gel and run for 45 min at 180V. The gel was stained with 1X SYBR Gold and visualized on a Typhoon 9410 Molecular Imager (GE Healthcare). The region of the gel containing PCR products from 200-300 bp was excised and the DNA

extracted as described above. The dsDNA was resuspended in 10 μL 10 mM Tris-HCl pH 8.0 and quantified on a Bioanalyzer 2100 (Agilent) using High Sensitivity DNA Analysis Kits before sequencing. Samples were pooled to a final molarity of 2 nM and sequenced at the JHU Genetic Resources Core Facility High Throughput Sequencing Center on a HiSeq2500 (Illumina) in Rapid Mode using 50 bp single reads.

3.2.6 Sequencing and analysis of cDNA libraries

The raw FASTQ files generated by Illumina sequencing were stripped of linker sequences using Cutadapt (Martin 2011), and the first 3 nucleotides at the 5' end were removed using FASTX trimmer (http://hannonlsb.cshl.edu/fastx_toolkit/). Reads without an identifiable 3' linker were discarded. The trimmed reads were aligned to the MRE600 consensus rDNA sequence using the ShapeMapper package (Siegfried 2014) and the mismatches at each position were counted. The mutation rate was calculated as the ratio of mismatches at an rRNA position divided by the number of trimmed reads overlapping that position. The error at a position was defined as the Poisson sampling error as previously described (Siegfried 2014). Any rRNA nucleotides with *in vivo* methylations in the absence of DMS probing were excluded from analysis. Mutation rates for untreated samples were not subtracted from the mutation rates of treated samples. The untreated samples had higher variability and their inclusion increased noise (Zubradt 2016). Log10 fold changes in DMS-induced mutation rates between treatment and control samples were calculated. RNA from exponential phase cells was used for the control samples. The control sample residues with reactivities in the top and bottom 1% were excluded from analysis. These cutoffs were meant to exclude residues with misleading changes in

mutation rate, such as those occurring when dividing two small numbers, and did not exclude any residues with significant changes in mutation rate. The log10 fold changes in the top and bottom 1% were set to the 99th and 1st percentile reactivities, respectively.

3.3 Results

3.3.1 Cells recovering from phosphate starvation do not accumulate free 50S subunits during the first 15 minutes of outgrowth

The kinetics of label incorporation and ribosome assembly were compared in exponential phase cells and cells recovering from phosphate starvation. Cells in exponential phase were dosed with ^{3}H-5-uridine and, at time points over the following 20 minutes, fractions of the culture were transferred to ice (Figure 3.3). Similarly, cells in a state of phosphate starvation were dosed with ^{3}H-5-uridine before outgrowth was induced and time points were collected during the first 15 minutes of outgrowth. Polysome profiles were determined using sucrose gradient sedimentation velocity.

In exponential phase cells, the label was found in the pools of free 30S and 50S subunits and also in full 70S ribosomes. The tritium label first entered the pool of free 30S subunits, then the pool of 50S subunits, and then the 70S ribosomes (Figure 3.4a). This subunit order is what would be predicted from the orientation of the *rrn* operons. After 3 minutes, the tritium content in the 30S fraction had reached its steady state level. It took about 5 minutes for this to occur in the 50S subunit. This likely reflects both the distal location of the 23S and 5S genes in the *rrn* operon and the increased complexity involved in the assembly of the 50S subunit. Based on the location in the *rrn* operon, the

23S rRNA will finish being transcribed approximately 45 s after the 16S rRNA finishes. After 10 minutes, the tritium label began to accumulate in 70S ribosomes as the labeled subunits began to take part in protein synthesis.

During starvation recovery, the tritium label readily entered the free 30S pool in the first minute of outgrowth, but no corresponding increase in tritium content was observed for free 50S subunits (Figure 3.4b). The 70S later began accumulating the radiolabeled nucleotide after approximately five minutes. The accumulation of label in 70S began earlier during starvation recovery than it did in exponential phase. It is possible that in exponential phase cells there are larger pools of unlabeled 30S and 50S subunits at the start of labeling. A higher proportion of unlabeled subunits would mean that they would be more likely to be used to translate protein and it would take longer for labeled subunits to be used.

The amount of tritium in the pool of free 30S subunits did not reach a steady state in the first 15 minutes of outgrowth. This also suggests that the pool of unlabeled free 30S subunits was reduced during phosphate starvation and will take longer to be replenished during starvation recovery. The free 50S subunits pool did not accumulate the tritium label in the first 15 minutes of outgrowth. This is far longer than the time needed to transcribe the 23S rRNA. This presents two possibilities: either new 50S subunits are not being made (either because they are not being synthesized or because they are being degraded) or the 50S subunits are immediately being incorporated into 70S ribosomes before they are able to accumulate as a free complex.

To determine the fate of these nascent 50S subunits, sucrose gradient fractions from the 30S, 50S, and 70S peaks were separated on an 3% acrylamide : 0.3% agarose

composite gel. In this way, it was possible to detect the amount of radiation in the 16S and 23S bands for both the free subunits and the complete ribosome. The free 30S subunits were found to contain the radiolabeled uridine in their 16S rRNA (Figure 3.4c), with large increases in radiolabel after 8 minutes of outgrowth. No radiolabeled 23S rRNA was found in the 30S fraction. The free 50S subunits showed a small increase in radiolabeled 23S in the first 15 min of outgrowth (Figure 3.4c). In 70S-containing fractions, the 16S band showed a small increase in the amount of radiolabeled uridine and the 23S band showed a large increase (Figure 3.4c).

There was a large increase in the radiolabel content in both 16S and 23S rRNA after 8 minutes of outgrowth (Figure 3.4d). This timing was similar to what was seen for 30S and 70S particles (Figure 3.4b), with those beginning to increase after approximately 6-8 minutes of outgrowth.

These results (Figure 3.4c and 3.4d) show that the label is incorporated into both 16S and 23S rRNA, but when 50S subunits are formed, they are more immediately incorporated into 70S ribosomes, whereas 30S subunits go into the pool of free 30S subunits with a smaller amount going into 70S ribosomes. This suggests that the pool of free 50S subunits is depleted to a greater degree than the pool of free 30S subunits during phosphate starvation.

To determine the effect of phosphate starvation on the ribosomal content in cells, cells were starved of phosphate for various lengths of time. The lysates from these cellular time points were separated using sucrose gradient sedimentation velocity to generate polysome profiles (Figure 3.5). These polysome profiles show that there is normally a large pool of free 50S subunits at the beginning of phosphate starvation. After

4-6 h of phosphate starvation, this pool has been largely depleted, whereas the free 30S pool has remained a similar size.

3.3.2 RNAs in exponential phase cells are generally modified by DMS according to their expected secondary structure

By coupling *in vivo* DMS probing with high-throughput sequencing (Figure 3.2), it was possible to observe ribosomes in the cell throughout their lifecycles. The cDNA was generated using a universal primer complementary to an adaptor, rather than a gene-specific prime. This allowed all RNAs in the cell to be analyzed, rather than just one selected RNA. These methods were ultimately used to examine ribosome assembly intermediates, but they were first used to probe *in vivo* ribosomes in exponential phase cells to determine the expected background for later studies and to validate the protocol.

The DMS probing was highly reproducible (Figure 3.6a-c). A range of DMS concentrations and exposure times were tested. All conditions gave highly-correlated mutation rates for each base. When the DMS-probed RNA was reverse transcribed, a significant fraction (91.2%) of mismatches were on adenines and cytosines (Figure 3.6d). There was a wide range of mutation rates (Figure 3.7a-b). The absolute error for every mutation rate was less than 0.01 (Figure 3.7c). The absolute error was proportional to the mutation rate. The percent error was inversely proportional to the mutation rate (Figure 3.7d). This is especially beneficial since it is the residues with higher mutation rates that will be of interest.

The DMS probing patterns in exponential phase cells were generally as expected (Figure 3.8), with single-stranded loop and bulge regions reacting more strongly than

base-paired regions. In the 16S rRNA, there were highly reactive regions in h9, h16, and h27 (Figure 3.8a). In the 23S rRNA, there were high levels of DMS modification in H19, H20, H28, H63, and H97 (Figure 3.8b). Residues on the subunit interface generally had a higher reactivity than those on the solvent face (Figure 3.9). The reactivity rates at the solvent interface were consistent with previous DMS probing experiments (Merryman 1999, 1999).

The DMS modification profile of the immature rRNA was also obtained from the sequencing libraries. The sequencing coverage was much lower for these regions, with a depth of 1500-2000 reads for the 16S leader and trailer (Table 3.1). The 5' leader of the 16S rRNA contains several notable modifications. The residues -44A and -35A both had a high mutation rate. These residues occur in regions that are predicted to be single stranded. Interestingly, the residues -66A and -67A also had high DMS reactivities, but are predicted to be in a helix and base paired with uridines. During the rRNA processing that occurs in ribosome biogenesis, RNase E cleaves the 5' leader between -66A and -67A.

Samples that were not probed with DMS showed lower reactivity than those that were probed with DMS, as expected. For cells probed with DMS, a base in 16S with a mutation rate in the 95th percentile would be modified 1.52% of the time (Table 3.1). In cells not probed with DMS, a base with a mutation rate at the 95th percentile was modified 0.49% of the time. There were several notable exceptions to this trend, however. Residues known to have naturally-occurring modifications had very high reactivities, even in the absence of DMS probing. All base modifications caused increased mutation rates, but modifications occurring in the Watson-Crick face, such as

3-methyluridine 1498 in the 16S rRNA and 1-methylguanosine 745 and 3-methylpseudouridine 1915 in the 23S rRNA, showed the highest mutation rates. Another interesting observation which does not currently have an explanation is from the 5' leader sequence of the 16S rRNA. In the absence of DMS, residue -73A still has an over 40% mutation rate. Based on the proposed structure for the 5' leader, this should be a single-stranded region. The mutation rate would suggest that this residue either contains a structural modification or has some other structural anomaly.

3.3.3 Nascent rRNA in cells recovering from phosphate starvation shows increased DMS modification

To observe ribosome assembly intermediates, cells were starved of phosphate for 4 h to halt transcription (Figure 3.1a). These cells were pulsed with 0.25 mM 4sU and fed with rich media high in phosphate to restart transcription. With transcription synchronized, culture fractions were probed at various time points with DMS for the first 20 min of outgrowth. After feeding, the 4sU pulse was chased with a 20-fold excess of unlabeled uridine in order to reduce the heterogeneity of the ribosome assembly intermediate population. The start of each time course (i.e. the 0 min time point) was considered to be the addition of food.

All of the rRNA sequences had full coverage and good depth (Table 3.1), with the 16S and 23S rRNA having 15,000 or more reads for ~95% or more nucleotides. The 5S had lower depth near its 5' and 3' ends, but still had nearly 4000 reads for ~95% or more nucleotides (Table 3.1). Nascent RNA in cells recovering from phosphate starvation generally had higher rates of DMS reactivity than total RNA in exponential phase cells

(Figure 3.10 and 3.11). This comparison reflects the reactivities of nascent 4sU-labeled rRNA that were pulled down being normalized to total non-4sU-labeled rRNA that was not pulled down. The change in reactivity could reflect a greater degree of disorder in the nascent RNA or it could be an artifact of the normalization process. In the future, pulled down 4sU-labeled nascent rRNA should be compared to pulled down 4sU-labeled total rRNA.

After 4 minutes of outgrowth, the DMS reactivity of the 4sU-labeled rRNA differed from that of exponential phase rRNA, with the RNA being generally more exposed. The 5' domain of the 16S rRNA had the greatest reactivity, with h15 and h17 being particularly reactive (Figure 3.12a). The 3' domain also had increased reactivity. Residues in the 16S central domain had comparable reactivity to RNA during starvation recovery and during exponential phase growth. After 12 minutes of outgrowth, h15 and h17 still had increased DMS reactivity and h3 also showed increased reactivity (Figure 3.12b), but the reactivity throughout the rest of the 16S rRNA was generally reduced.

In the 23S rRNA, domains I, II, V, and VI had high reactivities after 4 minutes of outgrowth. Domains III and IV were less reactive, with domain IV actually being more protected than in fully assembled ribosomes (Figure 3.13a-b). After 12 minutes of outgrowth, domains I, II, V, and VI had decreased in DMS reactivity, approaching levels more similar to those expected for assembled ribosomes. Domain IV, which was more protected after 4 minutes of outgrowth, also approached DMS reactivity rates comparable to those expected in exponential phase cells.

As can be seen on the crystal structures of the ribosome (Figure 3.14), bases that were most reactive to DMS are largely located on the surface of the mature ribosome. As

was seen in the secondary structures, there is a decrease in the overall DMS reactivity as ribosome assembly proceeds. This would be the expected result for ribosomes approaching maturity.

The distribution of DMS reactivity rates for all ribosomal adenine and cytosine bases showed a decrease in variance from 4 minutes of outgrowth to 12 minutes (Figure 3.10). The median DMS reactivity rate remained similar after both 4 minutes and 12 minutes of outgrowth. The median reactivity rate and the variance in reactivity should both decrease as ribosome assembly proceeds. The fact that the median reactivity rate does not decrease could reflect the way in which DMS reactivities were normalized. DMS reactivity rates in nascent rRNA were normalized relative to the total rRNA in exponential phase cells rather than 4sU-labeled rRNA that was pulled down from exponential phase cells. The normalization should be repeated using rRNA that was labeled with 4sU and subject to the same RNA pulldown procedure that nascent rRNA underwent.

3.3.4 Ribosomal assembly intermediates can be examined in exponential phase cells by treating with the antibiotic rifampicin

Studying the structures of ribosome assembly intermediates *in vivo* has historically been challenging. Under normal growth conditions, assembly intermediates only constitute 2-5% of the total rRNA in *E. coli* (Lindahl 1975). Cells that are emerging from starvation conditions yield only a small amount of nascent RNA and require large culture volumes to approach the yields necessary for the RNA analysis. This can make the starvation-recovery method of RNA labeling difficult to implement. To improve RNA

yield, a second method was developed which would allow exponential phase cells to be used.

Exponential phase cells synthesize RNA more rapidly than cells emerging from starvation, but there is no synchronization to their transcription. To improve the synchronization in exponential phase cells, cells were dosed with 4sU and then treated with rifampicin (Figure 3.1b). Rifampicin is an antibiotic that halts transcription initiation in bacteria, but does not affect transcription elongation. In doing so, only RNA currently being transcribed will be labeled. The transcripts that were in the earliest stages of elongation upon rifampicin treatment should all complete transcription at nearly the same time. For the earliest time points, the RNA should constitute a fully heterogeneous mixture of assembly intermediates. For later time points, the RNA will be composed of assembled RNA and late assembly intermediates. Deviations from the probing patterns seen in assembled RNA will be indicative of late assembly intermediate structures. For these experiments, the time course begins with the addition of 4sU and time points reflect the length of time following 4sU addition. Yumeng Hao performed the cell growth and cDNA library preparation for this experiment. I designed the experiment and performed all of the data analysis.

All of the rRNA sequences had full coverage and good depth, with the 16S and 23S rRNA generally having 15000 or more reads for ~95% or more nucleotides (Table 3.2). The 5S had lower depth near its 5' and 3' ends, but still had more than 2000 reads for ~95% or more nucleotides. Nascent RNA in exponential phase cells generally had a higher rate of DMS reactivity than total RNA in exponential phase cells (Figure 3.15).

The DMS reactivity of the nascent rRNA differed from that of assembled rRNA (Figure 3.15) and also the nascent RNA found in cells recovering from phosphate starvation. The nascent RNA was generally more exposed to DMS, with regions of notable exposure occurring in the 16S central domain in h21 and h22 and in the 3' domain in h41. Regions of higher exposure were distributed throughout the 16S 5' domain. The 23S rRNA also featured increased DMS reactivity. The DMS reactivity was fairly evenly distributed throughout domains I, II, and III, with high reactivities for: helices 1, 2, and 7-10 in domain I; helices 27, 28, 31, 33, 41, 43, and 44 in domain II; and helices 47, 50, 52, 53, and 56 in domain III. In the 3' half of the 23S, regions of high DMS reactivity were more localized, with high reactivities for: helices 64 and 66 in domain IV; helices 75-78 in domain V; and helices 96 and 101 in domain VI. There was no change in the modification pattern during the first 6 minutes of assembly.

3.4 Discussion

3.4.1 Sucrose gradients show that virtually all newly transcribed 50S is immediately incorporated into 70S ribosomes during starvation recovery

Polysome profiles for cells emerging from phosphate starvation showed a large increase in the amount of nascent, radiolabeled rRNA in the pool of free 30S subunits. There was not a commensurate increase in nascent rRNA found in the pool of free 50S subunits. These nascent 50S particles are instead incorporated more immediately into 70S ribosomes.

At the beginning of phosphate starvation, there is a large pool of free 50S (Figure 3.5). After 4-6 h of phosphate starvation, this has been largely depleted, whereas the free 30S pool has remained a similar size (Figure 3.5). Transcription of the *rrn* operon produces one 16S molecule for every one 23S synthesized. Likewise, 30S and 50S should be produced in equimolar amounts. As cells recover from starvation, much of their energy will be focused on protein translation. After 4-6 h of phosphate starvation, cells still contain a large enough pool of free 30S to start the translation initiation process. However, because the free 50S pool is so depleted, nascent 50S subunits will need to be rapidly incorporated into translating ribosomes.

3.4.2 17S leader region involved in RNase E cleavage during processing is more exposed *in vivo* than predicted from *in vitro* structures

In exponential phase cells, certain regions of the rRNA had higher levels of DMS probing than would be expected from the secondary structure of precursor rRNA predicted from thermodynamic calculations. DMS reacts with the Watson-Crick faces of A and C bases, so paired bases are expected to show virtually no reactivity. This is largely borne out in the probed RNA, where the most reactive residues are almost exclusively found regions of the RNA that are single-stranded in crystal structures of the ribosome (Figure 3.8). However, in the 5' leader of the 17S rRNA, the adenines at the RNase E cleavage site are very exposed, suggesting that they are not base paired. RNase E cleaves the 5' leader between -66A and -67A. RNase E has a strong preference for single-stranded cleavage sites (Kaberdin 2003; Mackie 1992; Mackie 1993; McDowall 1995). A typical cleavage site is single-stranded with the composition 5'-(A/G)N↓AU-3'.

Consistent with this, the RNase E cut site in the 5' leader of 17S rRNA is 5'-GA↓AU-3'. The sequence is predicted to be in a helix, however it is predicted to be next to a single-stranded region. It is possible that the stability of this region is low enough to allow the cleavage site to be single-stranded a high percentage of the time.

3.4.3 Nascent rRNA in cells recovering from phosphate starvation shows DMS reactivity levels consistent with progressing ribosomal maturity

Cells were starved of phosphate to halt transcription, pulsed with 4sU, and fed with rich media to restart transcription (Figure 3.1a). During synchronized transcription, culture fractions were probed at various time points with DMS to examine structural changes taking place in the rRNA during assembly.

The distribution of DMS reactivity rates for all ribosomal adenine and cytosine bases showed a decrease in variance from 4 minutes of outgrowth to 12 minutes (Figure 3.10). The median DMS reactivity rate remained similar after both 4 minutes and 12 minutes of outgrowth. A decrease in both overall reactivity and the reactivity variability would be expected as ribosomal assembly proceeds. As ribosomes mature, they should approach a generally homogeneous final structure, resulting in a reduction in variability. This is seen in the reactivity rates. The assembled structure should also have greater secondary and tertiary structure than the assembly intermediates, resulting in decreased probing and a lower rate of DMS modification. This is not seen in the reactivity rates. This could reflect the way in which DMS reactivities were normalized. DMS reactivity rates in nascent rRNA were normalized relative to the total rRNA in exponential phase cells rather than 4sU-labeled rRNA that was pulled down from exponential phase cells.

This may affect the baseline DMS reactivity ratio. The normalization should be repeated using rRNA that was labeled with 4sU and subject to the RNA pulldown procedure.

The decrease in variability in DMS reactivity suggest that ribosome intermediates have been isolated and probed and that they are maturing over time. This could be more compelling with a greater number of time points. Unfortunately, the low yield of nascent RNA found in cells emerging from phosphate starvation made it difficult to prepare sequencing libraries for all of the time intervals, with only two points from the time course resulting in enough RNA to proceed with sequencing.

A bulk method such as this will almost certainly lack the sensitivity to identify separate assembly intermediates that occur concurrently, as would be expected with multiple parallel assembly pathways. More sensitive isolation techniques, for instance sucrose gradient separation of the labeled assembly intermediates, will need to be used. This will require further improvements to the yield of nascent RNA.

3.4.4 Nascent rRNA in exponential phase cells treated with rifampicin does not experience changes in reactivity during the first six minutes of assembly

The DMS reactivity patterns that occurred in nascent RNA generated in exponential phase cells treated with rifampicin were different from the exposure patterns seen for assembled RNA in exponential phase cells (Figure 3.15). The nascent structures had greater regions of solvent accessibility and a higher incidence of single-stranded RNA. The exposure patterns did not change in any meaningful way during the first 6 minutes of assembly, that is, the first 6 minutes after 4sU was added to the media. It is possible that over a longer time course changes would be seen. But for exponential phase

cells, this should be sufficient time for rRNA to be transcribed and the subunits nearly assembled. This suggests two possibilities: treatment with rifampicin is unable to properly synchronize assembly or treatment with rifampicin is somehow interfering with assembly. Both of these reasons are highly problematic and would be unresolvable.

The use of rifampicin will likely not be a viable method for studying ribosome assembly in the future. A 4sU pulse with a uridine chase, whether used in exponential phase cells or cells coming out of starvation, appears to be a much more viable future direction. If the yield of nascent RNA can be improved for that method, a more detailed time course during assembly could be produced. It is still unlikely that the DMS probing alone will be sufficient to characterize ribosomal assembly intermediates given the amount of heterogeneity that will always exist with parallel assembly pathways. But in combination with another technique, like electron microscopy, it could provide valuable structural information.

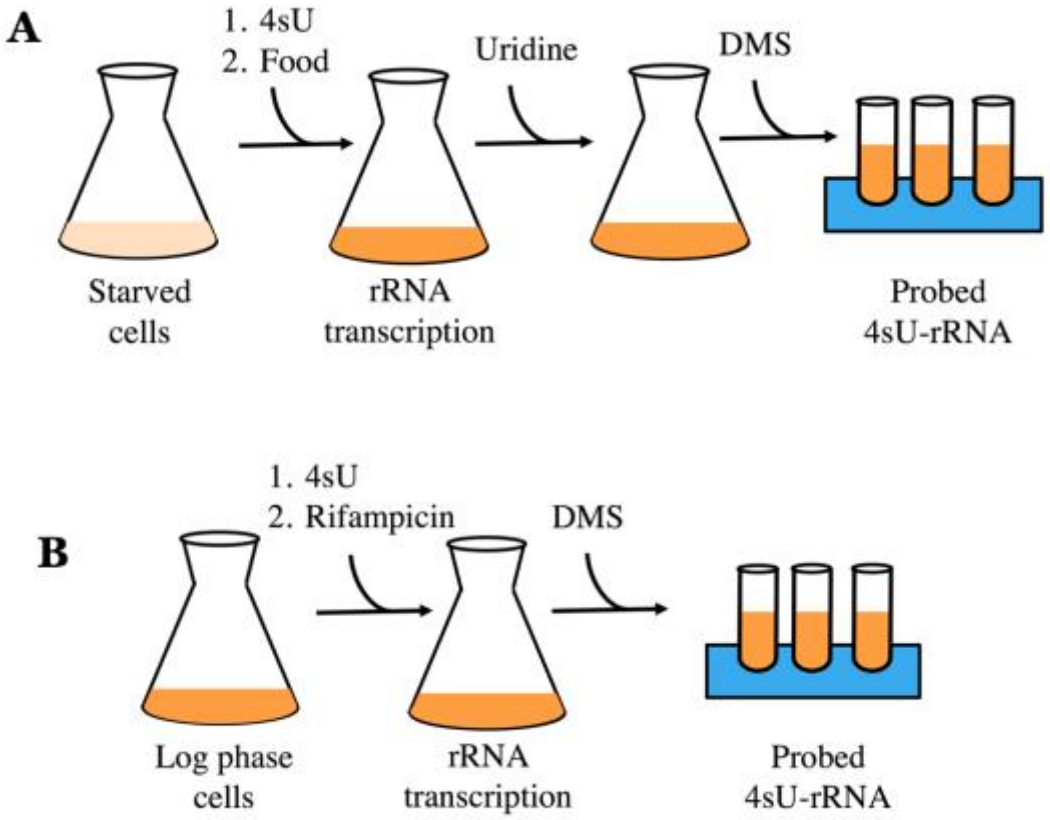

Figure 3.1. Labeling of nascent RNA during starvation recovery and during exponential phase (a) The labeling scheme occurs in three major parts: (1) phosphate starvation, (2) starvation recovery, and (3) *in vivo* DMS probing. Transcription of pre-rRNA is synchronized by starving cells of phosphate, then adding nutrients and phosphate to trigger de novo ribosome biogenesis. The modified nucleotide 4-thiouridine (4sU) is added to the media prior to food. During the recovery from starvation, the 4sU is chased with unlabeled uridine. The 4sU-labeled nascent rRNA is probed with DMS and the nascent transcripts will be able to be isolated and analyzed. (b) When using rifampicin, nascent RNA can be probed in exponential phase cells. After 4sU is added to the culture, rifampicin is added to halt transcription initiation. Cells are probed with DMS and the nascent transcripts can be isolated for analysis.

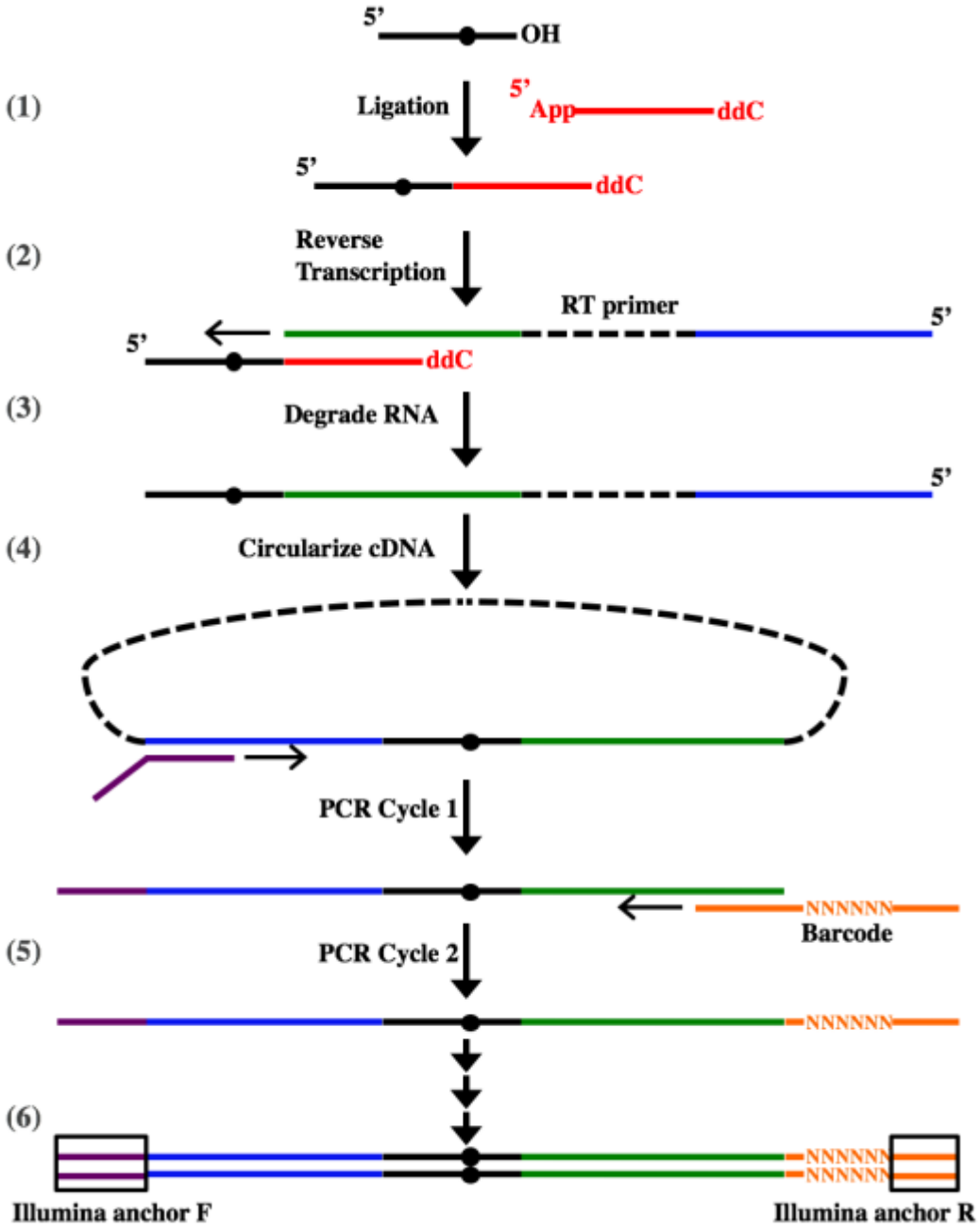

Figure 3.2. Overview of the DMS-MaPseq RNA probing protocol The method was adapted from (Zubradt 2016) and consists of six major parts: (1) Ligation of 3' adaptor (red) to RNA fragment. Adaptor is Linker-2 in Table A.1) (2) Reverse transcription using TGIRT to encode DMS methylations as cDNA mismatches. Primer (blue and green) is Linker-2 RT primer in Table A.1. (3) Isolation of cDNA fragments after degrading the probed RNA with NaOH. (4) Circularization of cDNA. (5) PCR addition of Illumina primers. Forward primer (purple) is NINI2 in Table A.1. Reverse primers (orange) are indexing primers RMH001-RMH024 in Table A.1. (6) Identification of mutations by Illumina sequencing.

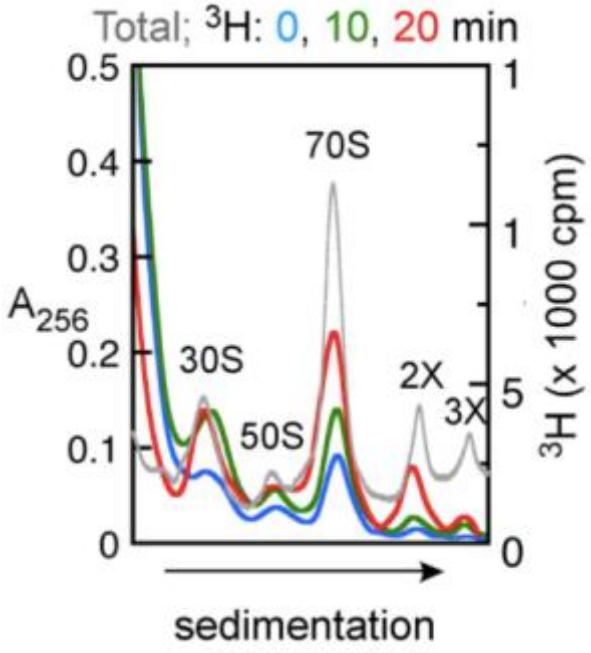

Figure 3.3. Polysome profiles of exponential phase MRE600 The left axis corresponds to the grey polysome profile depicting the total rRNA in the cell as measured by A_{256}. The right axis corresponds to the colored polysome profiles depicting the amount of nascent rRNA in the cell as measured by the incorporation of ^{3}H-labeled uridine. Cells dosed with ^{3}H-uridine at 0 min. The total RNA curve features approximately 14000 data points. The curves depicting ^{3}H content in RNA each contain approximately 60 data points which were joined with a smooth curve. Figure drawn by S. Woodson.

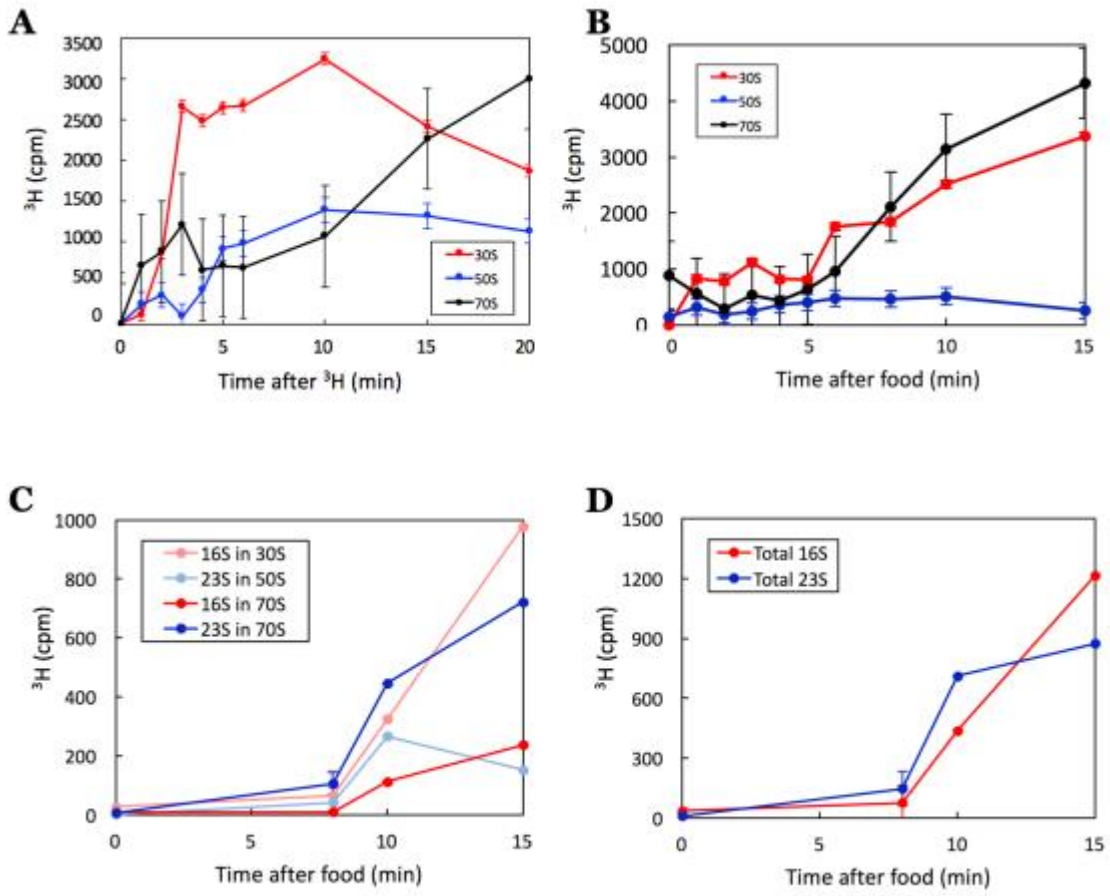

Figure 3.4. Ribosomal RNA labeling kinetics For (a and b), rRNA from each time point was separated on a sucrose gradient and the ^{3}H-uridine content of each gradient fraction was determined via scintillation counting. Each point represents the area under each ribosomal peak after a pre-food baseline is subtracted. For (c and d), sucrose gradient fractions were gel separated. Bands for 16S and 23S were excised to determine the amount of radiolabel going into free ribosomal subunits and 70S ribosomes. (a) Radiolabeled uridine entering ribosomes during exponential phase. (b) Radiolabeled uridine entering ribosomes during recovery from phosphate starvation. Labeled uridine was added 10 min before food. Food added at the 0 min mark. The experiment was performed once. The error bars reflect the variability in data collection and were estimated as follows: Before food was added, cells were collected at five time points. For each time, sucrose gradient fractions were collected and the ^{3}H-uridine content was determined via scintillation counting. The area under the curve for each ribosomal peak was calculated. The standard deviation of these points for the 30S, 50S, and 70S regions are used as the error bars for (a) and (b). (c) Presence of radiolabeled uridine in free subunits and in 70S ribosomes during recovery from phosphate starvation. (d) Presence of radiolabeled uridine in total 16S and 23S rRNA. For (c and d), experiments were repeated for the 0 and 8 minute time points. Data points are the average of two experiments and error bars are the standard deviation. The 10 and 15 minute time points reflect one experiment.

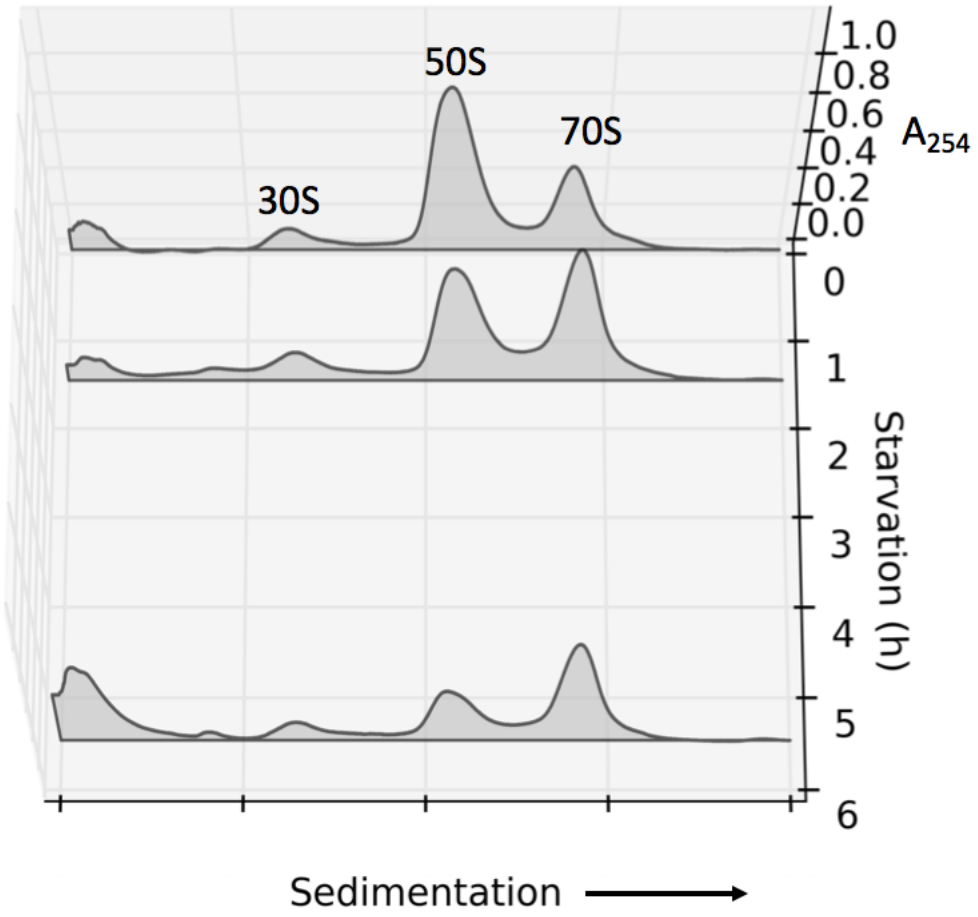

Figure 3.5. Polysome profiles of MRE600 undergoing phosphate starvation The three polysome profiles are from cells taken: immediately after, 1.5 h after, or 5.5 h after resuspension in phosphate-lacking minimal media. The z-axis depicts the raw A_{254} for the sucrose gradients.

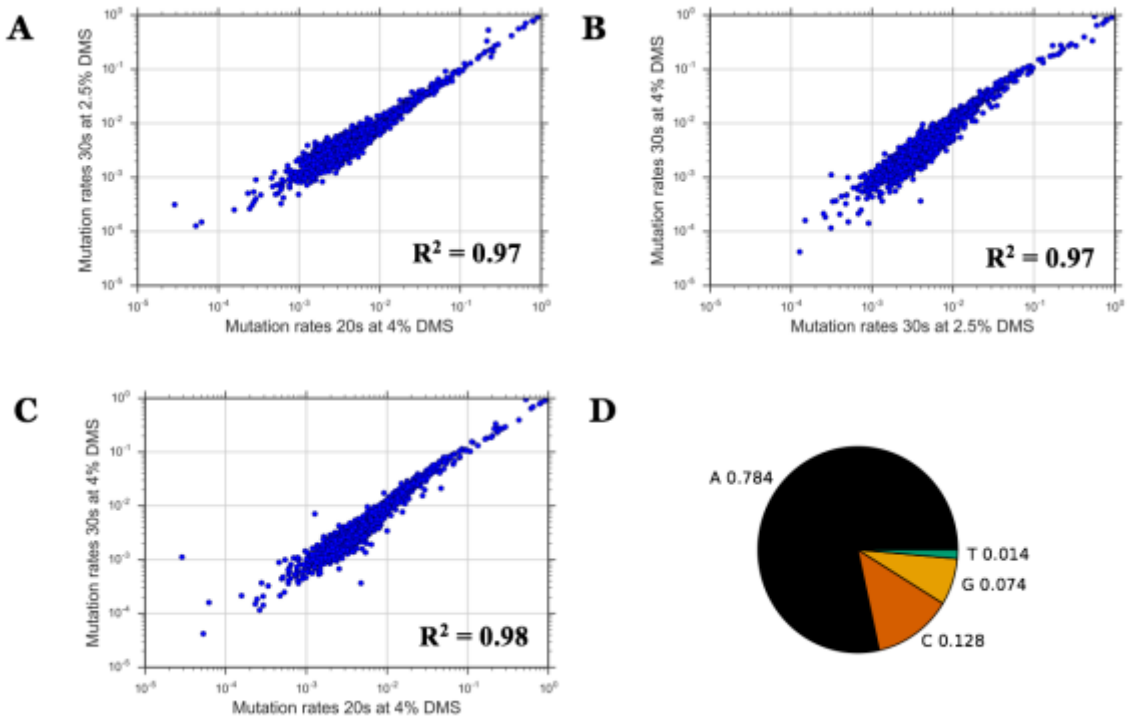

Figure 3.6. DMS probing results are highly reproducible and predominantly affect adenines and cytosines DMS probing results are reproducible between biological replicates and are robust to changes in DMS concentration and length of probing. Each individual point in (a-c) represents the mutation rate for specific bases in the 16S, 23S, and 5S rRNA. All ribosomal adenines and cytosines are included in these plots. Mutation rates for each base are compared between: (a) 20 s probing with 4% DMS and 30 s probing with 4% DMS, (b) 30 s probing with 2.5% DMS and 30 s probing with 4% DMS, and (c) 20 s probing with 4% DMS and 30 s probing with 2.5% DMS. (d) Nucleotide composition of mismatches in cDNA prepared from rRNA probed with DMS.

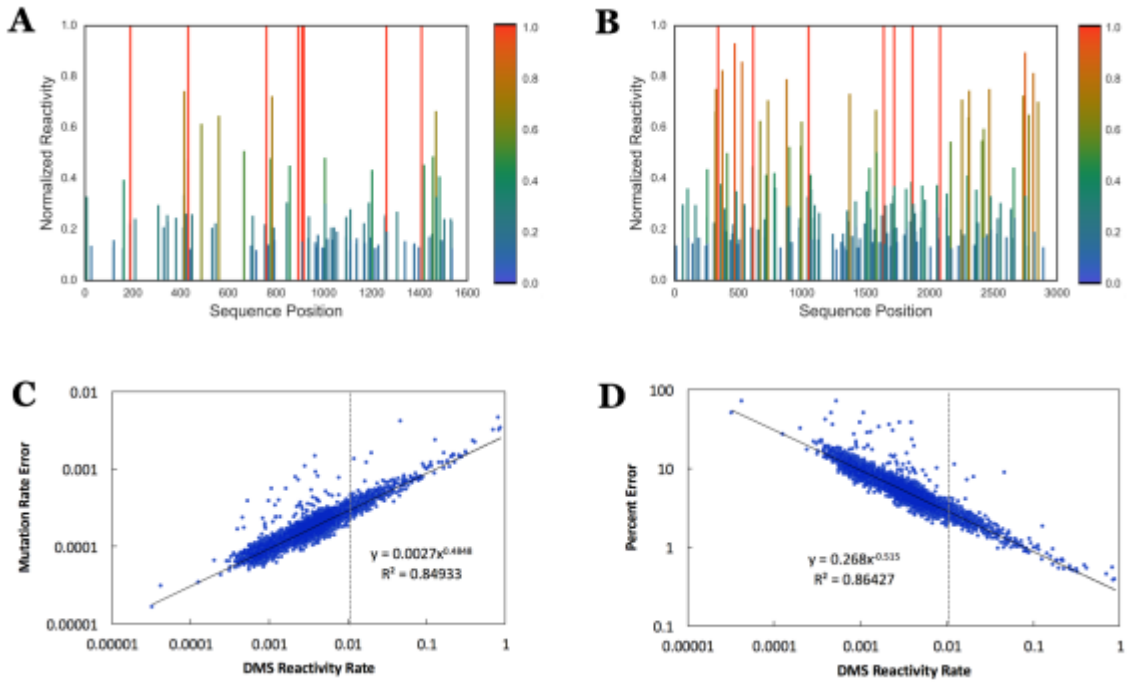

Figure 3.7. DMS reactivity rates in exponential phase cells For (a-b), mutation rates are normalized such that the 99th percentile reactivity is set to 1 and all reactivities are scaled to that value. For visual clarity, only the top 30% most reactive adenine and cytosine residues are shown in the line plots. In (c-d), the error in mutation rate is shown relative to the absolute mutation rate for all residues. The vertical line depicts the cutoff for the top 30%. (a) Line plot depicting mutation rate for each residue in the 16S. (b) Line plot depicting mutation rate for each residue in the 23S. (c) Absolute error for each base relative to absolute mutation rate. (d) Percent error for each base relative to absolute mutation rate.

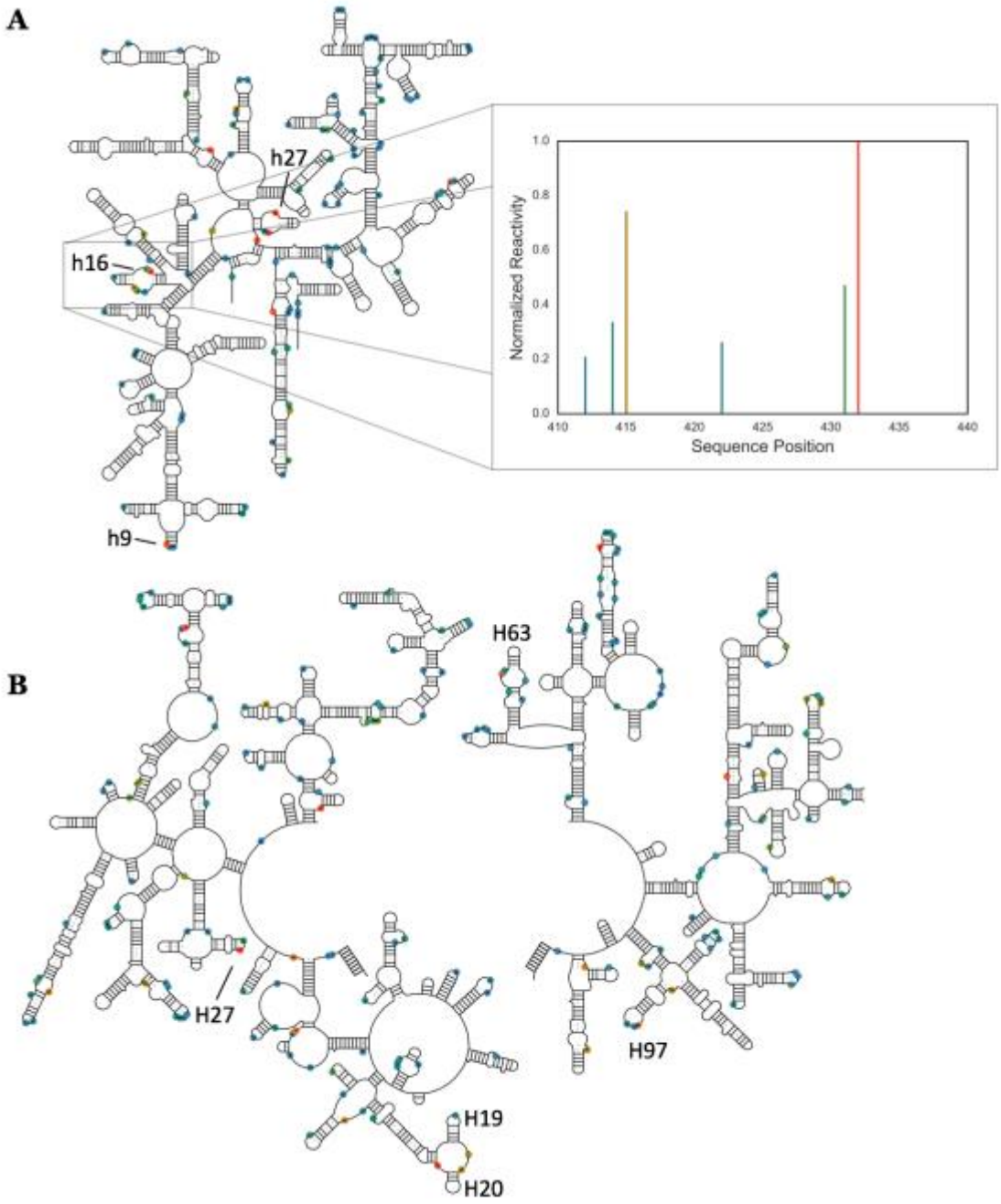

Figure 3.8. DMS probing patterns RNA species in exponential phase cells Mutation rates are normalized such that the 99th percentile reactivity is set to 1 and all reactivities are scaled to that value. For visual clarity, only the top 30% most reactive adenine and cytosine residues are shown in the secondary structures. (a) Secondary structure of 16S showing *in vivo* mutation rates. (Inset) Zoom of line plot for helix 16. (b) Secondary structure of 23S showing *in vivo* mutation rates.

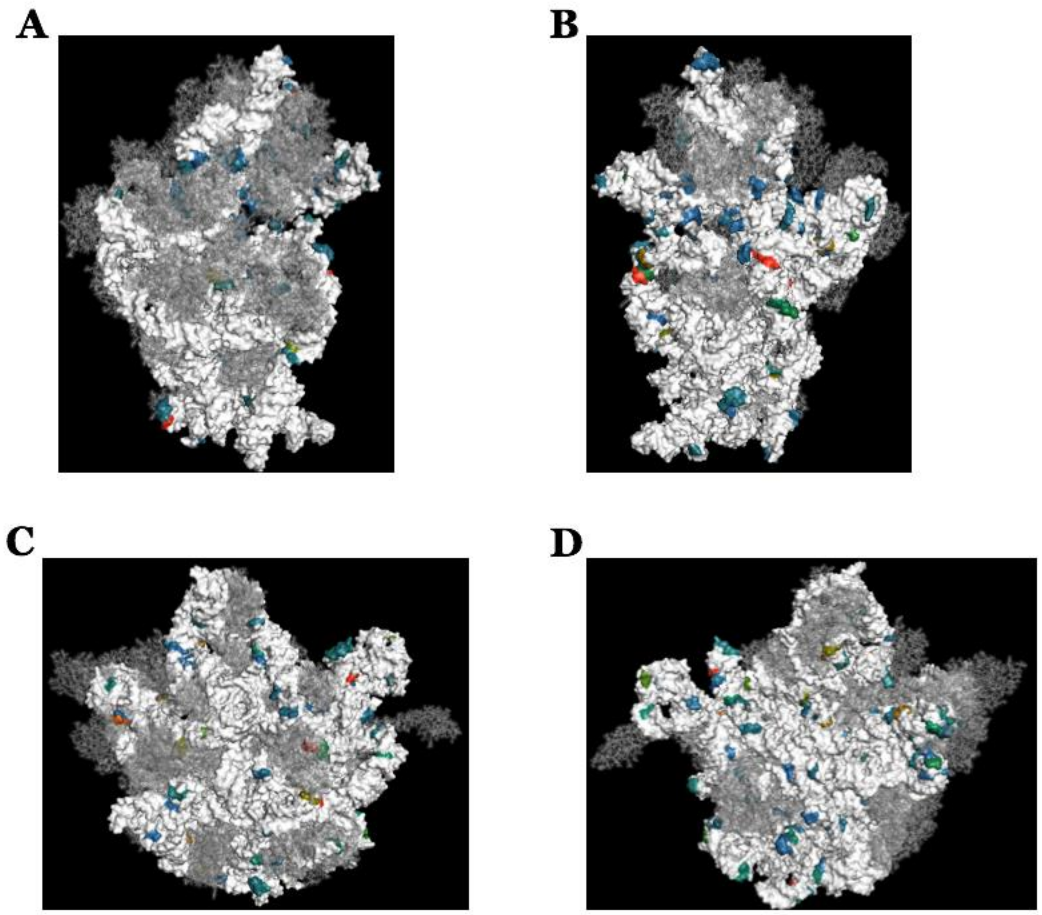

Figure 3.9. DMS probing patterns RNA species in exponential phase cells (a) The solvent view of the 30S. (b) The interface view of the 30S. (c) The solvent view of the 50S. (d) The interface view of the 50S. Ribosomal proteins are shown in transparent grey. Residues colored as in Figure 3.5. Only A and C bases with modification rates in the top 30% are colored.

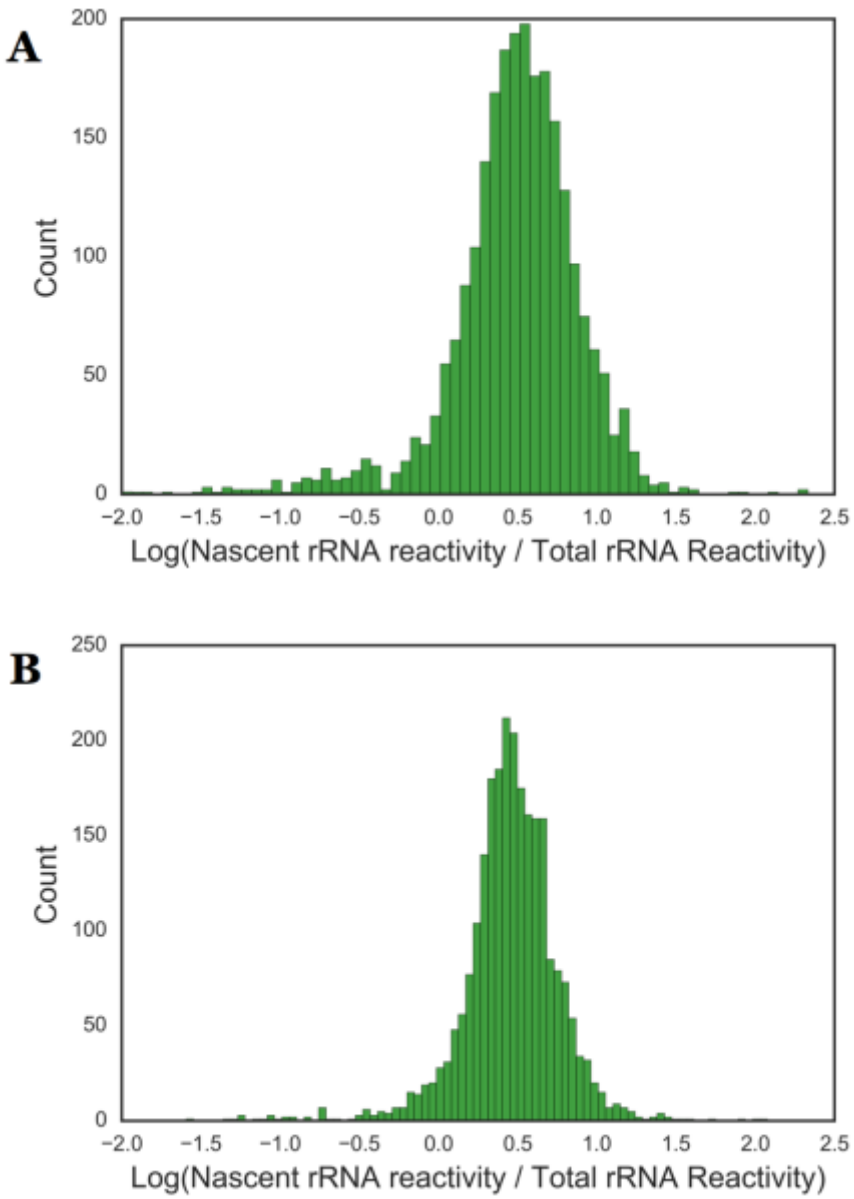

Figure 3.10. DMS mutation rates for *E. coli* cells recovering from phosphate starvation Histograms of the log ratio of the reactivity in RNA in cells recovering from phosphate starvation over the reactivity of total RNA in exponential phase cells. Ratios are the DMS reactivities of individual bases divided by the reactivity of the corresponding base in RNA found in exponentially growing cells. The RNA from exponential phase cells is total RNA, and not 4sU-labeled RNA that has been pulled down. Binwidth, *h*, for each histogram is calculated using a Freedman-Diaconis estimator: $h = 2*IQR/n^{1/3}$, where IQR is the interquartile range and n is the number of observations. Samples were collected after: (a) 4 minutes of outgrowth, with h=0.063, or (b) 12 minutes of outgrowth, with h=0.046.

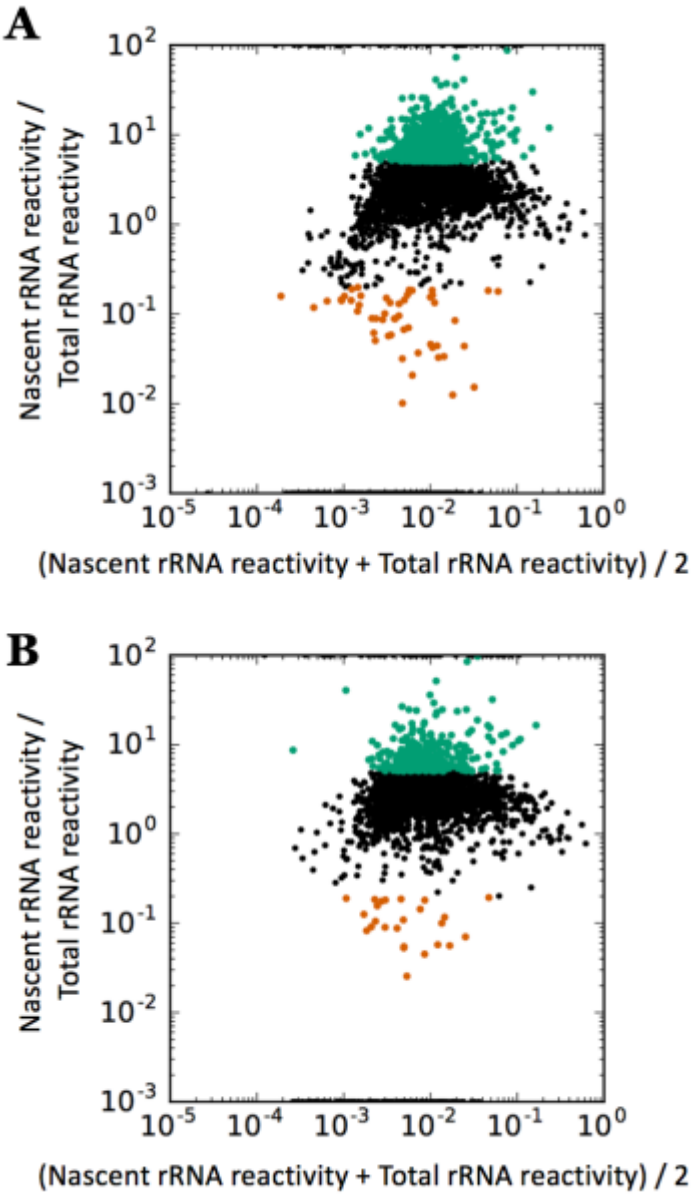

Figure 3.11. MA plots depicting DMS mutation rates for *E. coli* cells recovering from phosphate starvation Ratios are the DMS reactivities of individual bases divided by the reactivity of the corresponding base in RNA found in exponentially growing cells. The plots feature all ribosomal adenines and cytosines. The RNA from exponential phase cells is total RNA, and not 4sU-labeled RNA that has been pulled down. Green data points are bases that are at least five times more reactive in nascent rRNA compared to total rRNA. Orange data points are at least five times less reactive in nascent rRNA relative to total rRNA. Samples were collected after: (a) 4 minutes of outgrowth or (b) 12 minutes of outgrowth.

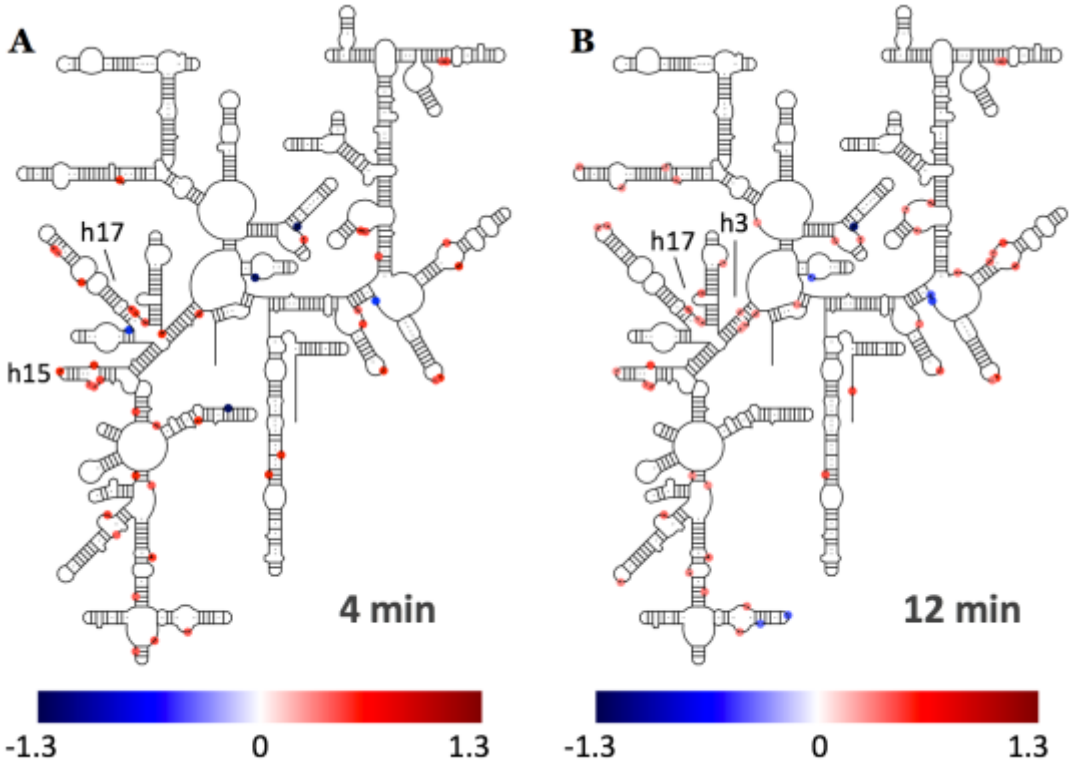

Figure 3.12. Overview of DMS-MaPseq results for *E. coli* cells recovering from phosphate starvation Color bar shows coloring of residues. The deepest red indicates largest $\log_{10}$(experimental reactivity rate / exponential phase reactivity rate). The deepest blue is the negative of this value. The color scheme is continuous, rather than binned. (a) Secondary structure of 16S showing *in vivo* mutation rates after 4 min of outgrowth, (b) Secondary structure of 16S showing *in vivo* mutation rates after 12 min of outgrowth.

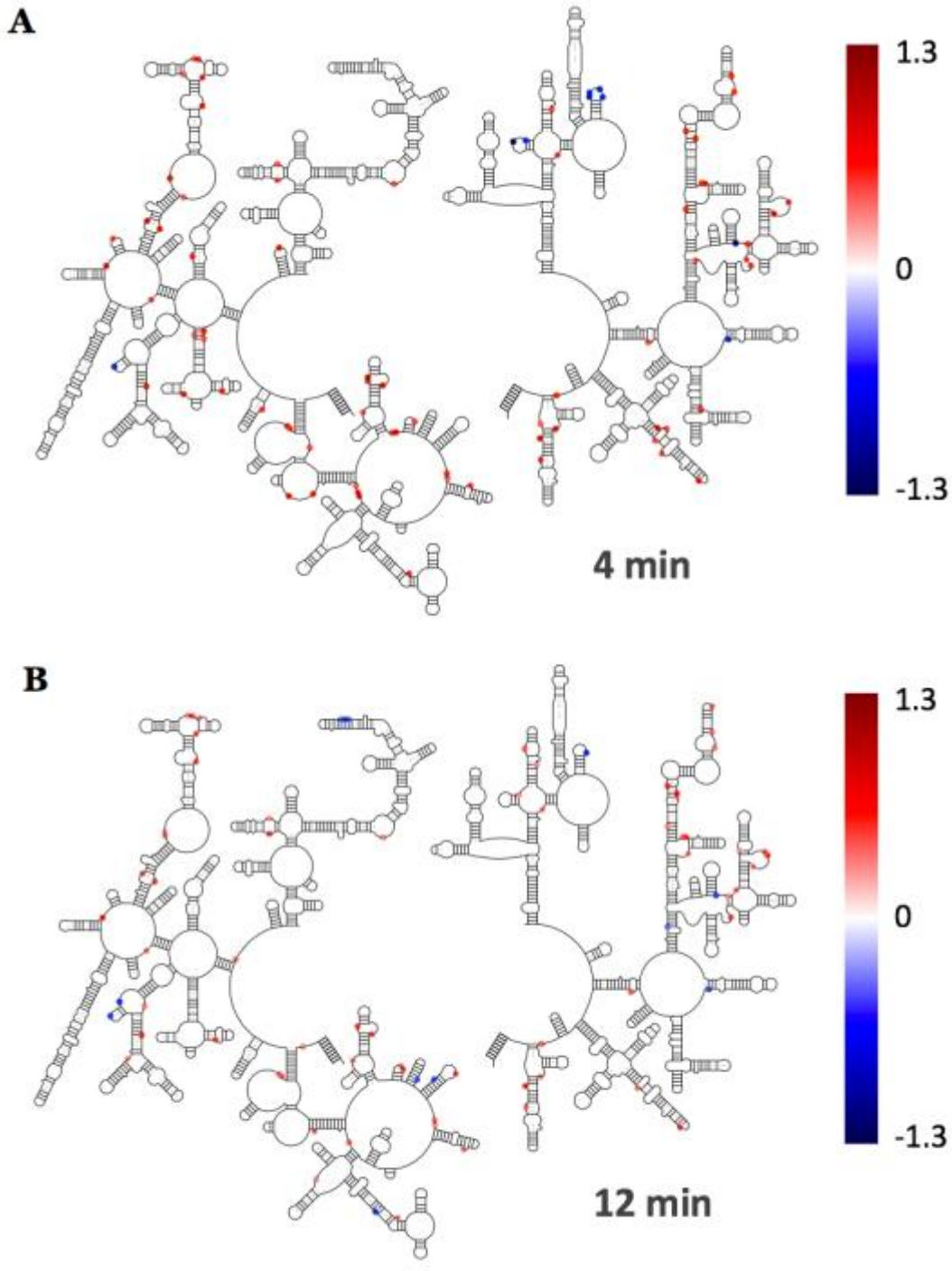

Figure 3.13. Overview of DMS-MaPseq results for *E. coli* cells recovering from phosphate starvation Color bar shows coloring of residues. The deepest red indicates largest $\log_{10}$(experimental reactivity rate / exponential phase reactivity rate). The deepest blue is the negative of this value. The color scheme is continuous, rather than binned. (a) Secondary structure of 23S showing *in vivo* mutation rates after 4 min of outgrowth, (b) Secondary structure of 23S showing *in vivo* mutation rates after 12 min of outgrowth.

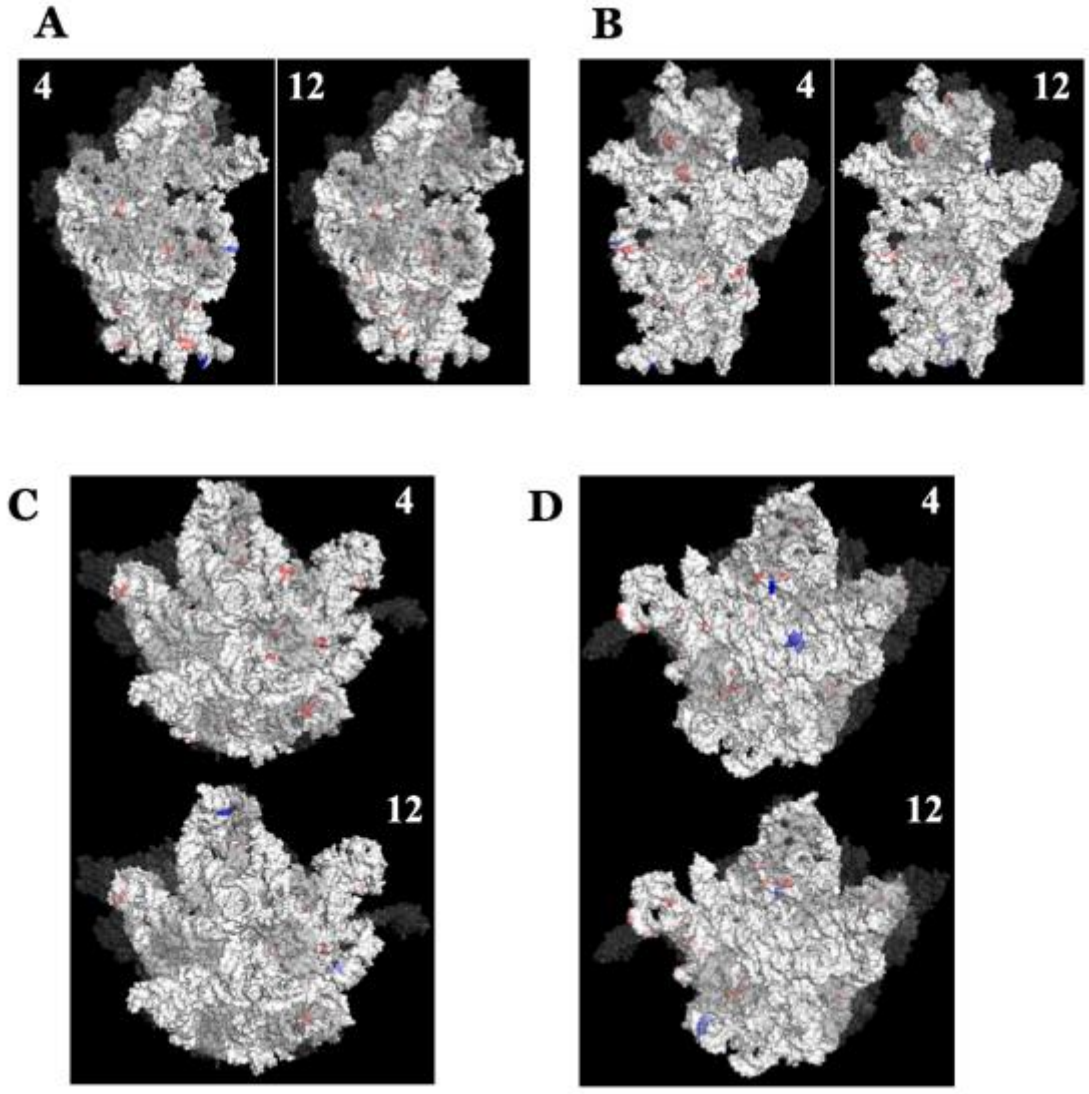

Figure 3.14. DMS mutation rates for rRNA in *E. coli* cells recovering from phosphate starvation (a) The solvent view of the 30S subunit after 4 min (left) and 12 min (right) of outgrowth. (b) The interface view of the 30S subunit after 4 min (left) and 12 min (right) of outgrowth. (c) The solvent view of the 50S subunit after 4 min (top) and 12 min (bottom) of outgrowth. (d) The interface view of the 50S subunit after 4 min (top) and 12 min (bottom) of outgrowth. Ribosomal proteins are shown in transparent grey. Residues colored as in Figure 3.8.

Figure 3.15. Overview of DMS-MaPseq results for exponential phase *E. coli* cells treated with rifampicin Color bar shows coloring of residues. The deepest red indicates largest $\log_{10}$(experimental reactivity rate / exponential phase reactivity rate). The deepest blue is the negative of this value. The color scheme is continuous, rather than binned. (a) Secondary structure of 16S showing *in vivo* mutation rates after 1 min of treatment, (b) Secondary structure of 16S showing *in vivo* mutation rates after 3 min of treatment, (c) Secondary structure of 16S showing *in vivo* mutation rates after 5 min of treatment, (d) Secondary structure of 16S showing *in vivo* mutation rates after 6 min of treatment. Color bar shows coloring of residues. The deepest red indicates largest $\log_{10}$(experimental reactivity rate / exponential phase reactivity rate). The deepest blue is the negative of this value.

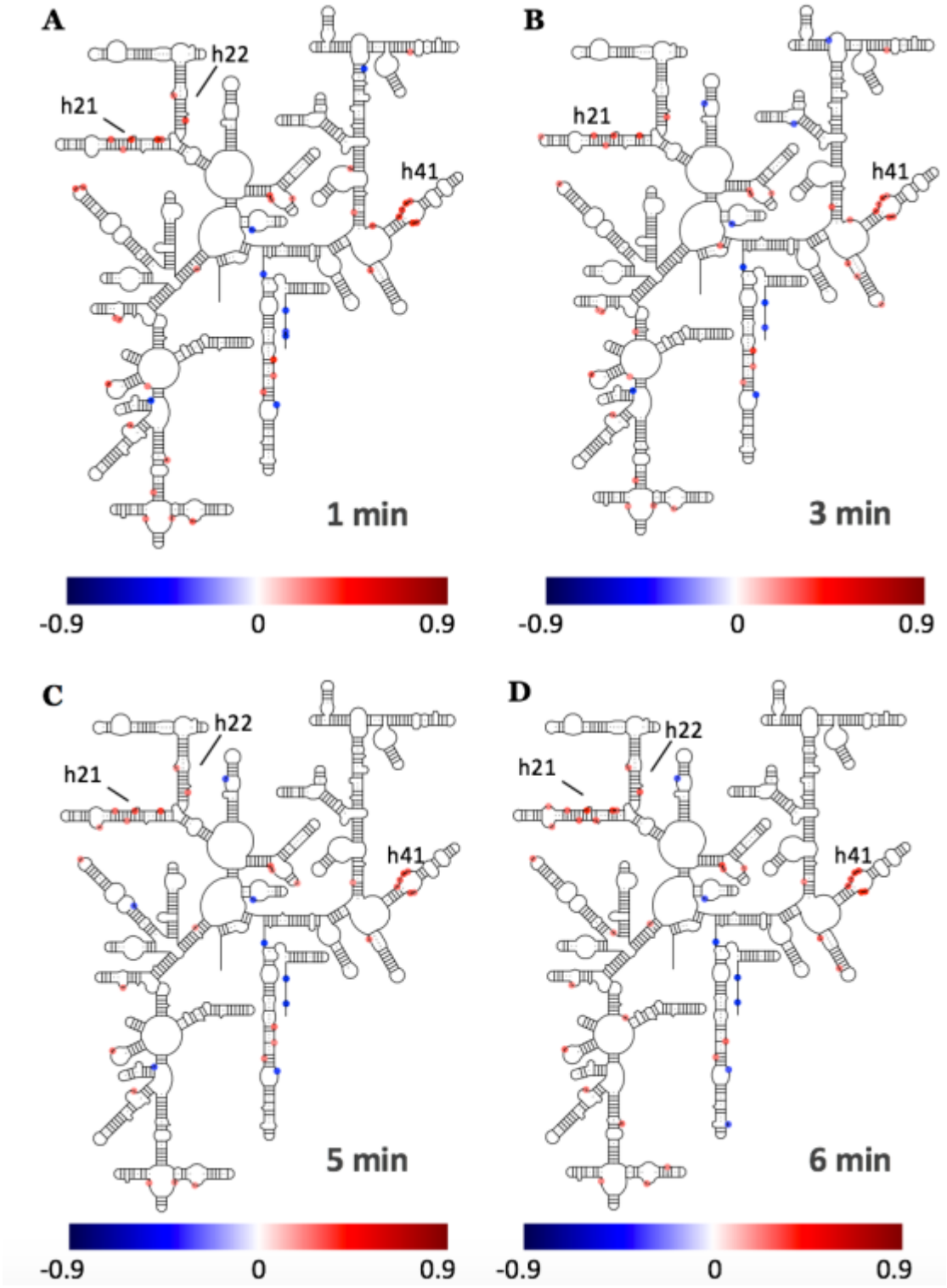
A
h22
h21
h41
1 min
-0.9
0
0.9
B
h21
h41
3 min
-0.9
0
0.9
C
h22
h21
h41
5 min
-0.9
0
0.9
D
h22
h21
h41
6 min
-0.9
0
0.9

Table 3.1. **Mutation rate and read depth for Illumina-sequenced RNA from exponential phase cells and cells emerging from phosphate starvation**.

	Mutation Rate (percent)		Read Depth	
RNA species	**Median**	**95th percentile**	**Median**	**5th percentile**
Exponential phase 16S	0.06	1.52	173610	100665
Exponential phase 23S	0.06	1.71	179309	100499
Exponential phase 5S	0.07	1.17	230084	10516
Exponential phase 16S 5' leader	0.19	2.84	1866	915
Exponential phase 16S 3' trailer	0.00	2.32	1685	61
Nascent 16S: 4 min	0.04	3.92	37679	15110
Nascent 23S: 4 min	0.03	4.15	42628	19062
Nascent 5S: 4 min	0.09	2.93	63158	3963
Nascent 16S: 12 min	0.11	3.66	48539	21253
Nascent 23S: 12 min	0.11	3.89	63689	26756
Nascent 5S: 12 min	0.06	3.21	44652	6590

Table 3.2. **Mutation rate and read depth for Illumina-sequenced RNA from exponential phase MRE600 treated with rifampicin**.

	Mutation Rate (percent)		Read Depth	
RNA species	**Median**	**95th percentile**	**Median**	**5th percentile**
Rifampicin 16S: 1 min	0.33	2.94	36960	13859
Rifampicin 23S: 1 min	0.33	3.06	46162	19517
Rifampicin 16S: 2 min	0.33	2.74	38679	15217
Rifampicin 23S: 2 min	0.37	2.93	52354	22616
Rifampicin 16S: 3 min	0.38	2.84	61336	18050
Rifampicin 23S: 3 min	0.4	3.04	79907	34071
Rifampicin 16S: 4 min	0.33	2.9	64078	17731
Rifampicin 23S: 4 min	0.34	3.09	85998	33325
Rifampicin 16S: 5 min	0.35	2.71	68240	28118
Rifampicin 23S: 5 min	0.36	3.01	85376	38828
Rifampicin 16S: 6 min	0.34	2.58	52400	27161
Rifampicin 23S: 6 min	0.36	2.77	60461	29372

CHAPTER 4: Changes in *E. coli* ribosome structure and composition during cellular stress

4.1 Introduction

E. coli are enteric bacteria that typically endure feast-or-famine nutrient conditions. The cells must make a number of adaptations when transitioning to nutrient-depleted conditions. Under these conditions, cellular growth and division are inhibited and protein translation is greatly reduced (Siegele 1992). During nutrient depletion, excess ribosomes are degraded (Ben-Hamida 1966; Davis 1986; Jacobson 1968; Kaplan 1975), releasing their nutrients and prolonging cell survival until more hospitable conditions are available. The process leading to rRNA degradation during starvation is not fully understood, but many of the RNases involved in the breakdown of rRNA have been identified (Basturea 2011; Sulthana 2016) and their regulation during exponential phase and stationary phase is starting to be elucidated (Sulthana 2017).

Determining how the degradation of stable RNA is regulated is a central question in understanding RNA metabolism. One possible regulatory mechanism is that RNAs are degraded by RNases unless they are somehow physically protected from cleavage. During exponential phase growth, the rRNA is largely in 70S ribosomes. The surface of the ribosome is protected by bound r-proteins and the interfacial regions of the subunits is protected by the presence of the other subunit. In cells that enter stationary phase, there are fewer translating ribosomes and more free ribosomal subunits. These free subunits would have a solvent-exposed interface. This interfacial region is acted on by RNase E

during starvation, ultimately leading to the complete degradation of the subunits (Sulthana 2016).

According to the model above, structural changes in ribosomes during bacterial stress increase their accessibility to RNases. Another possible mechanism for stable RNA degradation is that the rRNA structure remains similar and the activity of RNases is increased during periods of starvation (Deutscher 2009; Sulthana 2017).

I looked at MRE600 under five different stress conditions to determine if the cells responded to different stresses using different survival strategies (Figure 1). rRNA was degraded under all five conditions, but on different time scales. Cells were able to respond to some stresses much better than others. To provide greater insight into potential structural changes that occur in ribosomes during starvation, I also used *in vivo* DMS probing of rRNA over the duration of two of the cellular stress conditions: growth to late stationary phase and growth in minimal media lacking nitrogen. RNA appears less susceptible to degradation during nitrogen starvation, both in terms of the amount of rRNA remaining over time and the degree of modification by DMS.

Upon entry into the stationary phase, *E. coli* 70S ribosomes are known to dimerize to form a translationally inactive 100S ribosome (Wada 1998). The dimerization process is assisted by the ribosome modulation factor (RMF) and the hibernation promoting factor (HPF) (Maki 2000; Wada 1990). Both proteins bind to the 30S subunit. The RMF binding site overlaps the Shine-Dalgarno-anti-Shine-Dalgarno helix (Polikanov 2012). The HPF binding site overlaps with that of tRNA and mRNA in the A- and P-site of the 30S subunit (Polikanov 2012). These interactions could inhibit the binding of initiator tRNA and association of the ribosome with mRNA, preventing translation. The

binding of these proteins induces a conformational change in the 30S head domain that promotes 100S formation (Yoshida 2009). A third protein, YfiA, has been shown to bind to 70S ribosomes in stationary phase (Maki 2000). YfiA binds to 30S subunits at the subunit interface and prevents dissociation of the 70S ribosome (Agafonov 1999). YfiA also antagonizes the formation of 100S ribosome dimers (Ueta 2005). A fourth protein, RsfA, binds to L14 on 50S subunits, protecting the interfacial region and inhibiting 70S and 100S formation (Häuser 2012). The proteins YfiA and RsfA have not been observed to cause conformational changes in the 30S or 50S subunits.

Despite the extensive use of MRE600 cells for ribosomal and translational research, there has been limited research on ribosomal RNA in MRE600 during starvation or stationary phase. It is not known whether the ribosomes in these cells adopt the same survival strategies that they would in wild-type K12 *E. coli* strains. The experiments in this chapter will use sucrose gradient ribosome fractionation to address the kinetics of ribosome degradation in MRE600 during cellular stress, as well as structural studies highlighting reasons for which there might be differences in decay rates. The sucrose gradient studies will also depict the complexes that ribosomes in MRE600 maintain, with 70S ribosomes and ribosomal subunits present, but no formation of 100S ribosomal dimers.

4.2 Materials and methods

4.2.1 Starvation conditions (media for all conditions)

To prepare cultures, 3–5 mL of LB media was inoculated with a single MRE600 colony and grown overnight at 37 °C with shaking. The following day, the culture was diluted at a ratio of 1:100 to 1:1000 into the desired volume of media, usually 75 mL.

For experiments in stationary phase cells, cells were grown to late-stationary phase (OD_{600} = 3.5 – 4.0). For nutrient deprivation experiments, cells were grown to mid- to late-exponential phase (OD_{600} = 0.7 – 0.8). They were harvested by centrifugation and resuspended in one of four minimal media: minimal media lacking phosphate (100 mM Tris-HCl, 25 mM KCl, 10 mM NaCl, 20 mM NH_4Cl, 1 mM $MgSO_4$, 0.1 mM $CaCl_2$, 2 μM thiamine, 0.4% glucose, pH 7.8), minimal media lacking glucose (42 mM Na_2HPO_4, 24 mM KH_2PO_4, 9 mM NaCl, 19 mM NH_4Cl, 1 mM $MgSO_4$, 0.1 mM $CaCl_2$, 2 μM thiamine, pH 7.8), minimal media lacking nitrogen (42 mM Na_2HPO_4, 24 mM KH_2PO_4, 19 mM NaCl, 1 mM $MgSO_4$, 0.1 mM $CaCl_2$, 2 μM thiamine, 0.4% glucose, pH 7.8), and minimal media lacking magnesium (42 mM Na_2HPO_4, 24 mM KH_2PO_4, 9 mM NaCl, 19 mM NH_4Cl, 0.1 mM $CaCl_2$, 2 μM thiamine, 0.4% glucose, pH 7.8). The cells were harvested and resuspended twice more, each time in 1 volume minimal media, to more thoroughly deplete the nutrient of interest: phosphate, glucose, nitrogen, or magnesium, respectively. On the final step, minimal media was added until the cells were diluted to the desired final volume and had an OD_{600} in the mid- to late-log range (0.5–0.7). The cells were incubated in minimal media at 37 °C with shaking for the length of starvation (up to 14 days).

4.2.2 *In vivo* DMS probing

To probe the rRNA secondary structure with dimethyl sulfate (DMS), the *in vivo* DMS probing and quenching conditions of Wells et al. (Wells 2000) was adapted as previously described in Section 2.2.6. For a starvation time course, MRE600 cells were cultured as described in Section 4.2.1. DMS was diluted 1:2 (v/v) in 95% ethanol. At the desired times, a 5 mL aliquot was removed from the main culture and added to a tube containing diluted DMS. The ratio of DMS-ethanol solution to culture medium was typically 1:25 (v/v) in these experiments. After 30 s, the methylation reaction was quenched with the addition of a 1/2 vol ice-cold 0.6 M β-mercaptoethanol and a 1/2 vol of water-saturated isoamyl alcohol (Wells 2000). After DMS treatment, cells in each sample were pelleted by centrifugation and resuspended in one culture volume of 0.6 M β-mercaptoethanol (Wells 2000). Cells were pelleted again and the supernatant decanted. RNA was extracted using RNeasy Mini Kit Spin Columns (Qiagen).

4.2.3 Sucrose gradients

Analytical sucrose gradients were prepared as described (Spedding 1990) with several modifications. These are explained in detail in Section 3.2.2.

4.2.4 Preparation of cDNA libraries from DMS-probed RNA

The cDNA libraries were made using the DMS-MaPseq method (Zubradt 2016). A detailed protocol is given in Section 3.2.9.

4.3 Results

4.3.1 The amount of intracellular rRNA decreases during bacterial stress

To determine if different conditions result in changes in the regulation of rRNA degradation, cells were exposed to five different stresses: growth to high cell density, depletion of nitrogen, depletion of carbon, depletion of phosphate, or depletion of magnesium. These stresses were continued for up to 13 days. At various time points, cells were lysed and the cell lysates were separated on a sucrose gradient. Growth curves (Figure 4.2) and polysome profiles (Figure 4.3) show a steady decrease in cell viability and intracellular rRNA content, respectively. Polysome profiles were normalized to the starting optical density of the culture and the amount of total RNA extracted for each sample. This will provide relative changes in the polysome profiles per cell.

4.3.1.1 Cells grown to late stationary phase show more rapid degradation of 50S subunits than 30S subunits

Cells were grown to late stationary phase in rich media. For this experiment, the time scale began with 0 h corresponding to cells reaching their highest optical density (OD_{600} = 3.7). These cells showed a slight decrease in optical density over the first four days at stationary phase (Figure 4.2a). The number of colony forming units per mL of cells steadily decreased, with the cells having a half-life of 17 h (Figure 4.2b). The polysome profiles (Figure 4.3a) showed a steady decrease in the numbers of 70S ribosomes and the free 50S subunits during the first 18 h, such that both populations are depleted after 18 h in the late stationary phase. The free 30S subunit pool persisted

slightly longer, with a small amount of free 30S subunit after 27 h in the late stationary phase. The decrease in total 70S ribosomes over time is shown in Figure 4.4.

The changes in the total amount of 30S and 50S subunits can be calculated from the area under the peaks for the free 30S subunits, the free 50S subunits, and the 70S ribosomes. The fraction of the 70S ribosome peak area comprising the 30S and 50S subunits can be calculated based on the length of the respective rRNAs of the subunits and their contribution to the A_{254} signal. Figure 4.5a shows the decay of the 30S and 50S subunits during late stationary phase. These were normalized to the lengths of the rRNAs in each subunit, so that changes in the relative number of subunits is the observable, rather than the total A_{254} contributions from each subunit. Both the 30S and 50S subunits were degraded, with the 50S subunits being degraded more rapidly (k_{decay} = 0.116 h^{-1}, $t_{1/2}$ = 2.4 h) than the 30S subunits (k_{decay} = 0.293 h^{-1}, $t_{1/2}$ = 6.0 h) during late stationary phase (Table 4.1).

4.3.1.2 Cells starved of nitrogen show slow degradation of rRNA

Nitrogen depletion seemed to have had the least deleterious effect on ribosome populations of any of the stress conditions tested. These cells showed a slight decrease in optical density over the first four days of nitrogen starvation (Figure 4.2a). The number of colony forming units per mL of cells steadily decreased, with the cells having a half-life of 10 h (Figure 4.2b). The 70S ribosomes maintained a consistent level during the first 5.5 h of nitrogen starvation and steadily split into 30S and 50S subunits as starvation continued (Figure 4.3b). Of all of the bacterial stresses tested, the 70S ribosomes remained in the cells for the longest duration in nitrogen starvation (Figure 4.4), with

ribosomes still present after 60 h. The total 30S and 50S subunits were both degraded slowly (k_{decay} = 0.004 and 0.009 h^{-1}, respectively) during nitrogen starvation (Figure 4.5b and Table 4.1). These decay rates correspond to $t_{1/2}$ = 38.0 h for 30S and $t_{1/2}$ = 32.0 h for 50S (Figure 4.5f).

4.3.1.3 Cells starved of carbon slowly degrade 50S and have increased 70S

Cells grown to exponential phase in LB were depleted of carbon by resuspension in M9 salts lacking glucose. These cells showed a slight decrease in optical density over the first four days of carbon starvation (Figure 4.2a). The number of colony forming units per mL of cells steadily decreased, with the cells having a half-life of 10 h (Figure 4.2b). During glucose starvation, there was a large increase in 70S ribosomes from 0 to 5.5 h (Figure 4.3c and 4.4). This was followed by a steady decrease in the 70S ribosome population. After 44 h of carbon starvation, the 70S ribosomes were completely degraded. Along with nitrogen starvation, this was the longest that 70S ribosomes persisted in the cell, for over 24 h in both cases. The free 30S and 50S subunit pools followed similar decay patterns (Figure 4.5c) and rates (k_{decay} = 0.015 and 0.019 h^{-1}, respectively) and both retained small populations after 72 h of carbon starvation (Figure 4.3c and 4.5c). These decay rates correspond to $t_{1/2}$ = 23.0 h for 30S and $t_{1/2}$ = 18.0 h for 50S (Figure 4.5f).

4.3.1.4 Cells starved of phosphate rapidly degrade ribosomes

Cells starved of phosphate showed a greater depletion of rRNA than cells starved of nitrogen or carbon (Figure 4.3d). These cells were atypical in that they showed a

steady increase in optical density during the first four days of phosphate starvation (Figure 4.2a). However, the number of colony forming units per mL of cells steadily decreased, with the cells having a half-life of 14 h (Figure 4.2b). Because the number of viable cells is not increasing, the increase in OD_{600} likely reflects changes in the shape of phosphate-starved bacteria or of dead bacteria affecting the light scattering. The 70S ribosome population maintained a consistent level during the first 5.5 h of starvation (Figure 4.4). Beyond 5.5 h of phosphate starvation, there was a steady decrease in the number of 70S ribosomes in the cell and by 27 h of starvation, the 70S ribosomes had been fully degraded. The total 30S and 50S subunit populations decayed with similar rates (Figure 4.5d and Table 4.1) with $k_{decay} = 0.102\ h^{-1}$ for the total 30S and $k_{decay} = 0.152\ h^{-1}$ for the total 50S. These decay rates correspond to $t_{1/2} = 6.8$ h for 30S and $t_{1/2} = 4.6$ h for 50S (Figure 4.5f). As with the 70S ribosomes, by 27 h of phosphate starvation the 30S and 50S subunits were completely degraded.

4.3.1.5 Cells starved of magnesium rapidly degrade ribosomes

Cells grown to exponential phase in LB were depleted of magnesium by resuspension in M9 salts lacking magnesium. These cells showed a slight decrease in optical density over the first four days of magnesium starvation (Figure 4.2a). The number of colony forming units per mL of cells steadily decreased, with the cells having a half-life of 8 h (Figure 4.2b). Similar to phosphate starvation, depletion of magnesium appears to be quite deleterious to the rRNA in the stressed cells. After 5.5 h of magnesium starvation, the amounts of all three complexes were greatly reduced (Figure 4.3e, 4.4 and 4.5e). After 18 h of starvation, all three rRNA species had disappeared. The

decay rates for the total 30S and 50S subunits were fairly high with k_{decay} = 0.121 h^{-1} for the 30S subunits and k_{decay} = 0.200 h^{-1} for the 50S subunits (Table 4.1). These decay rates correspond to $t_{1/2}$ = 5.7 h for 30S and $t_{1/2}$ = 3.5 h for 50S (Figure 4.5f). These are likely underestimates of the half-lives. The cells have far less total RNA at the start of starvation than any of the other bacterial stress conditions (Figure 4.3). It appears that a significant portion of the total RNA that would have been present in the cell before resuspension in minimal media has degraded before the first sample was able to be collected.

4.3.2 Ribosomal RNA becomes more exposed during stationary phase

DMS probing was performed in cells that were grown in LB to late stationary phase. Time points were selected throughout the first four days of incubation. As with the sucrose gradients, the first time point was selected to be when the cells reached their maximum optical density (OD_{600} = 3.7) and seven samples were taken over the next 90 h. The rRNA sequences all showed good coverage and read depth. The probed RNA in stationary phase cells was generally more DMS reactive than RNA in exponential phase cells (Figure 4.6). This reflects a greater level of disorder in the ribosome structures in stationary phase cells, potentially improving cleavage opportunities for RNases.

In the small subunit of the ribosome, there were some slight changes in the DMS reactivity pattern in the first 5.5 h of late stationary phase. Around the time of entry to late stationary phase, as shown in the initial time point in Figure 4.6a, the 5' domain of the 16S had generally heightened DMS reactivity relative to exponential phase cells, with notable reactivity in h8, h15, and h17. The central domain had increased reactivity in h21

and h22, but otherwise had a similar modification profile as it would in exponential phase cells. The 3' domain had a few regions of increased DMS reactivity. These were mostly in h31, h41, h42, h43, and h44. There was also a very protected region at J44/45.

After 1.5 h in late stationary phase, there were additional changes in the reactivity profile (Figure 4.7b). There were fewer reactive bases in the 5' and 3' domains. The central domain still showed reactivity in h21, but the rest of the domain was similar to its exponential phase reactivity.

In the 5.5 h time point (Figure 4.7c and Figure 4.10), the 16S rRNA was generally slightly more protected. There were regions of greater protection throughout the 16S, with the possible exception of the 3' minor domain. The protection was notable in h6, h8, h13, and h33.

Over the next three days of incubation, the ribosomes steadily degraded. The reactivity profiles for the 16S were similar during these later time points, with increased DMS reactivity in h3, h15, h17, h21, and h41. Notable in all of these was that reactivity near the central pseudoknot was near the levels seen in exponential phase cells (Figure 4.9a). This suggests that this region is susceptible to endonucleolytic cleavage and could initiate the steady degradation of 30S subunits.

Entering into late stationary phase (0 h), the 23S showed increased DMS reactivity fairly evenly throughout all domains except domain IV (Figure 4.8a). This continued after 1.5 and 5.5 h of late stationary phase. Although the reactivity patterns were similar at the entry to late stationary phase and 5.5 h later, domain IV was more exposed and domain V was more protected after 5.5 h (Figure 4.8b). There were no large

changes seen in the protection of the peptidyl transferase center relative to cells in exponential phase (Figure 4.9b).

During degradation initiated by quality control or carbon starvation, it has been shown that RNase E cleaves the 23S rRNA after C1942 (Sulthana 2016). The two bases C1941 and C1942 had a perceptible change in DMS reactivity. In the first 18 h of incubation, C1941 was more reactive than in exponential phase and C1942 was more protected than exponential phase for every time point except 5.5 h. After 5.5 h, C1942 was still more protected than exponential phase and there was no change for C1941.

4.3.3 Structural changes occurring in the ribosome during nitrogen starvation

DMS probing was performed in cells that were suspended in minimal media lacking nitrogen. Time points were selected throughout the first four days of incubation. The rRNA sequences all showed full coverage and good read depth. The probed RNA in cells depleted of nitrogen was slightly more DMS reactive than RNA in exponential phase cells, but generally had very similar overall reactivity (Figure 4.11). As was seen in the polysome profiles (Figure 4.3), the cells starved of nitrogen retained high levels of rRNA, but still saw degradation over time (Figure 4.4 and 4.5b). The DMS reactivity reflects this slight increase in structural flexibility.

At the onset of nitrogen starvation (0 h), there were increases in the DMS reactivity in h17, h21, h22, h41, h42, and h43 (Figure 4.12a), similar to what was seen for 16S rRNA in cells grown to late stationary phase at high cell density. However, there were also large regions protected from DMS probing. The 3' domain is very protected in

h31, h33, and J44/45. The central pseudoknot was also well protected. This is likely a central reason why so little degradation is seen under nitrogen starvation conditions.

After 1.5 h of nitrogen starvation, the 5' domain became more protected, particularly h6, h8, and h13 (Figure 4.12b). The previously protected regions h31, J44/45, and the central pseudoknot were still protected.

From 5.5 h to 60 h of nitrogen starvation, the 16S reactivity profile was consistent, with h17 and h41 regularly exposed and much of the 3' domain protected. In the 3' domain, h31, h33, J44/45, and the central pseudoknot were consistently protected (Figure 4.14a) and h26 and h27 became more protected over time.

After 90 h of nitrogen starvation, the reactivity profiles began to change. The 5' domain was more reactive and the central pseudoknot was no longer protected. Beyond 90 h of nitrogen starvation, the RNA extraction yield was too low to perform sequencing.

In the large subunit, at the onset of nitrogen starvation (Figure 4.13a), there was a general increase in DMS reactivity in all domains except domain IV. Also, while there was a general increase in the reactivity in domain V, the peptidyl transferase center became more protected (Figure 4.14b). As nitrogen starvation continued, each of the domains became significantly more protected from DMS probing. The peptidyl transferase center remained protected throughout nitrogen starvation.

A region worth noting is the set of nucleotides just upstream of Helix 71: residues C1941 and C1942. During periods of starvation, RNase E cleaves the 23S rRNA after C1942 (Sulthana 2016). After 1.5 h of nitrogen starvation (Figure 4.13b), these residues were both more exposed and after 5.5 h, C1942 was much more exposed. Beyond 5.5 h, both bases exhibited DMS reactivity comparable to what would be seen in exponential

phase cells. These probing results would suggest a more rapid degradation of free 50S during the first few hours of starvation, followed by a slower degradation for the remainder of starvation. This difference in turnover rates is not seen in the polysome profiles, however (Figure 4.5b).

4.4 Discussion

4.4.1 Sucrose gradients show different ribosomal responses to different cellular stresses

Each of the five bacterial stress conditions resulted in slightly different ribosomal responses, but all cells exhibited the same general pattern. Over time, the 70S ribosomes were separated into their individual subunits. At the same time, free 30S and 50S subunits were also being degraded. The kinetics of ribosomal decay varied for the different stress conditions. Cells starved of nitrogen had the slowest decay of 70S ribosomes and the slowest decay of free subunits. Cells starved of carbon also had slow decay of 70S ribosomes and subunits, but the ribosomal RNA did not persist as long as in cells starved of nitrogen. The other stress conditions exhibited more rapid degradation of ribosomal RNA. Of the three, phosphate starvation showed the slowest degradation of 70S ribosome and subunits, then cells starved of magnesium, and finally, late stationary phase cells. However, cells in late stationary phase retained ribosomal complexes longer than magnesium-starved cells, owing to a much larger amount of total rRNA at the start of the bacterial stress.

The 50S subunits had faster decay rates than the 30S subunits for each of the stress conditions (Table 4.1). This may be slightly misleading for the starvation conditions. For each of the four starvation conditions, there are more 50S subunits at the start of starvation than 30S subunits (Figure 4.5). This could be occurring for multiple reasons. One possibility is that there is ribosomal degradation taking place during the time when cells are being resuspended in minimal media before the first time point is taken. This certainly seems to be the case for cells starved of magnesium. Another possibility is that in the starvation conditions, notably nitrogen, carbon, and magnesium starvation, there are overlapping peaks in the polysome profiles (Figure 4.3) and this is affecting the peak integration that is used for the calculations of relative subunit amounts (Figure 4.5). The ribosome subunit decay patterns were similar for each of the starvation conditions, suggesting decay was occurring at similar rates for the subunits and the differences are in the initial scaling. For cells that were grown to late stationary phase, the starting amounts of total 30S and 50S subunits were identical (Figure 4.5a). In that case, there was a difference in decay rate with 50S subunits being degraded more rapidly than 30S subunits. It is possible that cells engage in different degradation pathways under different circumstances. In cells grown to late stationary phase, it may be preferential to degrade 50S subunits more rapidly than 30S subunits. Degrading a 50S subunit releases almost twice the amount of nutrients to the cell that degrading a 30S subunit would release.

The different responses to starvation conditions clearly relates to the localization of different nutrients within the cell. Cells retained ribosomal particles the longest during nitrogen and carbon starvation, with cells in both conditions still containing large pools of

30S subunits, 50S subunits, and 70S ribosomes after 24 h of starvation. Cells starved of phosphate were almost completely depleted of rRNA after 24 h and cells starved of magnesium had lost all rRNA within the first 18 h of starvation. Ribosomes contain all four nutrients: nitrogen, carbon, phosphate, and magnesium. But nitrogen and carbon are readily available from protein sources in the cell that are also subject to degradation during starvation conditions. Turnover of mRNAs will also provide the cell with phosphate and magnesium, but the degradation of ribosomes will be the primary source from which nutrient-starved cells are replenished with phosphate and magnesium. Ribosomes are abundant and particularly rich in phosphate and magnesium. The total intracellular concentration of Mg^{2+} in *E. coli* has been determined to be near 100 mM (Akanuma 2014; Moncany 1981). The amount of Mg^{2+} associated with ribosomes is estimated to be near 12 mM during exponential phase growth (Nierhaus 2014). By comparison, the amount of free Mg^{2+} in a cell is near 1 mM (Alatossava 1985). For phosphate, the total intracellular concentration has been shown to be directly related to the concentration of total intracellular RNA (Wade 1952).

4.4.2 Effects of the late stationary phase and nitrogen starvation on ribosomes

DMS probing was performed in cells that were grown in LB to late stationary phase and in cells that were starved of nitrogen. Overall, cells in late stationary phase have higher mutation rates than those in exponential phase cells (Figure 4.6) and nitrogen starvation results in mutation rates that are similar to those seen in exponential phase cells (Figure 4.11). This suggests the rRNA in late stationary phase has a higher overall solvent accessibility than in either nitrogen starvation or exponential phase. Cells in late

stationary phase see a much greater degree of rRNA degradation than cells in nitrogen starvation conditions. This increase in exposure, and the corresponding increase in accessibility of RNases, would explain the more rapid rRNA degradation in late stationary phase.

It has previously been shown that during periods of carbon starvation, the 16S rRNA is cleaved by RNase E between A919 and U920, near the central pseudoknot (Sulthana 2016). The fragments derived from this cleavage event are rapidly degraded by exoribonucleases (Basturea 2011). For cells starved of nitrogen, there was an increase in protection for the central pseudoknot in 16S rRNA (Figure 4.14a). The degradation of 30S subunits likewise proceeded at a much slower rate than other conditions tested (Figure 4.5f). These subunits appear to be protected from RNase degradation by limiting the solvent exposure of RNA regions sensitive to degradation.

For stationary phase cells, there is no significant change in the protection of the central pseudoknot. This, combined with the general increase in solvent exposure of rRNA in stationary phase relative to exponential phase, could explain why the ribosomal subunits are degraded over six times faster in stationary phase cells than cells starved of nitrogen. The increased exposure of the central pseudoknot makes the small subunit more susceptible to RNase degradation during stationary phase.

The DMS probing patterns do not appreciably change over time for cells in late stationary phase or in cells starved of nitrogen. This suggests that the 70S ribosomes and the 30S and 50S subunits do not experience great structural changes during the course of their prolonged stress. It appears there is not a slow structural degeneration in ribosomes that occur over time, but instead more sudden changes in structure for individual

ribosomes or subunits during stress. This will result in their rapid degradation while the remaining pool is unaffected. This is consistent with previous results looking at ribosomal degradation during cellular stress (Deutscher 2009; Kaplan 1975a).

4.4.3 Absence of the 100S ribosomal particle during stationary phase

In the work presented in this chapter, the 100S ribosomal complex is not observed. Despite the extensive use of MRE600 cells for ribosomal and translational research, there have been no studies looking at ribosomal RNA in MRE600 during starvation or stationary phase. Studies have been performed with MRE600 during stationary phase (Ramagopal 1974; Subramanian 1980), but the polysome profile of the cells was never a consideration. As such, there is no mention in the literature regarding the appearance of the 100S ribosome in MRE600.

E. coli ribosomes are known to adopt a 100S dimer state in response to nutritional stress (Wada 1998). The dimerization process is assisted by the ribosome modulation factor (RMF) and the hibernation promoting factor (HPF) (Maki 2000; Wada 1990). A third protein, YfiA, has been shown to bind to 70S ribosomes in stationary phase (Maki 2000). YfiA binds to 30S subunits at the subunit interface and prevents dissociation of the 70S (Agafonov 1999). YfiA also antagonizes the formation of 100S ribosome dimers (Ueta 2005). A fourth protein, RsfA, binds to L14 on 50S subunits, protecting the interfacial region and inhibiting both the formation of 70S and 100S complexes (Häuser 2012).

As with the previously described probing experiments (Chapter 2 and 3), MRE600 *E. coli* cells were used for these studies. MRE600 is an *E. coli* strain that is

closely related to the genus *Shigella* (Kurylo 2016). MRE600 lacks RNase I activity and has been widely adopted for studies in which stable RNA will need to be extracted because of the reduced likelihood of non-specific RNA cleavage. Despite its extensive use in the ribosome and translation literature, there have been no studies looking at ribosomal RNA in MRE600 during starvation or stationary phase. Studies have been performed with MRE600 during stationary phase (Ramagopal 1974; Subramanian 1980), but the polysome profile of the cells was never a consideration. As such, there is no mention in the literature regarding the appearance of the 100S ribosome in MRE600. A phosphate starvation study was performed using an *E. coli* strain lacking RNase I (strain D10) and no 100S was observed (Davis 1986). The authors observed that the kinetics of cell death were similar in MRE600 and 100S was not mentioned. Other strains lacking RNase I have also been shown to not form 100S ribosomes (Kaplan 1975; Wada 2000). In strains that do possess the capacity to form 100S ribosomes, the cells are able to survive nutrient depletion for a longer period of time than cells that cannot form 100S ribosomes (Kalpaxis 1998).

In my work, the 100S ribosome was not observed in any of the stress conditions tested. The genome of MRE600 has been sequenced and it contains RMF, HPF, YfiA, and RsfA. Previous DMS probing studies have shown that the protein RMF inactivates ribosomes by covering the peptidyl transferase center (Yoshida 2004). It is possible that this protein is still functioning in this capacity, even though the ribosome dimerization does not occur. For cells starved of nitrogen, the peptidyl transferase center is highly protected (Figure 4.14b). Under conditions of nitrogen starvation, the 50S subunits degraded slower than under any other stress condition tested (Figure 4.5f). Conversely,

cells in late stationary phase showed no increase in protection in the peptidyl transferase center. The 50S subunits in stationary phase cells degraded over ten times faster than 50S subunits in cells starved of nitrogen (Figure 4.5f). This could reflect a role played by RMF in stabilizing the ribosome under nitrogen starvation.

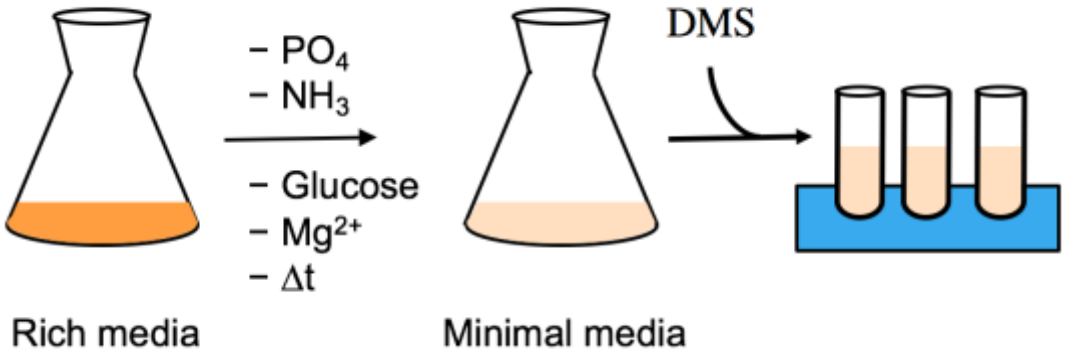

Figure 4.1. Schematic of DMS probing in *E. coli* cells depleted of nutrients Cells are either grown to late stationary phase in rich media or resuspended in a minimal media lacking one of four nutrients: phosphate, nitrogen, carbon, or magnesium. Aliquots from each are removed over time and probed with DMS.

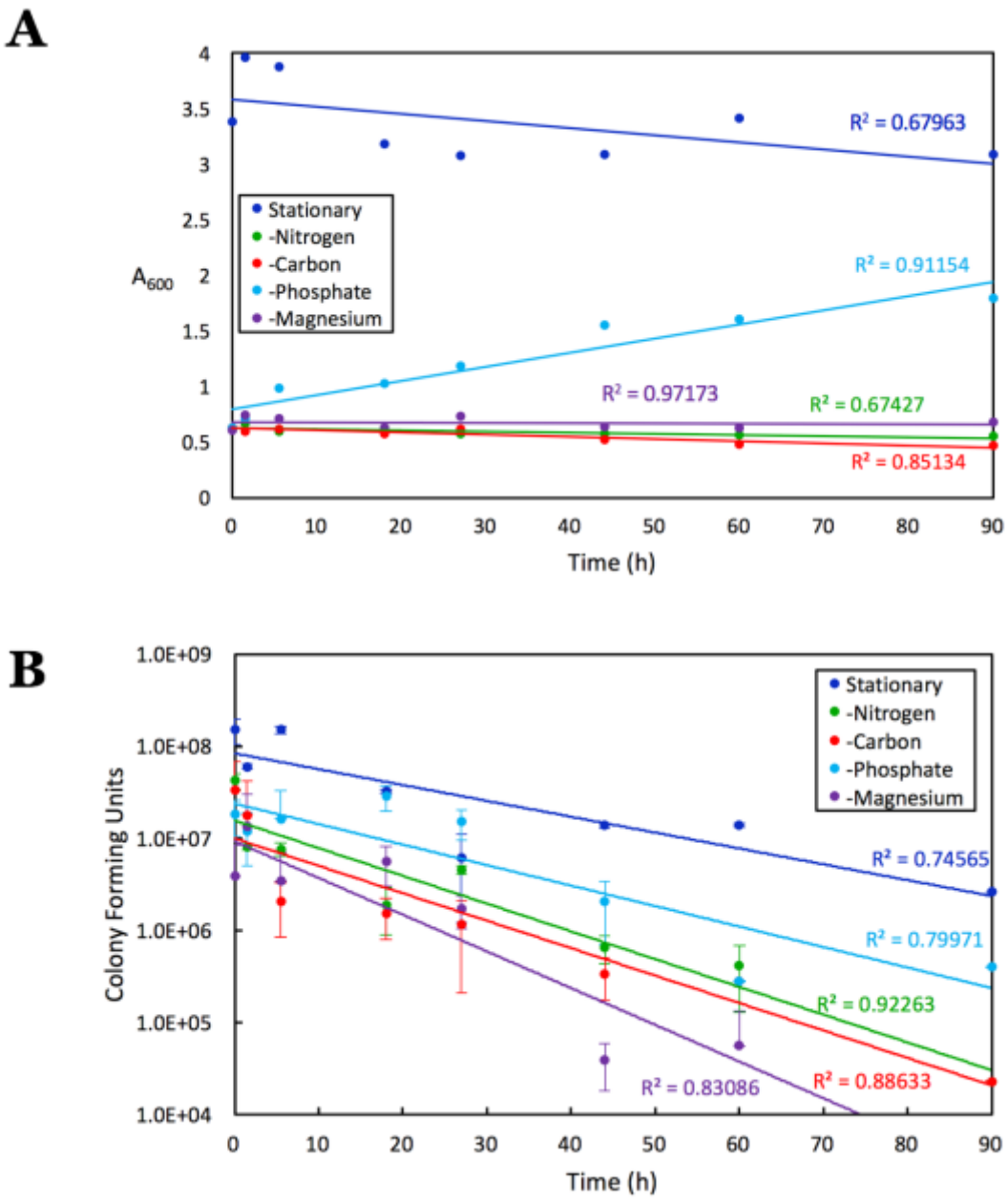

Figure 4.2. Growth curves of MRE600 during cellular stress Growth curves of MRE600 over the course of 90 h of cellular stress as measured by (a) OD_{600} and (b) colony forming units per mL of cells.

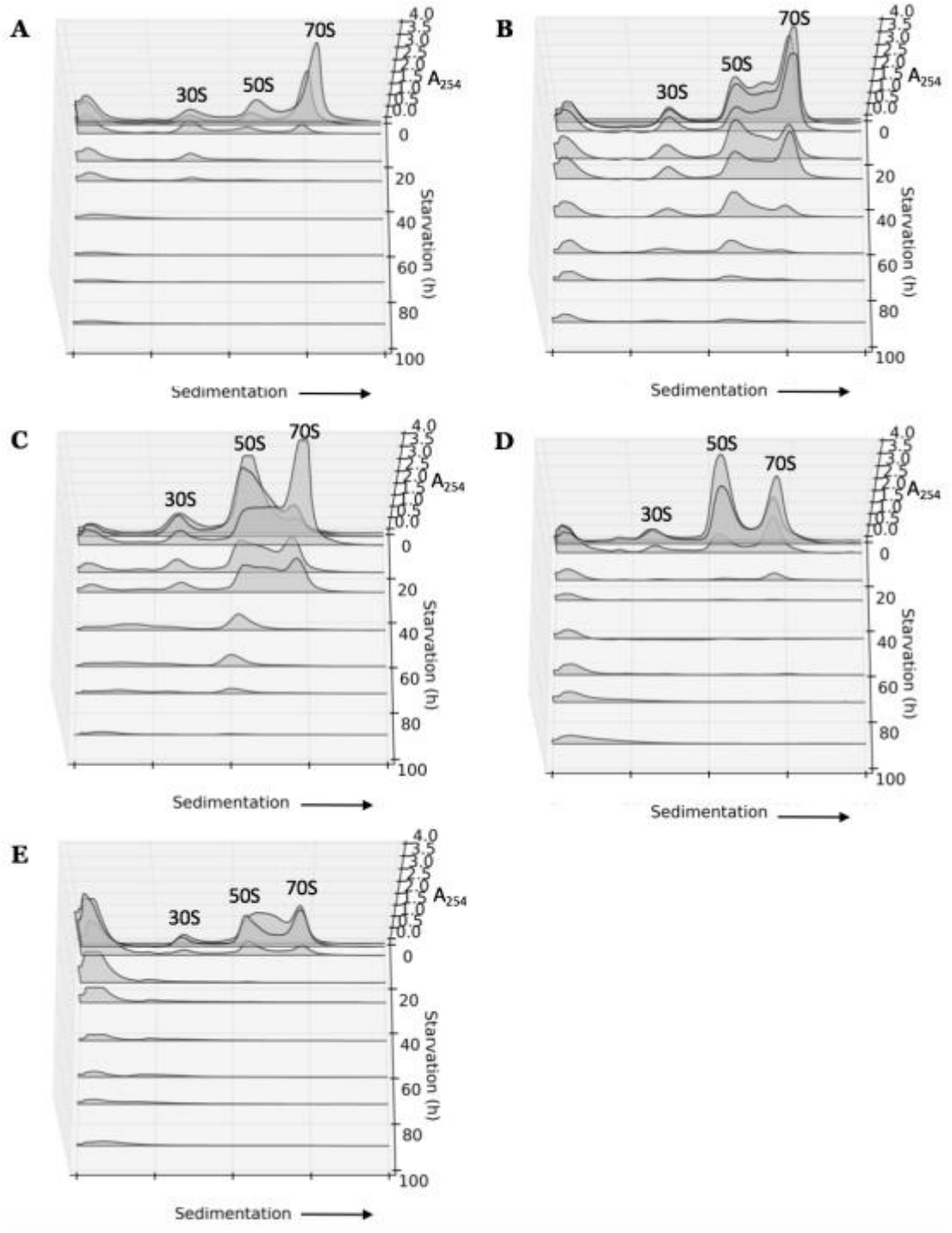

Figure 4.3. Kinetics of ribosome degradation in MRE600 during nutrient depletion
(a-e) Polysome profiles after 0 – 90 h of: (a) incubation in the stationary phase, (b) nitrogen starvation, (c) carbon starvation, (d) phosphate starvation, and (e) magnesium starvation. Absorbance was normalized by the starting OD600 and the RNA concentration at each time point to more clearly compare the amount of rRNA in between time points and between stress conditions.

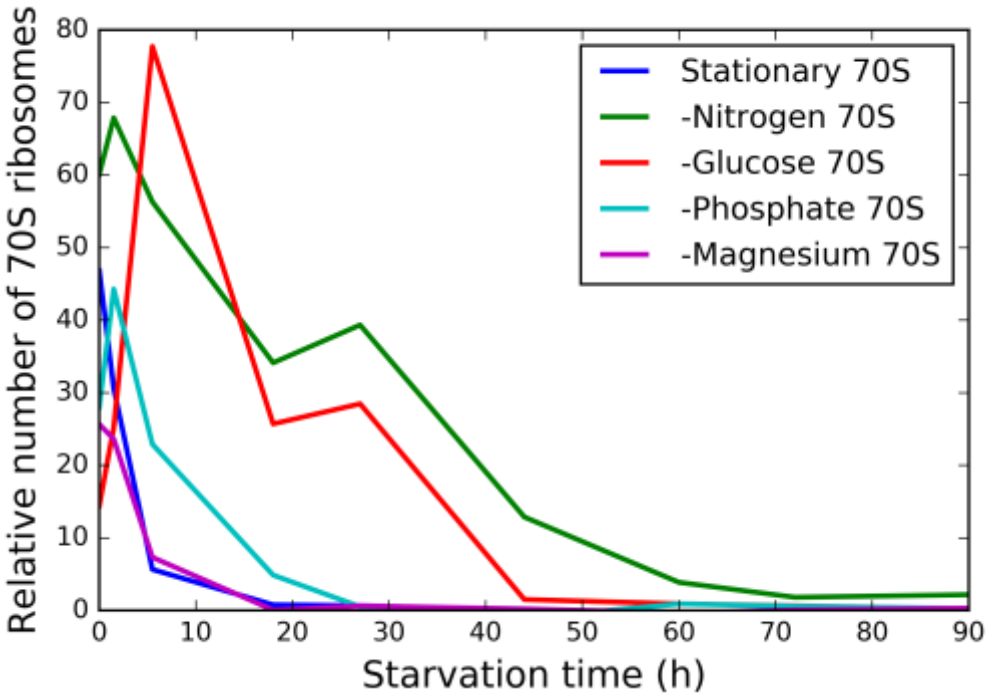

Figure 4.4. Rate of 70S ribosome breakdown in MRE600 under bacterial stress conditions These curves depict the area under the 70S peaks for each of the polysome profiles in Figure 4.2. For each bacterial stress condition, there is breakdown of 70S ribosomes over time. This process occurs on different time scales for the various stress conditions.

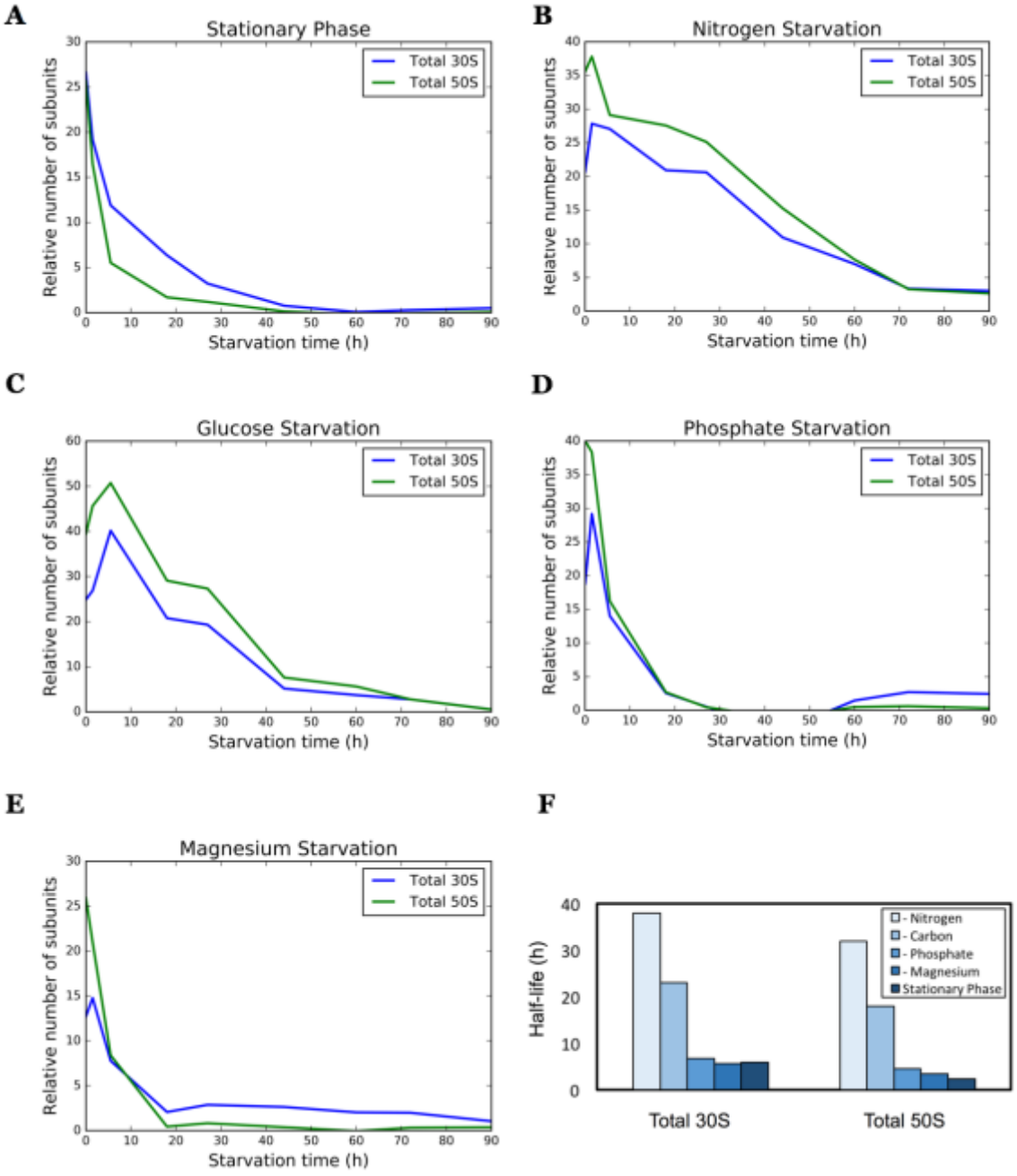

Figure 4.5. Kinetics of ribosomal subunit degradation in MRE600 under bacterial stress conditions The total amount of 30S and 50S subunits in cells was calculated from the area under the peaks of the polysome profiles in Figure 4.2. The contributions of each subunit to the 70S peak was calculated and included in the total intracellular subunit levels presented here. Curves shown here were normalized by the absorbance for each subunit, so that equal amounts of 30S to 50S would appear the same. (a) Stationary phase. (b) Nitrogen starvation. (c) Carbon starvation. (d) Phosphate starvation. (e) Magnesium starvation. (f) Half-lives for 30S and 50S subunits under each stress condition.

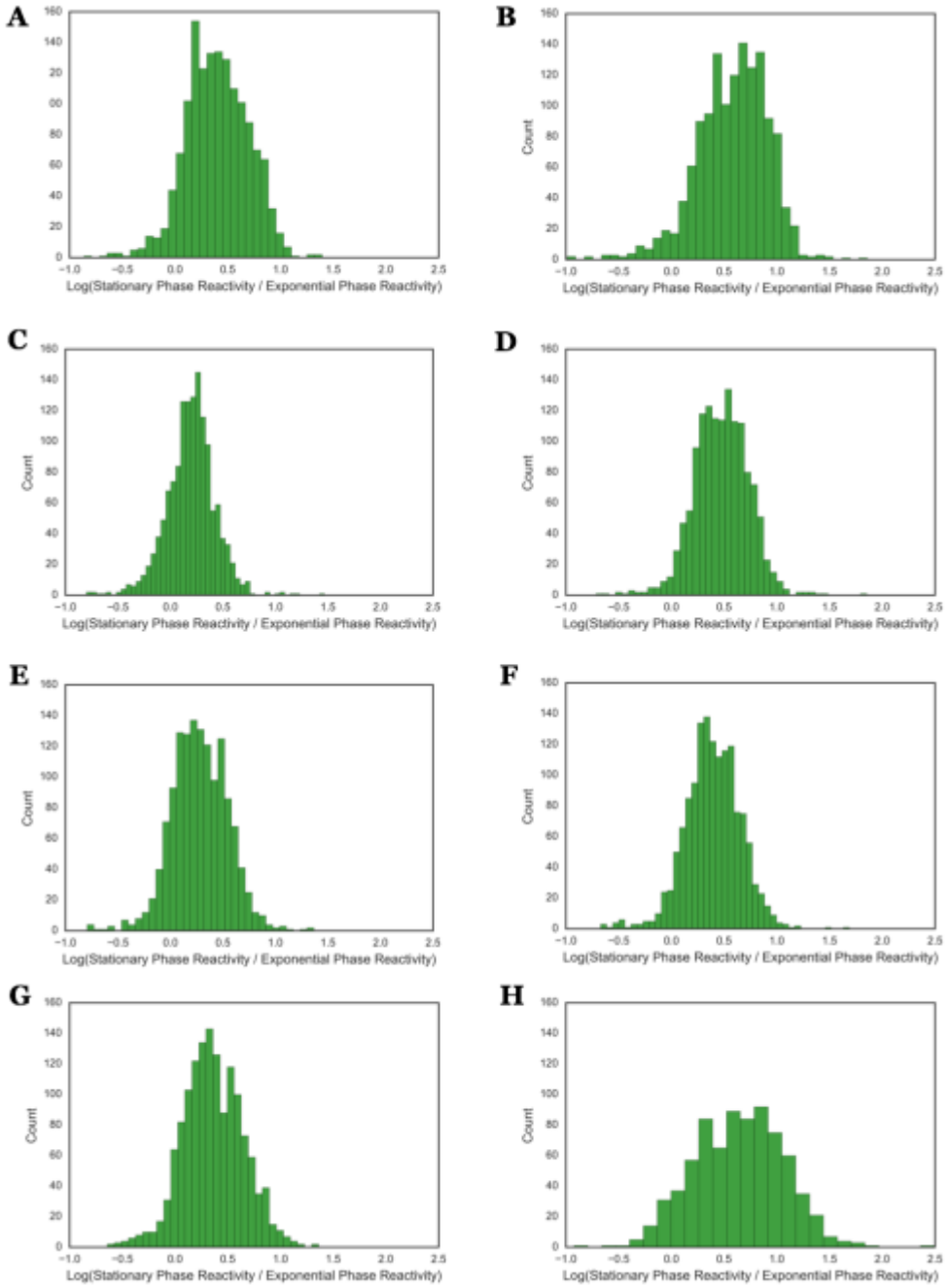

Figure 4.6. Mutation rates for *E. coli* cells in late stationary phase Histograms of the log ratio of the reactivity of each nucleotide in RNA in stationary phase cells over RNA in exponential phase cells. RNA in stationary phase cells experience higher levels of DMS probing than RNA in exponential phase cells. Binwidth, h, for each histogram is calculated using a Freedman-Diaconis estimator: $h = 2*IQR/n^{1/3}$, where IQR is the interquartile range and n is the number of observations. Samples were collected after: (a) cells entered late stationary phase (OD_{600} = 3.7), with h=0.072, (b) +1.5 h, with h=0.081, (c) +5.5 h, with h=0.047, (d) +18 h, with h=0.061, (e) +27 h, with h=0.065, (f) +44 h, with h=0.058, (g) +60 h, with h=0.067, and (h) +90 h, with h=0.131.

Figure 4.7. Secondary structures of 16S rRNA in late stationary phase *E. coli* Color bar shows coloring of residues. The deepest red indicates largest $\log_{10}$(experimental reactivity rate / exponential phase reactivity rate). The deepest blue is the negative of this value. The color scheme is continuous, rather than binned. (a-d) DMS reactivities in the 16S rRNA secondary structures after: (a) 0 h, (b) 1.5 h, (c) 5.5 h, and (d)18 h.

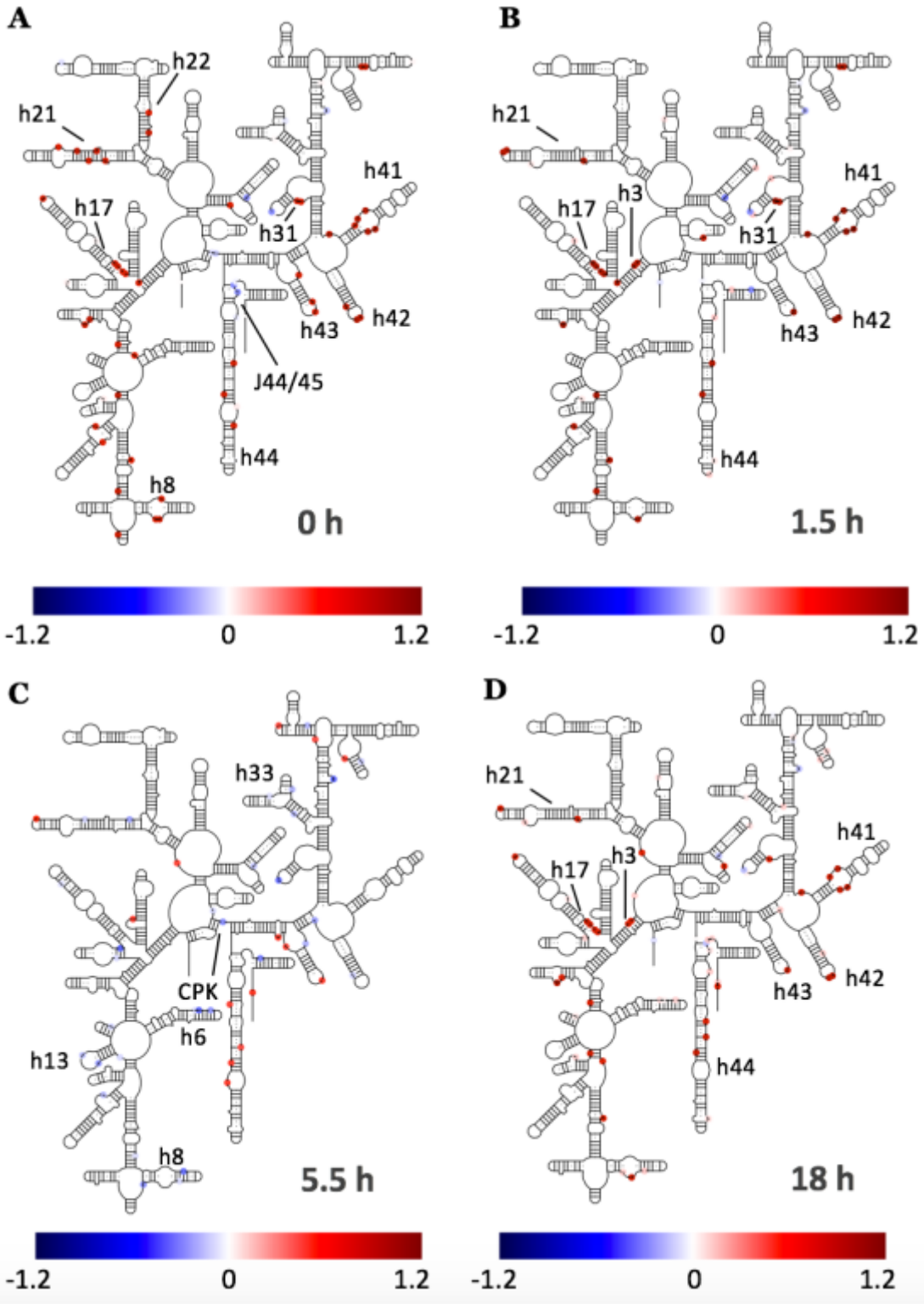
A
h22
h21
h41
h17
h31
h43
h42
J44/45
h44
h8
0 h
-1.2
0
1.2
B
h21
h3
h41
h17
h31
h43
h42
h44
1.5 h
-1.2
0
1.2
C
h33
CPK
h6
h13
h8
5.5 h
-1.2
0
1.2
D
h21
h41
h3
h17
h43
h42
h44
18 h
-1.2
0
1.2

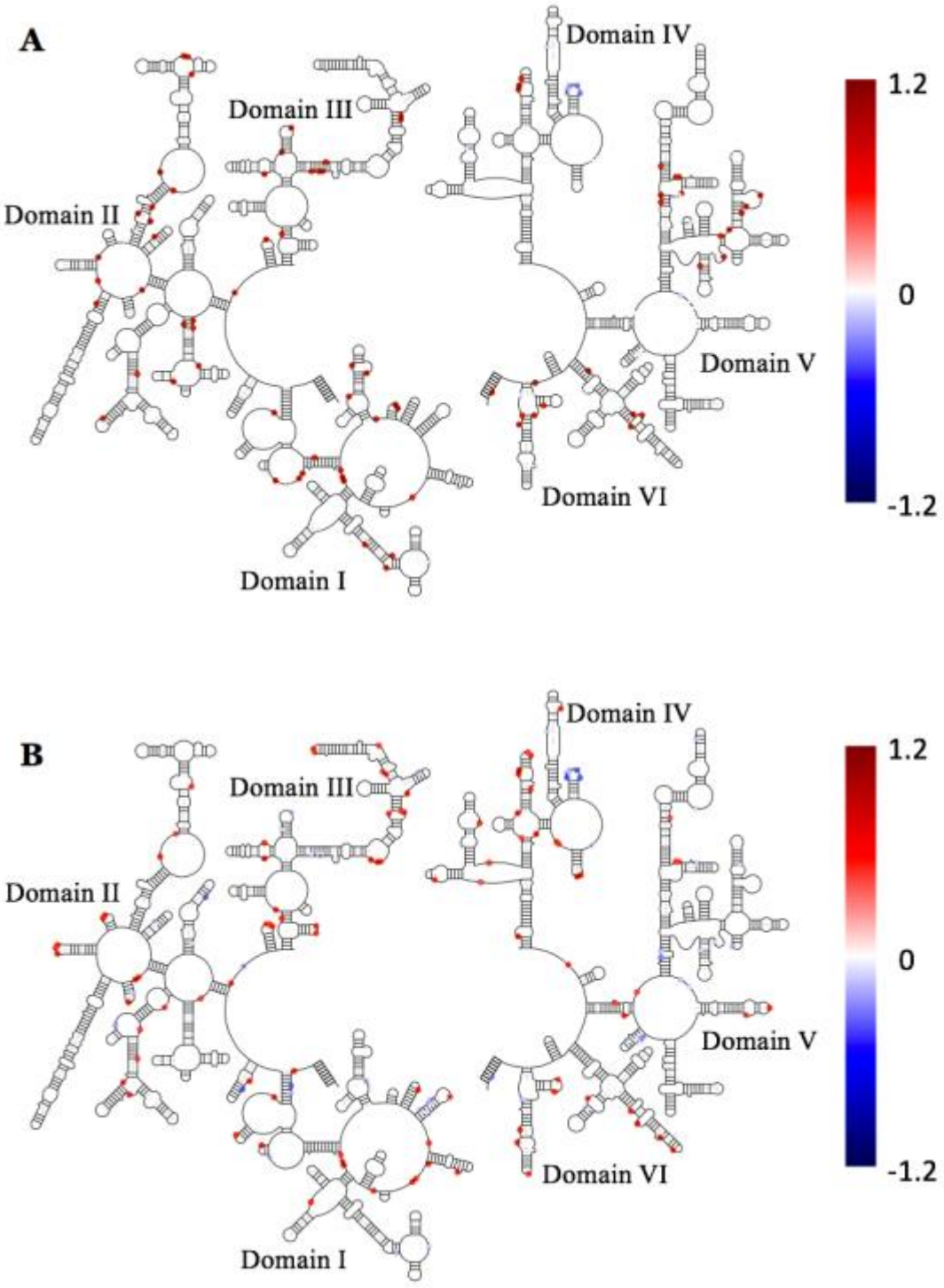

Figure 4.8. Secondary structures of 23S rRNA in late stationary phase *E. coli* Color bar shows coloring of residues. The deepest red indicates largest $\log_{10}$(experimental reactivity rate / exponential phase reactivity rate). The deepest blue is the negative of this value. The color scheme is continuous, rather than binned. DMS reactivities in the 23S rRNA secondary structures after: (a) 0 h and (b) 5.5 h.

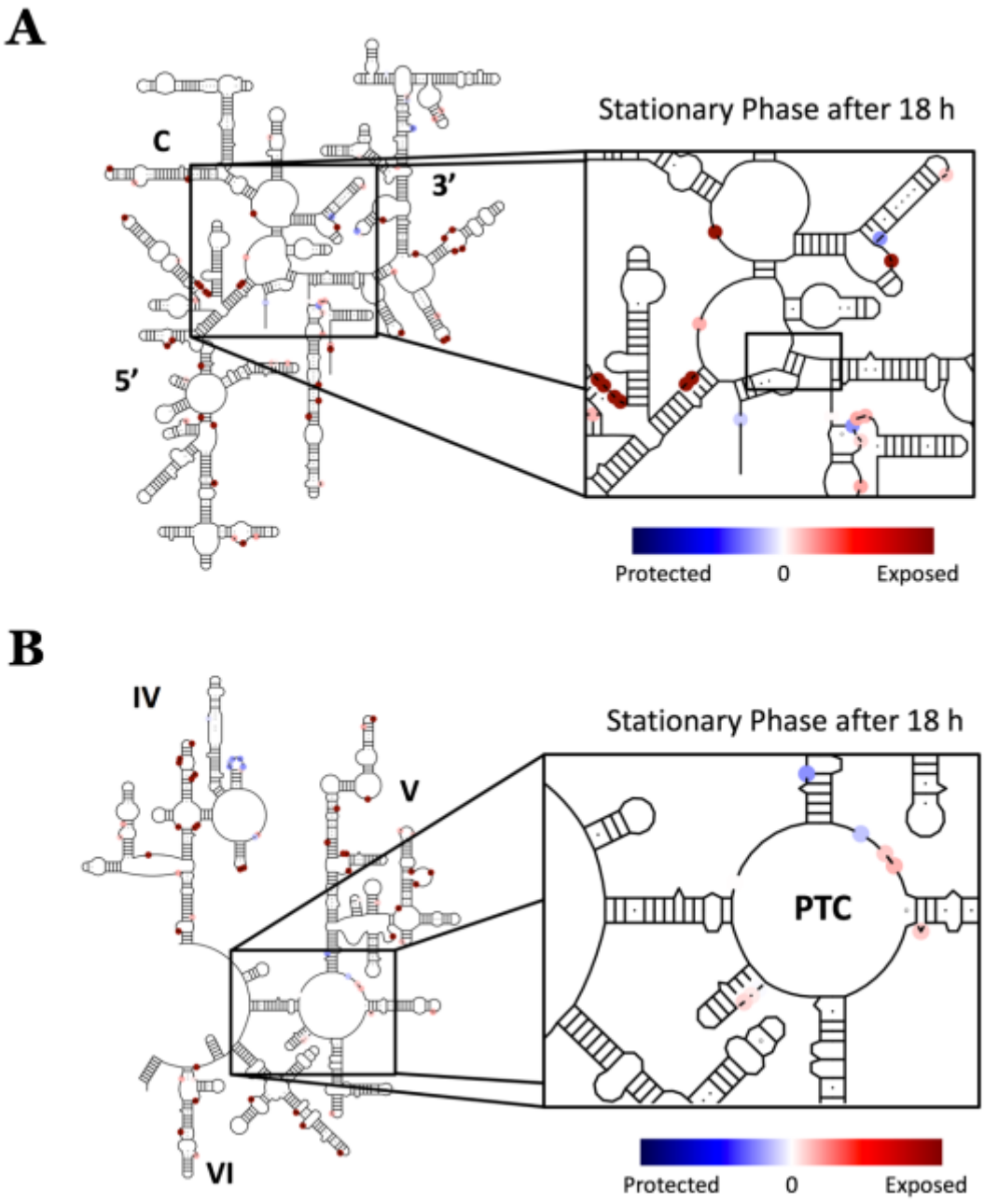

Figure 4.9. Secondary structures of rRNA in late stationary phase *E. coli* Color bar shows coloring of residues. The deepest red indicates largest $\log_{10}$(experimental reactivity rate / exponential phase reactivity rate). The deepest blue is the negative of this value. The color scheme is continuous, rather than binned. DMS reactivities in the 16S and 23S rRNA secondary structures after 18 h of incubation in stationary phase. (a) The central pseudoknot of the 16S rRNA. (b) The peptidyl transferase center of the 23S rRNA.

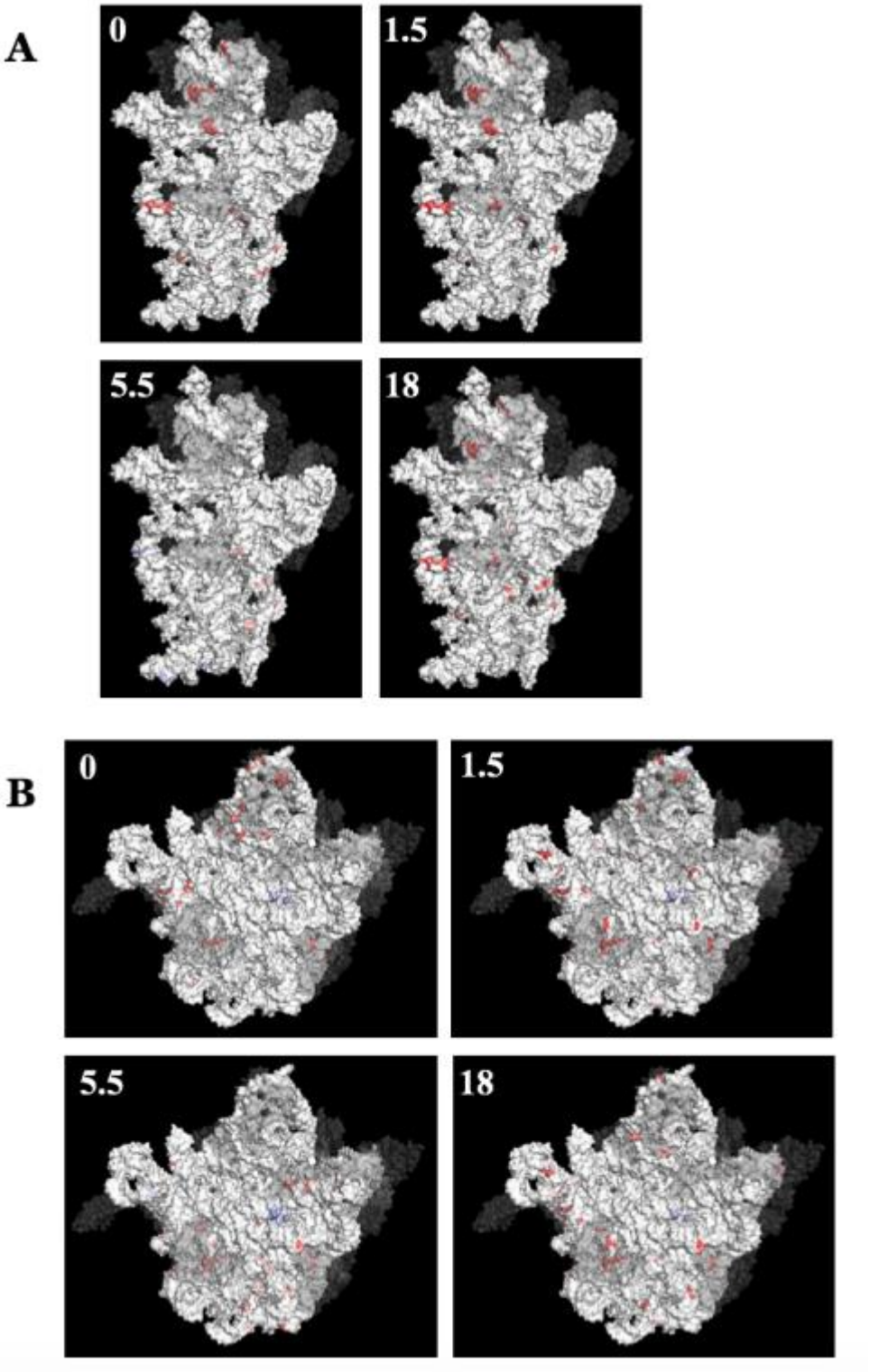

Figure 4.10. The 3D structures of ribosome subunits in late stationary phase *E. coli* (a) 30S subunit interface after 0, 1.5, 5.5, or 18 h. (b) 50S subunit interface after 0, 1.5, 5.5, or 18 h.

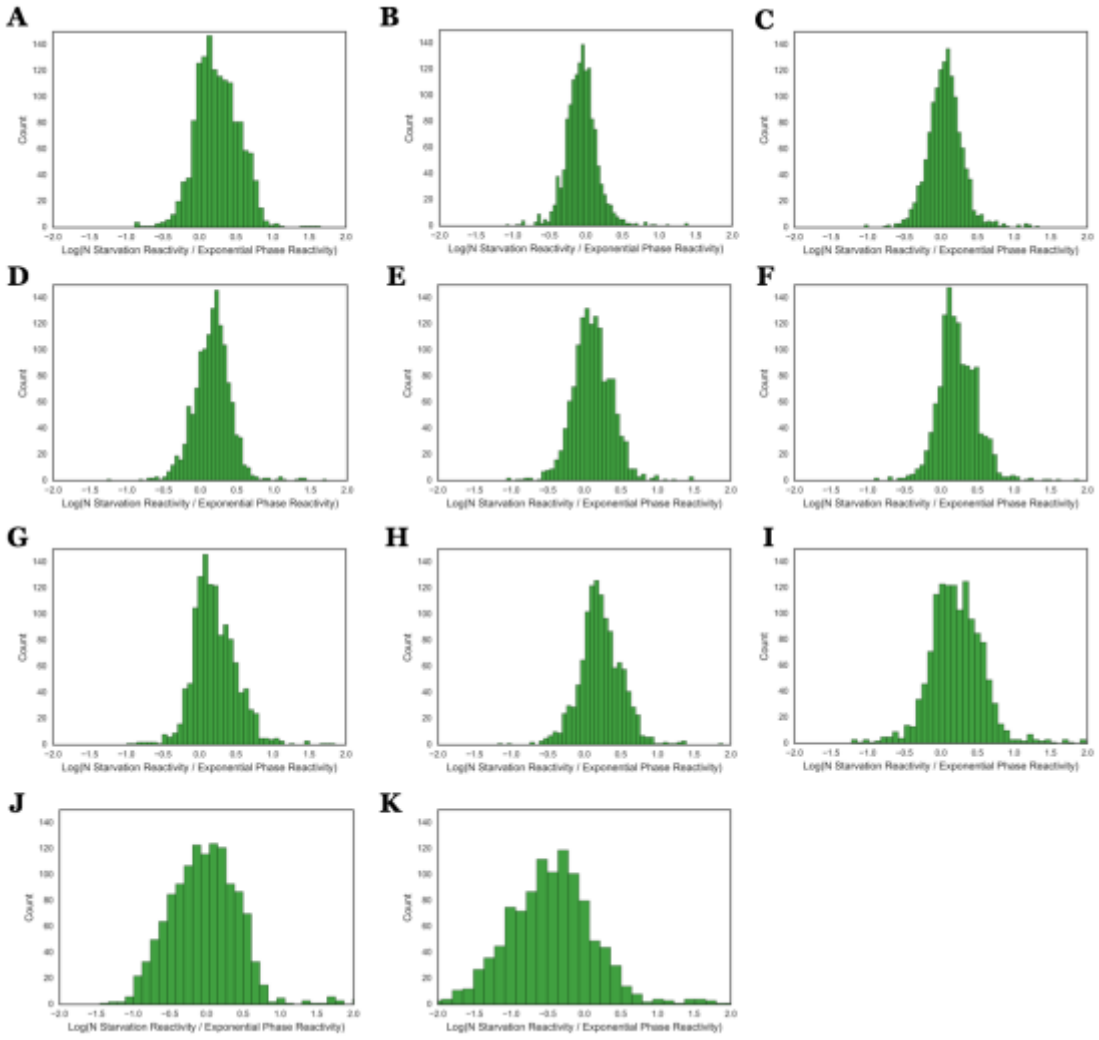

Figure 4.11. Mutation rates for *E. coli* cells starved of nitrogen Histograms of the log ratio of the reactivity of each nucleotide in RNA in cells starved of nitrogen over RNA in exponential phase cells. RNA in cells depleted of nitrogen experience similar levels of DMS probing as RNA in exponential phase cells. Binwidth, *h*, for each histogram is calculated using a Freedman-Diaconis estimator: $h = 2*IQR/n^{1/3}$, where IQR is the interquartile range and n is the number of observations. Samples were collected after incubation in nitrogen-lacking minimal media for: (a) 0 h, with *h*=0.071, (b) 1.5 h, with *h*=0.043, (c) 5.5 h, with *h*=0.051, (d) 18 h, with *h*=0.054, (e) 27 h, with *h*=0.059, (f) 44 h, with *h*=0.062, (g) 60 h, with *h*=0.069, (h) 90 h, with *h*=0.063, (i) 120 h, with *h*=0.080, (j) 186 h, with *h*=0.114, and (k) 336 h, with *h*=0.144.

Figure 4.12. Secondary structures of 16S rRNA in *E. coli* starved of nitrogen Color bar shows coloring of residues. The deepest red indicates largest $\log_{10}$(experimental reactivity rate / exponential phase reactivity rate). The deepest blue is the negative of this value. The color scheme is continuous, rather than binned. (a-d) DMS reactivities in the 16S rRNA secondary structures after being starved of nitrogen for: (a) 0 h, (b) 1.5 h, (c) 18 h, and (d) 90 h. Color bar shows coloring of residues.

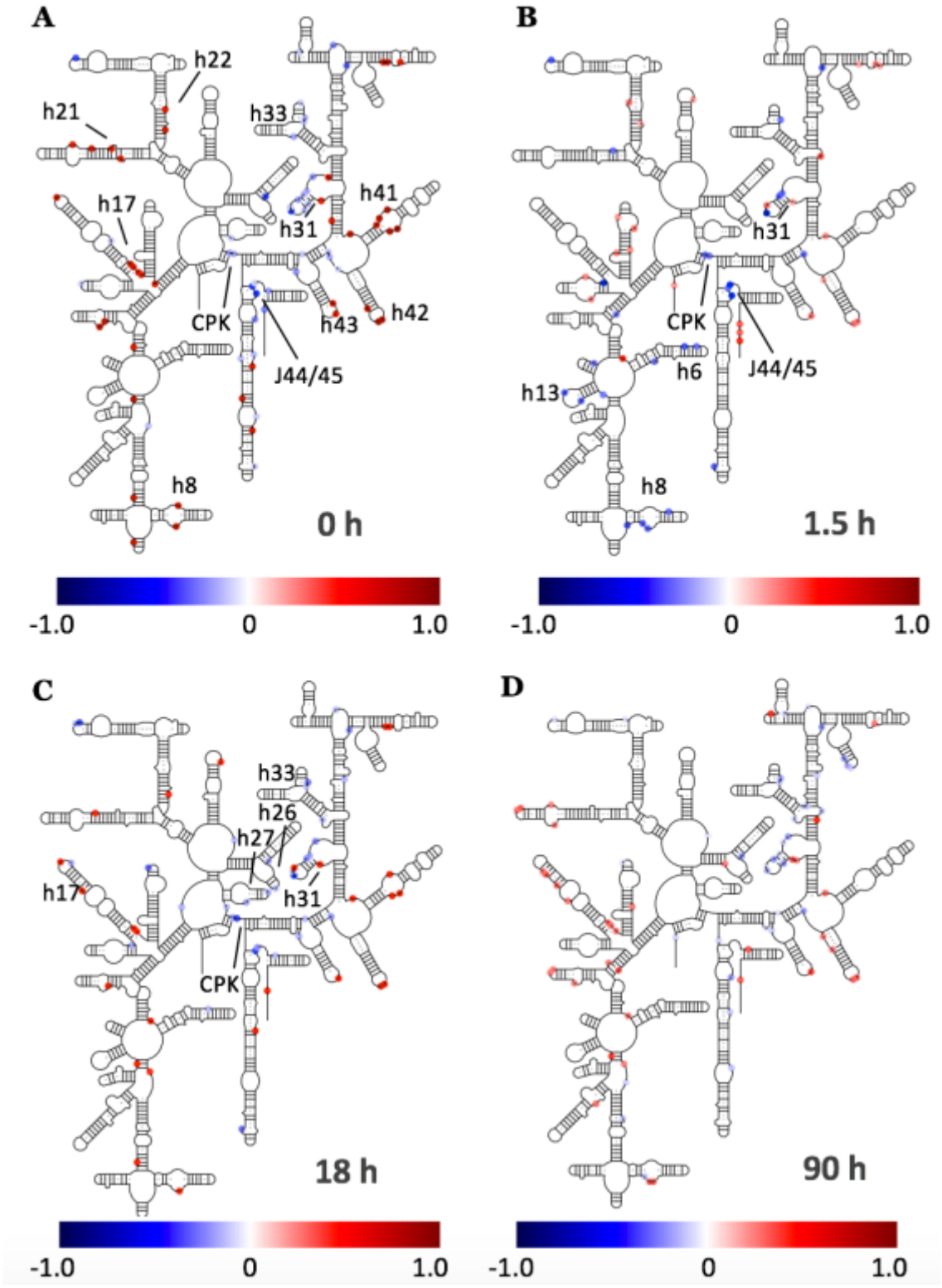
A
h22
h21
h33
h41
h17
h31
CPK
h43
h42
J44/45
h8
0 h
-1.0
0
1.0
B
h31
CPK
J44/45
h6
h13
h8
1.5 h
-1.0
0
1.0
C
h33
h26
h27
h17
h31
CPK
18 h
-1.0
0
1.0
D
90 h
-1.0
0
1.0

Figure 4.13. Secondary structures of 23S rRNA in *E. coli* starved of nitrogen Color bar shows coloring of residues. The deepest red indicates largest $\log_{10}$(experimental reactivity rate / exponential phase reactivity rate). The deepest blue is the negative of this value. The color scheme is continuous, rather than binned. (a-c) DMS reactivities in the 23S rRNA secondary structures after being starved of nitrogen for: (a) 0 h, (b) 1.5 h, and (c) 5.5 h. RNase E cleavage sites and the peptidyl transferase center (PTC) are labeled.

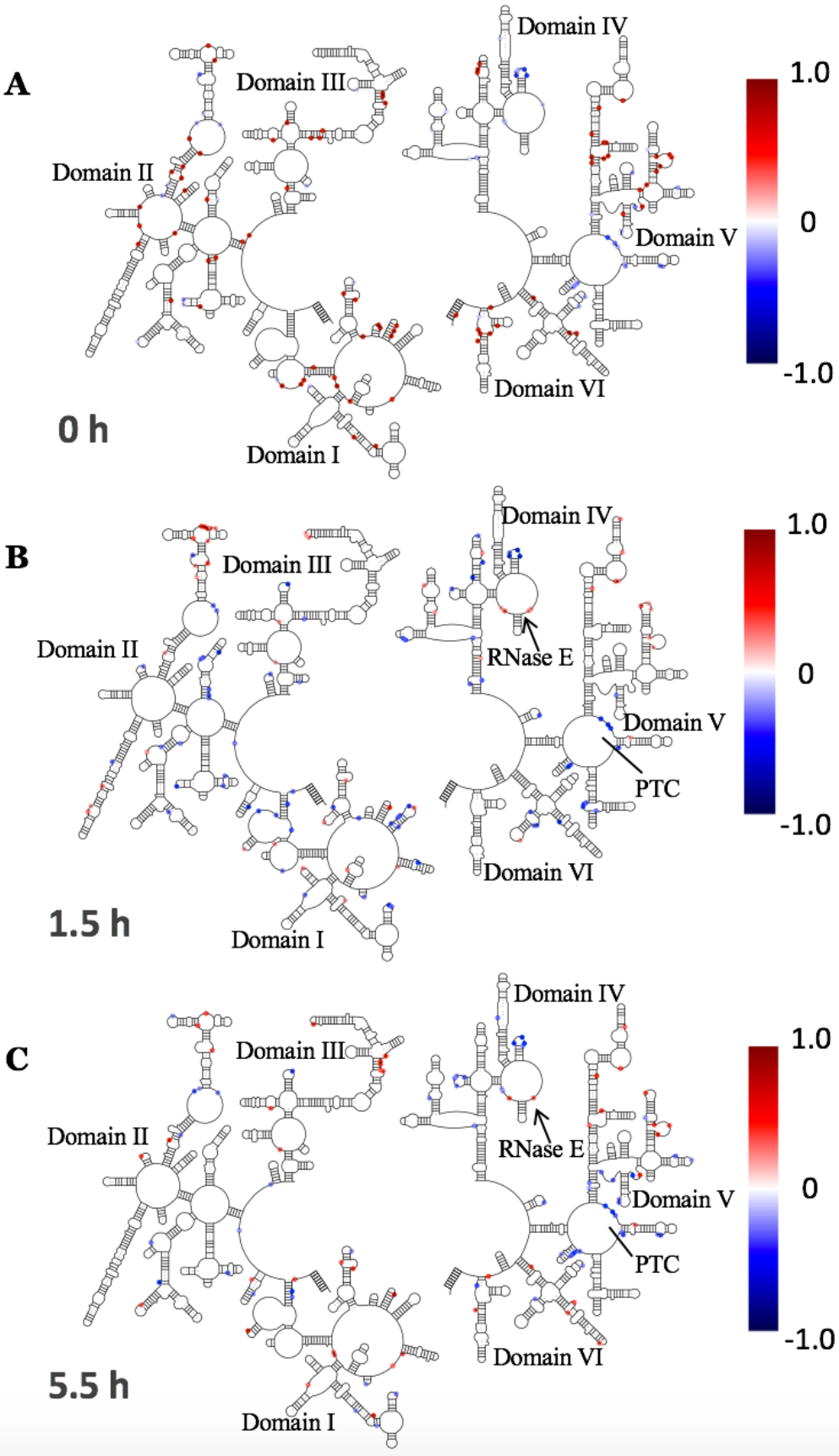
A
Domain IV
Domain III
Domain II
Domain V
Domain VI
Domain I
0 h
1.0
0
-1.0
B
Domain IV
Domain III
Domain II
RNase E
Domain V
PTC
Domain VI
Domain I
1.5 h
1.0
0
-1.0
C
Domain IV
Domain III
Domain II
RNase E
Domain V
PTC
Domain VI
Domain I
5.5 h
1.0
0
-1.0

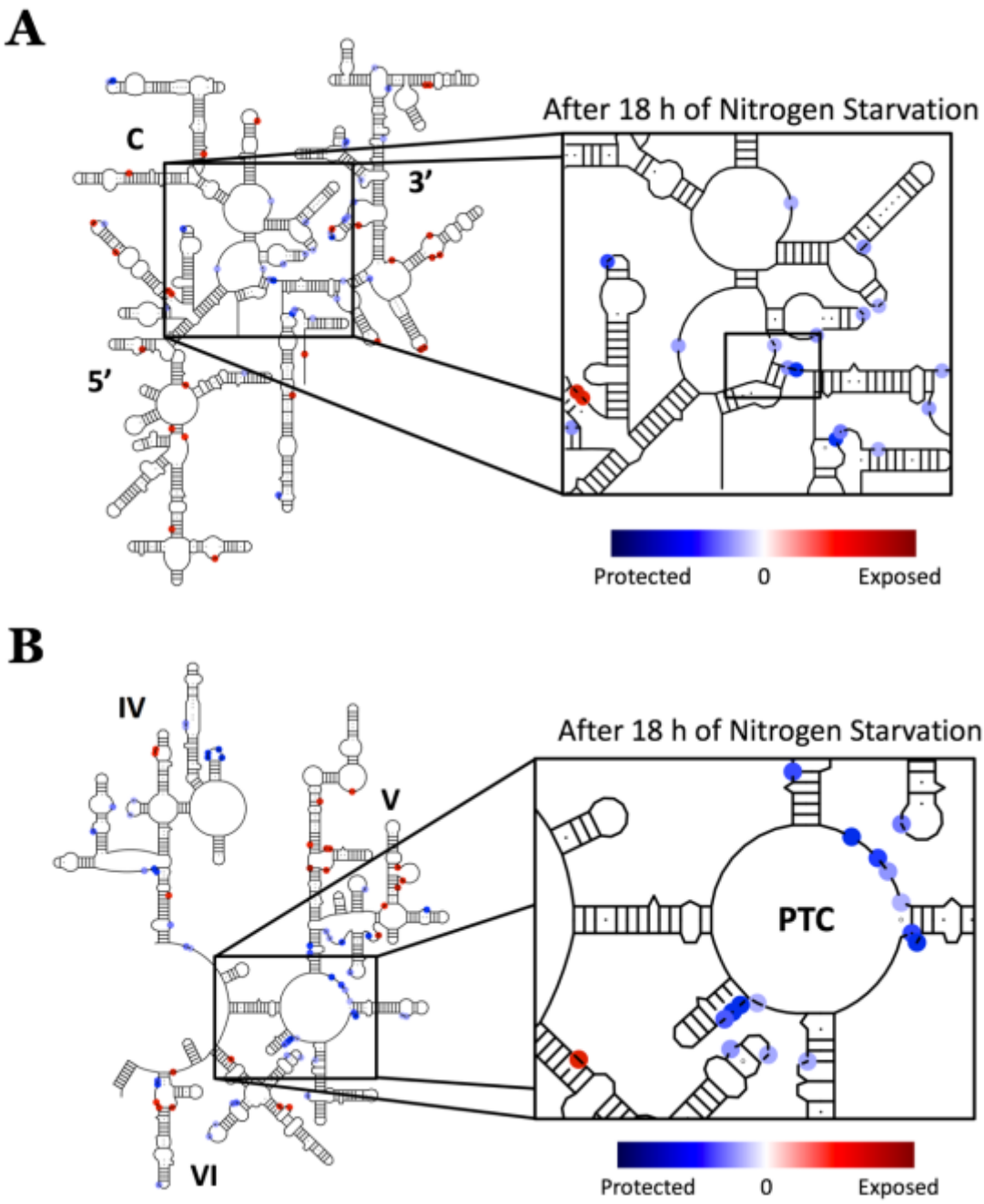

Figure 4.14. Secondary structures of rRNA in *E. coli* starved of nitrogen DMS reactivities in the 16S and 23S rRNA secondary structures after 18 h of incubation in media lacking nitrogen. Color bar shows coloring of residues. The deepest red indicates largest $\log_{10}$(experimental reactivity rate / exponential phase reactivity rate). The deepest blue is the negative of this value. The color scheme is continuous, rather than binned. (a) The central pseudoknot of the 16S rRNA. (b) The peptidyl transferase center of the 23S rRNA.

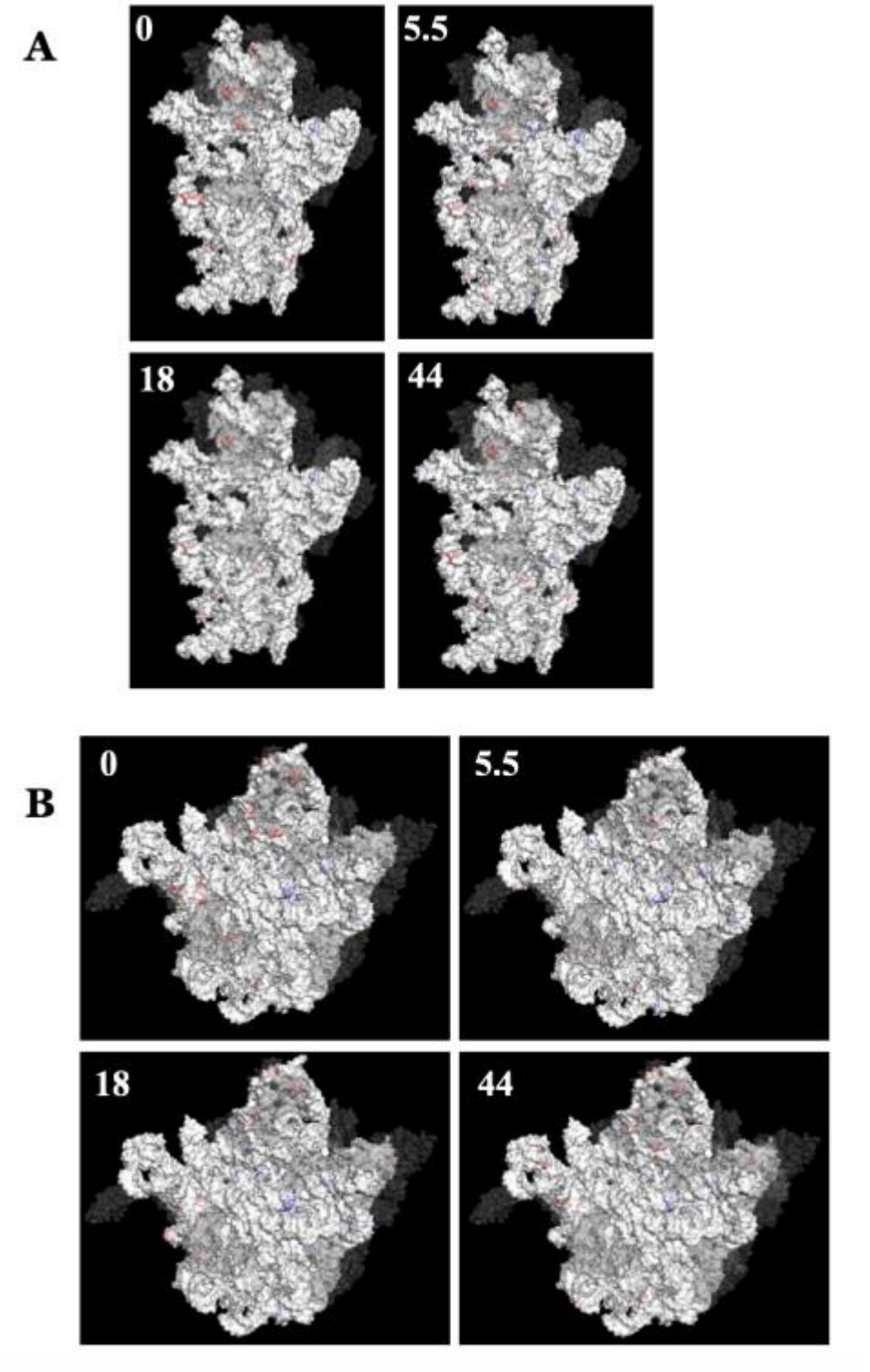

Figure 4.15. The 3D structures of ribosome subunits in *E. coli* starved of nitrogen (a) The 30S subunit interface after 0, 5.5, 18, or 44 h. (b) The 50S subunit interface after 0, 5.5, 18, or 44 h.

Table 4.1 **Ribosomal subunit decay rates**. Decay rates calculated from exponential curves fit to subunit decay curves in Figure 4.4.

Stress Condition	30S k_{decay} (h^{-1})	50S k_{decay} (h^{-1})
Stationary phase	0.116	0.293
Nitrogen starvation	0.004	0.009
Carbon starvation	0.015	0.019
Phosphate starvation	0.102	0.152
Magnesium starvation	0.121	0.200

CHAPTER 5: Conclusions

5.1 DMS probing shows global changes in rRNA structure

The goal of my research was to study structural changes that take place in the rRNA throughout ribosome metabolism. Changes that took place during assembly and degradation were studied by *in vivo* RNA probing using hydroxyl radicals and DMS. Probing with DMS ultimately proved to be most amenable to producing the RNA yields necessary for downstream analysis.

The probing was effective in assessing global exposure. For nascent rRNA in cells emerging from phosphate starvation, the rRNA was initially more exposed than it would be in an assembled structure and later approached exposure rates closer to those expected for an assembled ribosome (Figure 3.9). This is consistent with what would be expected for an assembling, nascent rRNA. Similarly, as cells grew beyond exponential phase and proceeded to late stationary phase, the rRNA showed a higher rate of exposure, suggesting that the structures were generally more disordered than in exponential phase. The local exposure patterns did not appreciably change during the duration of stationary phase. For cells starved of nitrogen, there were local changes in DMS exposure, but there was little change in the total rRNA exposure relative to rRNA in exponential phase cells. Over the course of starvation, the DMS exposure patterns did not undergo significant changes.

Local changes in protection were observed, particularly between nitrogen-starved cells and exponential phase cells. But within a stress condition, there were no large changes in protection seen between time points. There are a number of reasons that make

the determination of local structural changes difficult. For ribosome assembly, the assembly intermediates will be a heterogeneous mixture comprising all of the transcripts that were labeled during the duration of the 4sU pulse. A shorter pulse would decrease the heterogeneity, but it would also decrease the rRNA yield, which unfortunately has always been prohibitive.

In the case of ribosome degradation during starvation, it appears that the majority of the ribosomal particles are stable. Particles are undergoing structural changes that would make them susceptible to RNase cleavage appear to constitute a small percentage of the total number of ribosomal particles. Given that these particles are susceptible to RNase cleavage, it is also unlikely that these structurally perturbed complexes would persist long enough to accumulate in number. Using a bulk probing method, it will be difficult to distinguish the population of degrading ribosomal subunits from the much larger population of stable ribosomes and subunits.

5.2 DMS probing suggests a mechanism for ribosomal stability in cells starved of nitrogen

DMS probing was performed in cells that were starved of nitrogen. Of all stress conditions tested, rRNA degradation was slowest in nitrogen-starved cells. For these cells, the overall mutation rates were similar to those seen in exponential phase cells (Figure 4.11). Locally, there was an increase in protection near the central pseudoknot in the 16S rRNA (Figure 4.14a). It has previously been shown that during periods of carbon starvation, the 16S rRNA is cleaved by RNase E between A919 and U920, near the

central pseudoknot (Sulthana 2016). The fragments derived from this cleavage event are rapidly degraded by exoribonucleases (Basturea 2011). The greater protection of the central pseudoknot makes it less susceptible to RNase cleavage, resulting in decreased degradation. Accordingly, the degradation of 30S subunits did proceed at a much slower rate than all other stress conditions tested (Figure 4.5f). The increased protection of the central pseudoknot could be due to a conformational change in the rRNA or occlusion by a ribosomal factor. The use of mass spectrometry would help determine whether or not additional ribosome factors are involved.

5.3 MRE600 employ an unexpected cellular stress survival strategy

For most bacteria for which the ribosomes have been studied during stationary phase, the 70S ribosomes have dimerized to form 100S hibernation ribosomes to protect them from degradation. Once more nutrient-rich conditions are encountered, the 100S particles separate and the cell has a pool of 30S and 50S subunits that can be readily utilized for protein translation.

Though MRE600 cells contain the necessary proteins, RMF and HPF, to initiate the formation of 100S particles, they appear not to use them and instead stabilize their ribosomes as 30S, 50S, and 70S particles, likely with the proteins YfiA and RsfA, or potentially RMF. The protein RMF has been shown to protect the peptidyl transferase center from DMS probing (Yoshida 2004). DMS probing in cells starved of nitrogen showed a great increase in protection in the peptidyl transferase center relative to cells in exponential phase (Figure 4.14b).

When MRE600 cells encounter conditions of late stationary phase, the 50S subunits are degraded to a greater degree than the 30S subunits. This may affect the way that cells emerge from starvation. In cells that form 100S ribosomal complexes, the dimers separate when nutrients become available and there is a ready pool of free 30S and 50S subunits with which to begin protein translation. If cells are more depleted of 50S subunits, the start of outgrowth may occur similarly to how it occurred in cells starved of phosphate.

During outgrowth, cells emerging from phosphate starvation synthesize both 30S and 50S particles, but the 50S particles are immediately incorporated into 70S ribosomes to begin translation (Figure 3.4). At the start of outgrowth, the subunits that remain after late stationary phase are available for translation. There would be a surplus of 30S particles however, likely leading to the formation of 30S translation initiation complexes. As 50S are transcribed, they would be able to immediate enter these complexes and participate in translation.

The lack of active RNase I in MRE600 would impart a decreased need to protect the rRNA from non-specific degradation. Other stationary phase proteins are available to protect the interfaces of free subunits from being exposed to endonucleolytic cleavage by RNase E. By degrading the 50S more quickly than the 30S and not forming 100S hibernation ribosomes, MRE600 may be able to release a maximal amount of nutrients to the cell while still maintaining the ability to quickly emerge from stationary phase to resume growth and division once nutrients become available.

5.4 Future Directions

DMS probing reports on the solvent-accessibility of the Watson-Crick faces of adenines and cytosines. As such, it is not able to probe all of the structural changes that might occur during assembly and degradation. Hydroxyl radical footprinting would be a useful structure-probing technique to complement these studies. For the starvation-recovery method of synchronizing transcription, the culture would need to be pumped past the synchrotron X-ray beam through a 700 μm capillary tube. This limits the amount of RNA that can be probed during assembly to a level too low for our current analytical techniques. For cells enduring nutrient depletion, the time regime would be much slower and the cells would not have to be flowed past the X-ray beam. They could instead be prepared beforehand and frozen as cell pellets to be irradiated in much higher quantities. These results would help to corroborate the DMS probing data.

The study of stressed MRE600 cells has highlighted an unexplored bacterial survival strategy that does not employ the use of the 100S hibernation ribosome. This should be explored further. The use of mass spectrometry would provide information on the r-protein occupancy of the particles to determine if this changes as cellular stress is prolonged. This would also identify any other proteins associated with the 70S ribosomes and the subunits. For instance, it would be hypothesized that YfiA would be associated with free 30S subunits and 70S ribosomes, and RsfA would be associated with free 50S subunits. DMS probing has also suggested that RMF might be found interacting with the peptidyl transferase center in 50S subunits in cells starved of nitrogen (Figure 4.14b).

It would also be worth exploring the kinetics of RNA synthesis in cells emerging from stresses other than phosphate starvation to see if similar patterns emerge where 30S

and 50S are synthesized and the 50S subunits are immediately incorporated into 70S ribosomes.

APPENDIX

Table A.1 Oligonucleotides used in this work

Oligonucleotide primers used with numerical names denote the 16S nucleotide that anneals to the 3' end of the primer.

Name	Sequence (5' to 3')
46	TCGACTTGCATGTGTTAGGC
161	GCGGTATTAGCTACCGT
323	AGTCTGGACCGTGTCTC
540	TTCCGATTAACGCTTGCACCC
812	AACCTCCAAGTCGACATCGTTTAC
1046	GACAGCCATGCAGCACC
1257	GCTCTCGCGAGGTCGCT
1486	GGTTACCTTGTTACGACTTCACCCC
Linker2	5rApp/CACTCGGGCACCAAGGA/3ddC
Linker2 RT primer	5Phos/AGATCGGAAGAGCGTCGTGTAGGGAAAGAGTGT AGATCTCGGTGGTCGC/iSP18/CACTCA/iSp18/TTCAGACG TGTGCTCTTCCGATCTGTCCTTGGTGCCCGAGTG
NINI2	AATGATACGGCGACCACCGAGATCTACAC
RMH001	CAAGCAGAAGACGGCATACGAGATAAACCTGTGACTG GAGTTCAGACGTGTGCTCTTCCG
RMH002	CAAGCAGAAGACGGCATACGAGATCTCAGGGTGACTG GAGTTCAGACGTGTGCTCTTCCG
RMH003	CAAGCAGAAGACGGCATACGAGATGGGTTCGTGACTGG AGTTCAGACGTGTGCTCTTCCG
RMH004	CAAGCAGAAGACGGCATACGAGATTCTGAAGTGACTGG AGTTCAGACGTGTGCTCTTCCG
RMH005	CAAGCAGAAGACGGCATACGAGATACAGCAGTGACTG GAGTTCAGACGTGTGCTCTTCCG
RMH006	CAAGCAGAAGACGGCATACGAGATCACCGTGTGACTGG AGTTCAGACGTGTGCTCTTCCG
RMH007	CAAGCAGAAGACGGCATACGAGATGTGATGGTGACTG GAGTTCAGACGTGTGCTCTTCCG
RMH008	CAAGCAGAAGACGGCATACGAGATTGTTACGTGACTGG AGTTCAGACGTGTGCTCTTCCG
RMH009	CAAGCAGAAGACGGCATACGAGATAGATCCGTGACTG GAGTTCAGACGTGTGCTCTTCCG
RMH010	CAAGCAGAAGACGGCATACGAGATCCCGGAGTGACTG GAGTTCAGACGTGTGCTCTTCCG
RMH011	CAAGCAGAAGACGGCATACGAGATGAGCTTGTGACTGG AGTTCAGACGTGTGCTCTTCCG

Name	Sequence (5' to 3')
RMH012	CAAGCAGAAGACGGCATACGAGATTTTAAGGTGACTGG AGTTCAGACGTGTGCTCTTCCG
RMH013	CAAGCAGAAGACGGCATACGAGATAACTTGGTGACTGG AGTTCAGACGTGTGCTCTTCCG
RMH014	CAAGCAGAAGACGGCATACGAGATCTGGACGTGACTG GAGTTCAGACGTGTGCTCTTCCG
RMH015	CAAGCAGAAGACGGCATACGAGATGGTCCAGTGACTG GAGTTCAGACGTGTGCTCTTCCG
RMH016	CAAGCAGAAGACGGCATACGAGATTCAAGTGTGACTGG AGTTCAGACGTGTGCTCTTCCG
RMH017	CAAGCAGAAGACGGCATACGAGATACCATTGTGACTGG AGTTCAGACGTGTGCTCTTCCG
RMH018	CAAGCAGAAGACGGCATACGAGATCAGTAGGTGACTG GAGTTCAGACGTGTGCTCTTCCG
RMH019	CAAGCAGAAGACGGCATACGAGATGTTGCCGTGACTGG AGTTCAGACGTGTGCTCTTCCG
RMH020	CAAGCAGAAGACGGCATACGAGATTGACGAGTGACTG GAGTTCAGACGTGTGCTCTTCCG
RMH021	CAAGCAGAAGACGGCATACGAGATAGCCTAGTGACTG GAGTTCAGACGTGTGCTCTTCCG
RMH022	CAAGCAGAAGACGGCATACGAGATCCGAATGTGACTG GAGTTCAGACGTGTGCTCTTCCG
RMH023	CAAGCAGAAGACGGCATACGAGATGATTCGGTGACTGG AGTTCAGACGTGTGCTCTTCCG
RMH024	CAAGCAGAAGACGGCATACGAGATTTAGGCGTGACTGG AGTTCAGACGTGTGCTCTTCCG

REFERENCES

Adilakshmi T, Bellur DL, Woodson SA. (2008). Concurrent nucleation of 16S folding and induced fit in 30S ribosome assembly. *Nature*, *455*(7217), 1268–72. https://doi.org/10.1038/nature07298

Adilakshmi T, Soper SF, Woodson SA. (2009). Structural analysis of RNA in living cells by in vivo synchrotron X-ray footprinting. *Methods Enzymol*, *468*, 239–258. Retrieved from http://www.ncbi.nlm.nih.gov/entrez/query.fcgi?cmd=Retrieve&db=PubMed&dopt=Citation&list_uids=20946773

Agafonov DE, Kolb V a, Nazimov I V, Spirin a S. (1999). A protein residing at the subunit interface of the bacterial ribosome. *Proceedings of the National Academy of Sciences of the United States of America*, *96*(22), 12345–9. https://doi.org/10.1073/pnas.96.22.12345

Agalarov SC, Zheleznyakova EN, Selivanova OM, Zheleznaya LA, Matvienko NI, Vasiliev VD, Spirin AS. (1998). In vitro assembly of a ribonucleoprotein particle corresponding to the platform domain of the 30S ribosomal subunit. *Biochemistry*, *95*, 999–1003. Retrieved from http://www.pnas.org/content/95/3/999.full.pdf

Akanuma G, Kobayashi A, Suzuki S, Kawamura F, Shiwa Y, Watanabe S, … Ishizuka M. (2014). Defect in the Formation of 70S Ribosomes Caused by Lack of Ribosomal Protein L34 Can Be Suppressed by Magnesium. *Journal of Bacteriology*, *196*(22), 3820–3830. https://doi.org/10.1128/JB.01896-14

Alatossava T, Jütte H, Kuhn A, Kellenberger E. (1985). Manipulation of intracellular magnesium content in polymyxin B nonapeptide-sensitized Escherichia coli by

ionophore A23187. *Journal of Bacteriology*, *162*(1), 413–9. Retrieved from http://www.ncbi.nlm.nih.gov/pubmed/2984182

Balzer M, Wagner R. (1998). Mutations in the leader region of ribosomal RNA operons cause structurally defective 30 S ribosomes as revealed by in vivo structural probing. *Journal of Molecular Biology*, *276*(3), 547–557. https://doi.org/10.1006/jmbi.1997.1556

Basturea GN, Zundel MA, Deutscher MP. (2011). Degradation of ribosomal RNA during starvation: Comparison to quality control during steady-state growth and a role for RNase PH. *Rna*, *17*(2), 338–345. https://doi.org/10.1261/rna.2448911

Ben-Hamida F, Schlessinger D. (1966). Synthesis and breakdown of ribonucleic acid in Escherichia coli starving for nitrogen. *Biochimica et Biophysica Acta*, *119*, 183–191. Retrieved from http://www.sciencedirect.com/science/article/pii/0005278766900499

Besançon W, Wagner R. (1999). Characterization of transient RNA-RNA interactions important for the facilitated structure formation of bacterial ribosomal 16S RNA. *Nucleic Acids Research*, *27*(22), 4353–62. Retrieved from http://www.ncbi.nlm.nih.gov/pubmed/10536142

Bohon J, D'Mello R, Ralston C, Gupta S, Chance MR. (2014). Synchrotron X-ray footprinting on tour. *Journal of Synchrotron Radiation*, *21*(Pt 1), 24–31. https://doi.org/10.1107/S1600577513024715

Bram RJ, Young RA, Steitz JA. (1980). The ribonuclease III site flanking 23S sequences in the 30S ribosomal precursor RNA of E. coli. *Cell*, *19*(2), 393–401. Retrieved from http://www.ncbi.nlm.nih.gov/pubmed/6153577

Chen SS, Sperling E, Silverman JM, Davis JH, Williamson JR. (2012). Measuring the

dynamics of E. coli ribosome biogenesis using pulse-labeling and quantitative mass spectrometry. *Molecular bioSystems*, *8*(12), 3325–34. https://doi.org/10.1039/c2mb25310k

Chen SS, Williamson JR. (2013). Characterization of the ribosome biogenesis landscape in E. coli using quantitative mass spectrometry. *J Mol Biol*, *425*(4), 767–779. https://doi.org/10.1016/j.jmb.2012.11.040

Chen SS, Williamson JR. (2013). Characterization of the Ribosome Biogenesis Landscape in E. coli Using Quantitative Mass Spectrometry. *Journal of Molecular Biology*, *425*(4), 767–779. https://doi.org/10.1016/j.jmb.2012.11.040

Clatterbuck Soper SF, Dator RP, Limbach PA, Woodson SA. (2013). In vivo X-ray footprinting of pre-30S ribosomes reveals chaperone-dependent remodeling of late assembly intermediates. *Molecular Cell*, *52*(4), 506–16. https://doi.org/10.1016/j.molcel.2013.09.020

Culver GM. (2003). Assembly of the 30S ribosomal subunit. *Biopolymers*, *68*(2), 234–49. https://doi.org/10.1002/bip.10221

Culver GM, Noller HF. (1999). Efficient reconstitution of functional Escherichia coli 30S ribosomal subunits from a complete set of recombinant small subunit ribosomal proteins. *RNA (New York, N.Y.)*, *5*(6), 832–43. Retrieved from http://www.pubmedcentral.nih.gov/articlerender.fcgi?artid=1369808&tool=pmcentrez&rendertype=abstract

Das R, Laederach A, Pearlman SM, Herschlag D, Altman RB. (2005). SAFA: semi-automated footprinting analysis software for high-throughput quantification of nucleic acid footprinting experiments. *RNA (New York, N.Y.)*, *11*(3), 344–54.

https://doi.org/10.1261/rna.7214405

Davis BD, Luger SM, Tai12 PC. (1986). Role of Ribosome Degradation in the Death of Starved Escherichia coli Cells. *JOURNAL OF BACTERIOLOGY*, *166*(2), 439–445.

Davis JH, Tan YZ, Carragher B, Potter CS, Lyumkis D, Williamson JR. (2016). Modular Assembly of the Bacterial Large Ribosomal Subunit. *Cell*, *167*(6), 1610–1622.e15. https://doi.org/10.1016/j.cell.2016.11.020

Deutscher MP. (2009). Chapter 9 Maturation and Degradation of Ribosomal RNA in Bacteria. In C. Ciaran (Ed.), *Prog Mol Biol Transl Sci* (Vol. Volume 85, pp. 369–391). Academic Press. https://doi.org/http://dx.doi.org/10.1016/S0079-6603(08)00809-X

Dohme F, Nierhaus KH. (1976). Total reconstitution and assembly of 50 S subunits from Escherichia coli Ribosomes in vitro. *Journal of Molecular Biology*, *107*(4), 585–99. Retrieved from http://www.ncbi.nlm.nih.gov/pubmed/794489

Dölken L, Ruzsics Z, Rädle B, Friedel CC, Zimmer R, Mages J, … Koszinowski UH. (2008). High-resolution gene expression profiling for simultaneous kinetic parameter analysis of RNA synthesis and decay. *RNA (New York, N.Y.)*, *14*(9), 1959–72. https://doi.org/10.1261/rna.1136108

Ephrussi A, Church GM, Tonegawa S, Gilbert W. (1985). B lineage--specific interactions of an immunoglobulin enhancer with cellular factors in vivo. *Science (New York, N.Y.)*, *227*(4683), 134–40. Retrieved from http://www.ncbi.nlm.nih.gov/pubmed/3917574

Favre A, Bezerra R, Hajnsdorf E, Lemaigre Dubreuil Y, Expert-Bezancon A. (1986). Substitution of uridine in vivo by the intrinsic photoactivable probe 4-thiouridine in

Escherichia coli RNA. Its use for E. coli ribosome structural analysis. *Eur J Biochem*, *160*(3), 441–449. Retrieved from http://www.ncbi.nlm.nih.gov/pubmed/2430798

Gaal T, Bartlett MS, Ross W, Turnbough CL, Gourse RL. (1997). Transcription regulation by initiating NTP concentration: rRNA synthesis in bacteria. *Science (New York, N.Y.)*, *278*(5346), 2092–7. Retrieved from http://www.ncbi.nlm.nih.gov/pubmed/9405339

Gegenheimer P, Apirion D. (1975). Escherichia coli ribosomal ribonucleic acids are not cut from an intact precursor molecule. *The Journal of Biological Chemistry*, *250*(6), 2407–9. Retrieved from http://www.ncbi.nlm.nih.gov/pubmed/1090620

Gourse RL, Gaal T, Bartlett MS, Appleman JA, Ross W. (1996). rRNA transcription and growth rate-dependent regulation of ribosome synthesis in Escherichia coli. *Annual Review of Microbiology*, *50*, 645–77. https://doi.org/10.1146/annurev.micro.50.1.645

Gourse RL, Nomura M. (1984). Level of rRNA, not tRNA, synthesis controls transcription of rRNA and tRNA operons in Escherichia coli. *Journal of Bacteriology*, *160*(3), 1022–6. Retrieved from http://www.pubmedcentral.nih.gov/articlerender.fcgi?artid=215812&tool=pmcentrez&rendertype=abstract

Guerrier-Takada C, Gardiner K, Marsh T, Pace N, Altman S. (1983). The RNA moiety of ribonuclease P is the catalytic subunit of the enzyme. *Cell*, *35*(3 Pt 2), 849–57. Retrieved from http://www.ncbi.nlm.nih.gov/pubmed/6197186

Gupta N, Culver GM. (2014). Multiple in vivo pathways for Escherichia coli small

ribosomal subunit assembly occur on one pre-rRNA. *Nature Structural & Molecular Biology*, *21*(10), 937–43. https://doi.org/10.1038/nsmb.2887

Gupta S, Celestre R, Petzold CJ, Chance MR, Ralston C. (2014). Development of a microsecond X-ray protein footprinting facility at the Advanced Light Source. *Journal of Synchrotron Radiation*, *21*(Pt 4), 690–9. https://doi.org/10.1107/S1600577514007000

Gupta S, Sullivan M, Toomey J, Kiselar J, Chance MR. (2007). The Beamline X28C of the Center for Synchrotron Biosciences: a national resource for biomolecular structure and dynamics experiments using synchrotron footprinting. *Journal of Synchrotron Radiation*, *14*(Pt 3), 233–43. https://doi.org/10.1107/S0909049507013118

Gutgsell NS, Jain C. (2012). Gateway Role for rRNA Precursors in Ribosome Assembly. *Journal of Bacteriology*, *194*(24), 6875–6882. https://doi.org/10.1128/JB.01467-12

Hage A El, Tollervey D. (2014). A Surfeit of Factors: Why is Ribosome Assembly So Much More Complicated in Eukaryotes than Bacteria? *RNA Biology*, *1*(1), 9–14. https://doi.org/10.4161/rna.1.1.932

Häuser R, Pech M, Kijek J, Yamamoto H, Titz B, Naeve F, … Uetz P. (2012). RsfA (YbeB) Proteins Are Conserved Ribosomal Silencing Factors. *PLoS Genetics*, *8*(7), e1002815. https://doi.org/10.1371/journal.pgen.1002815

Held WA, Ballou B, Mizushima S, Nomura M. (1974). Assembly mapping of 30 S ribosomal proteins from Escherichia coli. Further studies. *The Journal of Biological Chemistry*, *249*(10), 3103–11. Retrieved from http://www.ncbi.nlm.nih.gov/pubmed/4598121

Held WA, Mizushima S, Nomura M. (1973). Reconstitution of Escherichia coli 30 S ribosomal subunits from purified molecular components. *The Journal of Biological Chemistry*, *248*(16), 5720–30. Retrieved from http://www.ncbi.nlm.nih.gov/pubmed/4579428

Holmes KL, Culver GM. (2004). Mapping structural differences between 30S ribosomal subunit assembly intermediates. *Nature Structural & Molecular Biology*, *11*(2), 179–186. https://doi.org/10.1038/nsmb719

Holmes KL, Culver GM. (2005). Analysis of conformational changes in 16 S rRNA during the course of 30 S subunit assembly. *Journal of Molecular Biology*, *354*(2), 340–57. https://doi.org/10.1016/j.jmb.2005.09.056

Hsieh M, Brenowitz M. (1996). Quantitative kinetics footprinting of protein-DNA association reactions. *Methods in Enzymology*, *274*, 478–92. Retrieved from http://www.ncbi.nlm.nih.gov/pubmed/8902826

Inoue T, Cech TR. (1985). Secondary structure of the circular form of the Tetrahymena rRNA intervening sequence: a technique for RNA structure analysis using chemical probes and reverse transcriptase. *Proceedings of the National Academy of Sciences of the United States of America*, *82*(3), 648–52. Retrieved from http://www.pubmedcentral.nih.gov/articlerender.fcgi?artid=397102&tool=pmcentrez&rendertype=abstract

Jacobson A, Gillespie D. (1968). Metabolic events occurring during recovery from prolonged glucose starvation in Escherichia coli. *Journal of Bacteriology*, *95*(3), 1030–9. Retrieved from http://www.ncbi.nlm.nih.gov/pubmed/4868350

Jomaa A, Jain N, Davis JH, Williamson JR, Britton RA, Ortega J. (2014). Functional

domains of the 50S subunit mature late in the assembly process. *Nucleic Acids Research*, *42*(5), 3419–35. https://doi.org/10.1093/nar/gkt1295

Kaberdin VR. (2003). Probing the substrate specificity of Escherichia coli RNase E using a novel oligonucleotide-based assay. *Nucleic Acids Research*, *31*(16), 4710–6. Retrieved from http://www.ncbi.nlm.nih.gov/pubmed/12907711

Kaczanowska M, Rydén-Aulin M. (2007). Ribosome biogenesis and the translation process in Escherichia coli. *Microbiology and Molecular Biology Reviews : MMBR*, *71*(3), 477–94. https://doi.org/10.1128/MMBR.00013-07

Kalpaxis DL, Karahalios P, Papapetropoulou M. (1998). Changes in ribosomal activity of Escherichia coli cells during prolonged culture in sea salts medium. *Journal of Bacteriology*, *180*(12), 3114–9. Retrieved from http://www.ncbi.nlm.nih.gov/pubmed/9620960

Kaplan R, Apirion D. (1975a). Decay of ribosomal ribonucleic acid in Escherichia coli cells starved for various nutrients. *The Journal of Biological Chemistry*, *250*(8), 3174–8. Retrieved from http://www.ncbi.nlm.nih.gov/pubmed/1091648

Kaplan R, Apirion D. (1975b). The fate of ribosomes in Escherichia coli cells starved for a carbon source. *The Journal of Biological Chemistry*, *250*(5), 1854–63. Retrieved from http://www.ncbi.nlm.nih.gov/pubmed/1089666

Katibah GE, Qin Y, Sidote DJ, Yao J, Lambowitz AM, Collins K. (2014). Broad and adaptable RNA structure recognition by the human interferon-induced tetratricopeptide repeat protein IFIT5. *Proceedings of the National Academy of Sciences*, *111*(33), 12025–12030. https://doi.org/10.1073/pnas.1412842111

King TC, Schlessinger D. (1983). S1 nuclease mapping analysis of ribosomal RNA

processing in wild type and processing deficient Escherichia coli. *The Journal of Biological Chemistry*, *258*(19), 12034–42. Retrieved from http://www.ncbi.nlm.nih.gov/pubmed/6311836

Kjeldgaard NO, Maaløe O. (1966). *Control of macromolecular synthesis a study of DNA, RNA, and protein synthesis in bacteria*. New York: W.A. Benjamin. Retrieved from http://www.worldcat.org/title/control-of-macromolecular-synthesis-a-study-of-dna-rna-and-protein-synthesis-in-bacteria/oclc/561292

Krzyzosiak W, Denman R, Nurse K, Hellmann W, Boublik M, Gehrke CW, … Ofengand J. (1987). In vitro synthesis of 16S ribosomal RNA containing single base changes and assembly into a functional 30S ribosome. *Biochemistry*, *26*(8), 2353–64. Retrieved from http://www.ncbi.nlm.nih.gov/pubmed/3304424

Kubota M, Tran C, Spitale RC. (2015). Progress and challenges for chemical probing of RNA structure inside living cells. *Nature Chemical Biology*, *11*(12), 933–941. https://doi.org/10.1038/nchembio.1958

Kurylo CM, Alexander N, Dass RA, Parks MM, Altman RA, Vincent CT, … Blanchard SC. (2016). Genome Sequence and Analysis of Escherichia coli MRE600, a Colicinogenic, Nonmotile Strain that Lacks RNase I and the Type I Methyltransferase, EcoKI. *Genome Biology and Evolution*, *8*(3), 742–52. https://doi.org/10.1093/gbe/evw008

Lewicki BT, Margus T, Remme J, Nierhaus KH. (1993). Coupling of rRNA transcription and ribosomal assembly in vivo. Formation of active ribosomal subunits in Escherichia coli requires transcription of rRNA genes by host RNA polymerase which cannot be replaced by bacteriophage T7 RNA polymerase. *Journal of*

Molecular Biology, *231*(3), 581–93. https://doi.org/10.1006/jmbi.1993.1311

Li N, Chen Y, Guo Q, Zhang Y, Yuan Y, Ma C, … Gao N. (2013). Cryo-EM structures of the late-stage assembly intermediates of the bacterial 50S ribosomal subunit. *Nucleic Acids Research*, *41*(14), 7073–7083. https://doi.org/10.1093/nar/gkt423

Li Z, Deutscher MP. (1995). The tRNA processing enzyme RNase T is essential for maturation of 5S RNA. *Proceedings of the National Academy of Sciences of the United States of America*, *92*(15), 6883–6. Retrieved from http://www.ncbi.nlm.nih.gov/pubmed/7542780

Lindahl L. (1975). Intermediates and time kinetics of the in vivo assembly of Escherichia coli ribosomes. *J Mol Biol*, *92*(1), 15–37. Retrieved from http://www.ncbi.nlm.nih.gov/pubmed/1097701

Mackie GA. (1992). Secondary structure of the mRNA for ribosomal protein S20. Implications for cleavage by ribonuclease E. *The Journal of Biological Chemistry*, *267*(2), 1054–61. Retrieved from http://www.ncbi.nlm.nih.gov/pubmed/1370457

Mackie GA, Genereaux JL. (1993). The Role of RNA Structure in Determining RNase E-dependent Cleavage Sites in the mRNA for Ribosomal Protein S20 in vitro. *Journal of Molecular Biology*, *234*(4), 998–1012. https://doi.org/10.1006/jmbi.1993.1654

Maki Y, Yoshida H, Wada A. (2000). Two proteins, YfiA and YhbH, associated with resting ribosomes in stationary phase Escherichia coli. *Genes to Cells*, *5*(12), 965–974. https://doi.org/10.1046/j.1365-2443.2000.00389.x

Martin M. (2011). Cutadapt removes adapter sequences from high-throughput sequencing reads. *EMBnet.journal*, *17*(1), 10. https://doi.org/10.14806/ej.17.1.200

Maruyama H, Mizuno D. (1970). Ribosome degradation and the degradation products in

starved Escherichia coli. II. Changes in base sequence of ribosomal RNA during degradation induced by phosphate and magnesium starvation. *BBA Section Nucleic Acids And Protein Synthesis*, *199*(1), 166–175. https://doi.org/10.1016/0005-2787(70)90705-7

McCarthy BJ. (1962). The effects of magnesium starvation on the ribosome content of Escherichia coli. *Biochimica et Biophysica Acta (BBA) - Specialized Section on Nucleic Acids and Related Subjects*, *55*(6), 880–889. https://doi.org/10.1016/0926-6550(62)90345-6

McDowall KJ, Kaberdin VR, Wu S-W, Cohen SN, Lin-Chao S. (1995). Site-specific RNase E cleavage of oligonucleotides and inhibition by stem–loops. *Nature*, *374*(6519), 287–290. https://doi.org/10.1038/374287a0

Merryman C, Moazed D, Daubresse G, Noller HF. (1999). Nucleotides in 23S rRNA protected by the association of 30S and 50S ribosomal subunits. *Journal of Molecular Biology*, *285*(1), 107–13. https://doi.org/10.1006/jmbi.1998.2243

Merryman C, Moazed D, McWhirter J, Noller HF. (1999). Nucleotides in 16S rRNA protected by the association of 30S and 50S ribosomal subunits. *Journal of Molecular Biology*, *285*(1), 97–105. https://doi.org/10.1006/jmbi.1998.2242

Mizushima S, Nomura M. (1970). Assembly mapping of 30S ribosomal proteins from E. coli. *Nature*, *226*(5252), 1214. Retrieved from http://www.ncbi.nlm.nih.gov/pubmed/4912319

Mohr S, Ghanem E, Smith W, Sheeter D, Qin Y, King O, … Lambowitz AM. (2013). Thermostable group II intron reverse transcriptase fusion proteins and their use in cDNA synthesis and next-generation RNA sequencing. *RNA (New York, N.Y.)*,

19(7), 958–970. https://doi.org/10.1261/rna.039743.113

Moncany ML, Kellenberger E. (1981). High magnesium content of Escherichia coli B. *Experientia*, *37*(8), 846–7. Retrieved from http://www.ncbi.nlm.nih.gov/pubmed/7026272

Mortimer SA, Kidwell MA, Doudna JA. (2014). Insights into RNA structure and function from genome-wide studies. *Nature Reviews. Genetics*, *15*(7), 469–79. https://doi.org/10.1038/nrg3681

Mulder AM, Yoshioka C, Beck AH, Bunner AE, Milligan RA, Potter CS, … Williamson JR. (2010). Visualizing ribosome biogenesis: parallel assembly pathways for the 30S subunit. *Science (New York, N.Y.)*, *330*(6004), 673–7. https://doi.org/10.1126/science.1193220

Murray HD, Appleman JA, Gourse RL. (2003). Regulation of the Escherichia coli rrnB P2 promoter. *Journal of Bacteriology*, *185*(1), 28–34. Retrieved from http://www.pubmedcentral.nih.gov/articlerender.fcgi?artid=141837&tool=pmcentrez&rendertype=abstract

Murray HD, Gourse RL. (2004). Unique roles of the rrn P2 rRNA promoters in Escherichia coli. *Molecular Microbiology*, *52*(5), 1375–87. https://doi.org/10.1111/j.1365-2958.2004.04060.x

Murray HD, Schneider DA, Gourse RL. (2003). Control of rRNA expression by small molecules is dynamic and nonredundant. *Molecular Cell*, *12*(1), 125–34. Retrieved from http://www.ncbi.nlm.nih.gov/pubmed/12887898

Nguyenle T, Laurberg M, Brenowitz M, Noller HF. (2006). Following the dynamics of changes in solvent accessibility of 16 S and 23 S rRNA during ribosomal subunit

association using synchrotron-generated hydroxyl radicals. *Journal of Molecular Biology*, *359*(5), 1235–48. https://doi.org/10.1016/j.jmb.2006.04.030

Nierhaus KH. (2014). Mg2+, K+, and the ribosome. *Journal of Bacteriology*, *196*(22), 3817–9. https://doi.org/10.1128/JB.02297-14

Nierhaus KH, Dohme F. (1974). Total reconstitution of functionally active 50S ribosomal subunits from Escherichia coli. *Proceedings of the National Academy of Sciences of the United States of America*, *71*(12), 4713–7. Retrieved from http://www.pubmedcentral.nih.gov/articlerender.fcgi?artid=433966&tool=pmcentrez&rendertype=abstract

Nierhaus KH, Dohme F. (1979). Total reconstitution of 50 S subunits from Escherichia coli ribosomes. *Methods in Enzymology*, *59*, 443–9. Retrieved from http://www.ncbi.nlm.nih.gov/pubmed/374949

Noller HF, Kop J, Wheaton V, Brosius J, Gutell RR, Kopylov AM, … Waese CR. (1981). Secondary structure model for 23S ribosomal RNA. *Nucleic Acids Research*, *9*(22), 6167–89. Retrieved from http://www.pubmedcentral.nih.gov/articlerender.fcgi?artid=327592&tool=pmcentrez&rendertype=abstract

Ottinger LM, Tullius TD. (2000). High-Resolution in Vivo Footprinting of a Protein−DNA Complex Using γ-Radiation. *Journal of the American Chemical Society*, *122*(24), 5901–5902. https://doi.org/10.1021/ja000285f

Pardon B, Wagner R. (1995). The Escherichia coli ribosomal RNA leader nut region interacts specifically with mature 16S RNA. *Nucleic Acids Research*, *23*(6), 932–41. Retrieved from http://www.ncbi.nlm.nih.gov/pubmed/7731806

Paul BJ, Ross W, Gaal T, Gourse RL. (2004). rRNA Transcription in Escherichia coli. *Annual Review of Genetics*, *38*(1), 749–770. https://doi.org/10.1146/annurev.genet.38.072902.091347

Peattie DA, Gilbert W. (1980). Chemical probes for higher-order structure in RNA. *Proceedings of the National Academy of Sciences of the United States of America*, *77*(8), 4679–82. Retrieved from http://www.ncbi.nlm.nih.gov/pubmed/6159633

Polikanov YS, Blaha GM, Steitz TA. (2012). How hibernation factors RMF, HPF, and YfiA turn off protein synthesis. *Science (New York, N.Y.)*, *336*(6083), 915–8. https://doi.org/10.1126/science.1218538

Popova AM, Williamson JR. (2014). Quantitative analysis of rRNA modifications using stable isotope labeling and mass spectrometry. *Journal of the American Chemical Society*, *136*(5), 2058–69. https://doi.org/10.1021/ja412084b

Powers T, Daubresse G, Noller HF. (1993). Dynamics of in vitro assembly of 16 S rRNA into 30 S ribosomal subunits. *Journal of Molecular Biology*, *232*(2), 362–74. https://doi.org/10.1006/jmbi.1993.1396

Powers T, Noller HF. (1995). Hydroxyl radical footprinting of ribosomal proteins on 16S rRNA. *RNA (New York, N.Y.)*, *1*(2), 194–209. Retrieved from http://www.pubmedcentral.nih.gov/articlerender.fcgi?artid=1369073&tool=pmcentrez&rendertype=abstract

Ralston CY, Sclavi B, Sullivan M, Deras ML, Woodson SA, Chance MR, Brenowitz M. (2000). Time-resolved synchrotron X-ray footprinting and its application to RNA folding. *Methods in Enzymology*, *317*, 353–68. Retrieved from http://www.ncbi.nlm.nih.gov/pubmed/10829290

Ramagopal S, Subramanian AR. (1974). Alteration in the Acetylation Level of Ribosomal Protein L12 During Growth Cycle of Escherichia coli (ribosome heterogeneity/regulation of acetylation/stationary phase adaptation), *71*(5), 2136–2140. Retrieved from http://www.pnas.org/content/71/5/2136.full.pdf

Rouskin S, Zubradt M, Washietl S, Kellis M, Weissman JS. (2014). Genome-wide probing of RNA structure reveals active unfolding of mRNA structures in vivo. *Nature*, *505*(7485), 701–5. https://doi.org/10.1038/nature12894

Roy MK, Singh B, Ray BK, Apirion D. (1983). Maturation of 5-S rRNA: ribonuclease E cleavages and their dependence on precursor sequences. *European Journal of Biochemistry*, *131*(1), 119–27. Retrieved from http://www.ncbi.nlm.nih.gov/pubmed/6339234

Samaha RR, O 'brien B, O 'brient TW, Noller HF. (1994). Independent in vitro assembly of a ribonucleoprotein particle containing the 3' domain of 16S rRNA (ribosomes/in vitro reconstitution/ribosomal proteins/spectinomycin). *Biochemistry*, *91*, 7884–7888. Retrieved from http://www.pnas.org/content/91/17/7884.full.pdf

Sashital DG, Greeman CA, Lyumkis D, Potter CS, Carragher B, Williamson JR. (2014). A combined quantitative mass spectrometry and electron microscopy analysis of ribosomal 30S subunit assembly in E. coli. *eLife*, *3*. https://doi.org/10.7554/eLife.04491

Schneider DA, Gourse RL. (2004). Relationship between growth rate and ATP concentration in Escherichia coli: a bioassay for available cellular ATP. *The Journal of Biological Chemistry*, *279*(9), 8262–8. https://doi.org/10.1074/jbc.M311996200

Sclavi B, Sullivan M, Chance MR, Brenowitz M, Woodson SA. (1998). RNA folding at

millisecond intervals by synchrotron hydroxyl radical footprinting. *Science (New York, N.Y.)*, *279*(5358), 1940–3. Retrieved from http://www.ncbi.nlm.nih.gov/pubmed/9506944

Shajani Z, Sykes MT, Williamson JR. (2011). Assembly of bacterial ribosomes. *Annual Review of Biochemistry*, *80*, 501–26. https://doi.org/10.1146/annurev-biochem-062608-160432

Sieber G, Nierhaus KH. (1978). Kinetic and thermodynamic parameters of the assembly in vitro of the large subunit from Escherichia coli ribosomes. *Biochemistry*, *17*(17), 3505–11. Retrieved from http://www.ncbi.nlm.nih.gov/pubmed/356881

Siegele DA, Kolter R. (1992). MINIREVIEW Life After Log. *Journal of Bacteriology*, *174*(2), 345–348. Retrieved from http://jb.asm.org/content/174/2/345.full.pdf

Siegfried NA, Busan S, Rice GM, Nelson JAE, Weeks KM. (2014). RNA motif discovery by SHAPE and mutational profiling (SHAPE-MaP). *Nature Methods*, *11*(9), 959–65. https://doi.org/10.1038/nmeth.3029

Spedding G (Gary). (1990). *Ribosomes and Protein Synthesis: A Practical Approach (The Practical Approach Series)*. Oxford University Press.

Spillmann S, Dohme F, Nierhaus KH. (1977). Assembly in vitro of the 50 S subunit from Escherichia coli ribosomes: proteins essential for the first heat-dependent conformational change. *Journal of Molecular Biology*, *115*(3), 513–23. Retrieved from http://www.ncbi.nlm.nih.gov/pubmed/338913

Steitz TA, Ban N, Nissen P, Hansen J, Capel M, Moore PB. (1999). Placement of protein and RNA structures into a 5 A-resolution map of the 50S ribosomal subunit. *Nature*, *400*(6747), 841–847. https://doi.org/10.1038/23641

Stern S, Moazed D, Noller HF. (1988). Structural analysis of RNA using chemical and enzymatic probing monitored by primer extension. *Methods in Enzymology*, *164*, 481–9. Retrieved from http://www.ncbi.nlm.nih.gov/pubmed/2468070

Stern S, Powers T, Changchien LM, Noller HF. (1989). RNA-protein interactions in 30S ribosomal subunits: folding and function of 16S rRNA. *Science (New York, N.Y.)*, *244*(4906), 783–90. Retrieved from http://www.ncbi.nlm.nih.gov/pubmed/2658053

Subramanian AR, Subramanian AR. (1980). Evidence for a repeated protein structure in the 30 S subunit of Escherichia coli ribosome. *The Journal of Biological Chemistry*, *255*(14), 6941–6. Retrieved from http://www.ncbi.nlm.nih.gov/pubmed/6993481

Sullivan MR, Rekhi S, Bohon J, Gupta S, Abel D, Toomey J, Chance MR. (2008). Installation and testing of a focusing mirror at beamline X28C for high flux x-ray radiolysis of biological macromolecules. *The Review of Scientific Instruments*, *79*(2 Pt 1), 25101. https://doi.org/10.1063/1.2839027

Sulthana S, Basturea GN, Deutscher MP. (2016). Elucidation of pathways of ribosomal RNA degradation: an essential role for RNase E. *RNA (New York, N.Y.)*, *22*(8), 1163–71. https://doi.org/10.1261/rna.056275.116

Sulthana S, Quesada E, Deutscher MP. (2017). RNase II regulates RNase PH and is essential for cell survival during starvation and stationary phase. *RNA*, rna.060558.116. https://doi.org/10.1261/rna.060558.116

Swiatkowska A, Wlotzka W, Tuck A, Barrass JD, Beggs JD, Tollervey D. (2012). Kinetic analysis of pre-ribosome structure in vivo. *RNA (New York, N.Y.)*, *18*(12), 2187–200. https://doi.org/10.1261/rna.034751.112

Sykes MT, Shajani Z, Sperling E, Beck AH, Williamson JR. (2010). Quantitative

proteomic analysis of ribosome assembly and turnover in vivo. *Journal of Molecular Biology*, *403*(3), 331–45. https://doi.org/10.1016/j.jmb.2010.08.005

Talkington MW, Siuzdak G, Williamson JR. (2005). An assembly landscape for the 30S ribosomal subunit. *Nature*, *438*(7068), 628–632. https://doi.org/10.1038/nature04261

Talkish J, May G, Lin Y, Woolford JL, McManus CJ. (2014). Mod-seq: high-throughput sequencing for chemical probing of RNA structure. *RNA (New York, N.Y.)*, *20*(5), 713–20. https://doi.org/10.1261/rna.042218.113

Traub P, Nomura M. (1968). Structure and function of E. coli ribosomes. V. Reconstitution of functionally active 30S ribosomal particles from RNA and proteins. *Proceedings of the National Academy of Sciences of the United States of America*, *59*(3), 777–84. Retrieved from http://www.ncbi.nlm.nih.gov/pubmed/4868216

Tullius TD, Dombroski BA. (1986). Hydroxyl radical "footprinting": high-resolution information about DNA-protein contacts and application to lambda repressor and Cro protein. *Proceedings of the National Academy of Sciences of the United States of America*, *83*(15), 5469–73. Retrieved from http://www.pubmedcentral.nih.gov/articlerender.fcgi?artid=386308&tool=pmcentrez&rendertype=abstract

Tullius TD, Dombroski BA, Churchill ME, Kam L. (1987). Hydroxyl radical footprinting: a high-resolution method for mapping protein-DNA contacts. *Methods in Enzymology*, *155*, 537–58. Retrieved from http://www.ncbi.nlm.nih.gov/pubmed/2828876

Tullius TD, Greenbaum JA. (2005). Mapping nucleic acid structure by hydroxyl radical cleavage. *Current Opinion in Chemical Biology*, *9*(2), 127–34. https://doi.org/10.1016/j.cbpa.2005.02.009

Udenfriend S, Clark CT, Axelrod J, Brodie BB. (1954). Ascorbic acid in aromatic hydroxylation. I. A model system for aromatic hydroxylation. *The Journal of Biological Chemistry*, *208*(2), 731–9. Retrieved from http://www.ncbi.nlm.nih.gov/pubmed/13174582

Ueta M, Yoshida H, Wada C, Baba T, Mori H, Wada A. (2005). Ribosome binding proteins YhbH and YfiA have opposite functions during 100S formation in the stationary phase of Escherichia coli. *Genes to Cells*, *10*(12), 1103–1112. https://doi.org/10.1111/j.1365-2443.2005.00903.x

Wada A. (1998). Growth phase coupled modulation of Escherichia coli ribosomes. *Genes to Cells*, *3*(4), 203–208. https://doi.org/10.1046/j.1365-2443.1998.00187.x

Wada A, Mikkola R, Kurland CG, Ishihama A. (2000). Growth phase-coupled changes of the ribosome profile in natural isolates and laboratory strains of Escherichia coli. *Journal of Bacteriology*, *182*(10), 2893–9. https://doi.org/10.1128/JB.182.10.2893-2899.2000

Wada A, Yamazaki Y, Fujita N, Ishihama A. (1990). Structure and probable genetic location of a "ribosome modulation factor" associated with 100S ribosomes in stationary-phase Escherichia coli cells. *Proceedings of the National Academy of Sciences of the United States of America*, *87*(7), 2657–61. Retrieved from http://www.ncbi.nlm.nih.gov/pubmed/2181444

Wade HE. (1952). Variation in the phosphorus content of Escherichia coli during

cultivation. *Journal of General Microbiology*, *7*, 24–30. https://doi.org/10.1099/00221287-7-1-2-24

Waldsich C, Grossberger R, Schroeder R. (2002). RNA chaperone StpA loosens interactions of the tertiary structure in the td group I intron in vivo. *Genes & Development*, *16*(17), 2300–12. https://doi.org/10.1101/gad.231302

Walker KA, Mallik P, Pratt TS, Osuna R. (2004). The Escherichia coli Fis promoter is regulated by changes in the levels of its transcription initiation nucleotide CTP. *The Journal of Biological Chemistry*, *279*(49), 50818–28. https://doi.org/10.1074/jbc.M406285200

Weitzmann CJ, Cunningham PR, Nurse K, Ofengand J. (1993). Chemical evidence for domain assembly of the Escherichia coli 30S ribosome. *FASEB Journal : Official Publication of the Federation of American Societies for Experimental Biology*, *7*(1), 177–80. Retrieved from http://www.ncbi.nlm.nih.gov/pubmed/7916699

Wells SE, Hughes JM., Haller Igel A, Ares M. (2000). *RNA-Ligand Interactions Part B*. *Methods in Enzymology* (Vol. 318). Elsevier. https://doi.org/10.1016/S0076-6879(00)18071-1

Wilson DN, Nierhaus KH. (2007). The weird and wonderful world of bacterial ribosome regulation. *Critical Reviews in Biochemistry and Molecular Biology*, *42*(3), 187–219. https://doi.org/10.1080/10409230701360843

Woese CR, Magrum LJ, Gupta R, Siegel RB, Stahl DA, Kop J, … Noller HF. (1980). Secondary structure model for bacterial 16S ribosomal RNA: phylogenetic, enzymatic and chemical evidence. *Nucleic Acids Research*, *8*(10), 2275–93. Retrieved from

http://www.pubmedcentral.nih.gov/articlerender.fcgi?artid=324077&tool=pmcentrez&rendertype=abstract

Yoshida H, Ueta M, Maki Y, Sakai A, Wada A. (2009). Activities of *Escherichia coli* ribosomes in IF3 and RMF change to prepare 100S ribosome formation on entering the stationary growth phase. *Genes to Cells*, *14*(2), 271–280. https://doi.org/10.1111/j.1365-2443.2008.01272.x

Yoshida H, Yamamoto H, Uchiumi T, Wada A. (2004). RMF inactivates ribosomes by covering the peptidyl transferase centre and entrance of peptide exit tunnel. *Genes to Cells*, *9*(4), 271–278. https://doi.org/10.1111/j.1356-9597.2004.00723.x

Young RA, Steitz JA. (1978). Complementary sequences 1700 nucleotides apart form a ribonuclease III cleavage site in Escherichia coli ribosomal precursor RNA. *Proceedings of the National Academy of Sciences of the United States of America*, *75*(8), 3593–7. Retrieved from http://www.pubmedcentral.nih.gov/articlerender.fcgi?artid=392831&tool=pmcentrez&rendertype=abstract

Zubradt M, Gupta P, Persad S, Lambowitz AM, Weissman JS, Rouskin S. (2016). DMS-MaPseq for genome-wide or targeted RNA structure probing in vivo. *Nature Methods*, *14*(1), 75–82. https://doi.org/10.1038/nmeth.4057

CURRICULUM VITAE

PERSONAL

Ryan Hulscher
ryan.hulscher@gmail.com
(253) 686-0993

Born: April 20th, 1983
Location: Puyallup, WA, USA

EDUCATION

Ph.D., Molecular biophysics 2017
The Johns Hopkins University, Baltimore, MD

B.S., Biochemistry 2010
University of Puget Sound, Tacoma, WA

B.S., Mathematics 2006
University of Puget Sound, Tacoma, WA

RESEARCH EXPERIENCE

Doctoral and Postdoctoral Research
2010-present
The Johns Hopkins University, Department of Biophysics
Advisor: Dr. Sarah Woodson
Thesis: "Structural changes in the *E. coli* ribosome during assembly and cellular stress"

- Created and optimized a method for isolating nascent ribosomes and combined this with *in vivo* RNA structure probing techniques to study changes in the structure of ribosomal RNA during ribosome biogenesis

Undergraduate Research
2009-2010
University of Puget Sound, Department of Chemistry
Advisor: Dr. Steven Neshyba
Topic: "Molecular dynamics simulations of growing and ablating hexagonal ice crystals"

- Performed molecular dynamics simulations of ice crystal formation and ablation

LEADERSHIP AND TEACHING EXPERIENCE

Teaching Assistant for Protein Engineering and Biochemistry Laboratory
Spring 2016
The Johns Hopkins University, Department of Biophysics

Teaching Assistant for Introduction to Scientific Computing
Spring 2015
The Johns Hopkins University, Department of Biophysics

Graduate Student Speaker Series Organizer
Fall 2012 – Spring 2014
The Johns Hopkins University

Teaching Assistant for Proteins and Nucleic Acids
Fall 2011
The Johns Hopkins University, Department of Biophysics

PUBLICATIONS

Hulscher, R.M.; Woodson, S.A. (2017). Changes in the *E. coli* ribosome structure and composition during cellular stress. In preparation.

Hulscher, R.M.; Bohon, J.; Rappé, M.C.; Gupta, S.; D'Mello, R.; Sullivan, M.; Ralston, C.Y.; Chance, M.R.; Woodson, S.A. (2016). Probing the structure of ribosome assembly intermediates *in vivo* using DMS and hydroxyl radical footprinting. Methods. *103*, 49-56.

Pfalzgraff, W.C.; Hulscher, R.M.; Neshyba, S.P. (2010). Scanning electron microscopy and molecular dynamics of growing and ablating hexagonal ice crystals. Atmos. Chem. Phys. *10(6)*, 2927-2935.

PRESENTATIONS

Oral presentation delivered at the 26th Annual Institute for Biophysical Research Retreat in Baltimore, MD, September 2017.

Hulscher, R.M.; Woodson, S.A. Structural changes in the *E. coli* ribosome during cellular stress.

Poster presentation delivered at the 25th Annual Institute for Biophysical Research Retreat in Baltimore, MD, September 2016.

Hulscher, R.M.; Woodson, S.A. Using *in vivo* DMS probing to determine the structures of ribosome assembly intermediates in *E. coli*.

Oral presentation delivered at the 21st Annual Meeting of the RNA Society in Kyoto, Japan, June 2016.

Hulscher, R.M.; Woodson, S.A. Determining the structures of ribosome assembly intermediates in *E. coli* by time-resolved intracellular footprinting.

Poster presentation delivered at the North Carolina Symposium on RNA Biology XI in Durham, NC, October 2015.

Hulscher, R.M.; Woodson, S.A. Using hydroxyl radical footprinting to observe ribosome assembly intermediates *in vivo*.

Poster presentation delivered at the 24th Annual Institute for Biophysical Research Retreat in Baltimore, MD, September 2015.

Hulscher, R.M.; Woodson, S.A. *In vivo* probing of ribosome assembly intermediates.

Poster presentation delivered at the National Cancer Institute Symposium "RNA Biology 2015" in Bethesda, MD, March 2015.

Hulscher, R.M.; Woodson, S.A. Using hydroxyl radical footprinting to observe ribosome assembly intermediates *in vivo*.

Poster presentation delivered at the 59th Annual Meeting of the Biophysical Society in Baltimore, MD, February 2015.

Hulscher, R.M.; Woodson, S.A. Using hydroxyl radical footprinting to observe ribosome assembly intermediates *in vivo*.

Poster presentation delivered at the 23rd Annual Institute for Biophysical Research Retreat in Baltimore, MD, September 2014.

Hulscher, R.M.; Woodson, S.A. Probing ribosome assembly intermediates *in vivo* using hydroxyl radical footprinting.

Poster presentation delivered at the 26th Annual Gibbs Conference on Biothermodynamics in Carbondale, IL, September 2012.

Hulscher, R.M.; Draper, D.E. Measurement of *in vivo* ion activity in *E. coli*.